

**ANALOG JOINT SOURCE CHANNEL CODING FOR MULTI  
TERMINAL AND NON-LINEAR CHANNELS**

by

Mohamed K Hassanin

A dissertation submitted to the Faculty of the University of Delaware in partial fulfillment of the requirements for the degree of Doctor of Philosophy in Electrical and Computer Engineering

Summer 2018

© 2018 Mohamed K Hassanin  
All Rights Reserved

ANALOG JOINT SOURCE CHANNEL CODING FOR MULTI  
TERMINAL AND NON-LINEAR CHANNELS

by

Mohamed K Hassanin

Approved: \_\_\_\_\_  
Kenneth E. Barner, Ph.D.  
Chair of the Department of Electrical and Computer Engineering

Approved: \_\_\_\_\_  
Babatunde A. Ogunnaike, Ph.D.  
Dean of the College of Engineering

Approved: \_\_\_\_\_  
Ann L. Ardis, Ph.D.  
Senior Vice Provost for Graduate and Professional Education

I certify that I have read this dissertation and that in my opinion it meets the academic and professional standard required by the University as a dissertation for the degree of Doctor of Philosophy.

Signed: \_\_\_\_\_  
Javier Garcia-Frias, Ph.D.  
Professor in charge of dissertation

I certify that I have read this dissertation and that in my opinion it meets the academic and professional standard required by the University as a dissertation for the degree of Doctor of Philosophy.

Signed: \_\_\_\_\_  
Gonzalo R. Arce, Ph.D.  
Member of dissertation committee

I certify that I have read this dissertation and that in my opinion it meets the academic and professional standard required by the University as a dissertation for the degree of Doctor of Philosophy.

Signed: \_\_\_\_\_  
Xiang-Gen Xia, Ph.D.  
Member of dissertation committee

I certify that I have read this dissertation and that in my opinion it meets the academic and professional standard required by the University as a dissertation for the degree of Doctor of Philosophy.

Signed: \_\_\_\_\_  
Luis Castedo, Ph.D.  
Member of dissertation committee

## ACKNOWLEDGEMENTS

In the name of God, the most merciful.

I would like to thank my mentor and advisor Professor Javier Garcia-Frias for supporting and encouraging me all the way through my research, and for offering me the opportunity to join the amazing small family of the Information Processing and Communications Lab. His passion for research, patience, and critical mind forced me to hone and evolve my “intuitive” arguments into solid well developed ideas. I am truly indebted to him for where I am today. Also special thanks to my lab-mates: Bo Lu and Lu Li, who made this journey much more enjoyable.

I am grateful for the companionship of my friends Sergio Matiz, Ana Ramirez, and Cesar Duarte, and our lunch discussions. They made me feel among family during my early days at UD. I will always remember the fun times I had with my friends Nimer Abusalem, Zakariya Nawasraeh, Lassad Mahmadi, Hesan Babtain and Abdulkader. I am also very grateful for Luisa Polania and Hadi Al-Khateeb for their continuous support, professional and personal advice.

I thank Tom Kenney and Shahrnaz Azizi for their great mentorship and support during my internship at Intel Corp. I enjoyed Tom’s stories about his early days in the Wireless and his opinions on its future directions. His great dedication and passion reminded me why I chose this field. I am truly grateful for Shahrnaz’s support and career advice, she showed me what it means to be a very successful professional who truly cares about the lives and careers of her team.

I would also like to acknowledge the great power of open education, the equal opportunity it provides, and the tremendous empowerment effects it can have on the individual, enabling him to truly achieve his potential. In particular, I am grateful for

the Digital Communications series of the MIT Open CourseWare, which made it clear early on that this is the right career for me.

Finally, I would like to thank my family for supporting me in taking the long journey of Graduate school. In particular, I dedicate this dissertation to my Mother, Naglaa. Without her prayers, support, and encouragement, I would not have made it half way through.

## TABLE OF CONTENTS

<b>LIST OF TABLES</b> . . . . .	<b>ix</b>
<b>LIST OF FIGURES</b> . . . . .	<b>x</b>
<b>ABSTRACT</b> . . . . .	<b>xvi</b>
 <b>Chapter</b>	
<b>1 INTRODUCTION</b> . . . . .	<b>1</b>
<b>2 ANALOG JOINT SOURCE CHANNEL CODING SYSTEMS</b> . . . . .	<b>7</b>
2.1 Framework for Digital Communications . . . . .	9
2.2 Analog JSCC Systems . . . . .	11
2.2.1 Linear Analog Systems . . . . .	13
2.2.2 Space filling curves . . . . .	14
2.2.3 Analog vs Digital Tradeoff . . . . .	16
2.3 Theoretical Limits . . . . .	17
2.3.1 Rate Distortion Function . . . . .	18
2.3.2 Channel Capacity . . . . .	19
2.3.3 Optimal Performance Theoretically Attainable . . . . .	20
<b>3 ANALOG JSCC FOR UNDERWATER COMMUNICATIONS</b> . . . . .	<b>22</b>
3.1 Introduction . . . . .	22
3.1.1 Introduction to Underwater channels . . . . .	22
3.1.2 Space Filling Curves . . . . .	23
3.1.3 Overall Channel Model . . . . .	24
3.2 Theoretical Analysis . . . . .	26
3.2.1 Simplified Non-linear Channel (No ISI) . . . . .	26

3.2.2	End-to-end Channel (with ISI) . . . . .	28
3.3	Power Allocation for the End-to-end Channel . . . . .	31
3.3.1	Optimal Power Allocation Scheme for $C_B$ . . . . .	31
3.3.2	Heuristic Power Allocation Scheme for $C_B$ . . . . .	32
3.4	Proposed System . . . . .	35
3.4.1	Decoder Structure . . . . .	38
3.5	Simulation Results . . . . .	40
3.5.1	Simplified non-linear Channel (no ISI) . . . . .	40
3.5.2	End-to-end non-linear ISI Channel . . . . .	41
3.6	Conclusion . . . . .	42
<b>4</b>	<b>ANALOG JSCC FOR THE MULTIPLE ACCESS CHANNEL . . . . .</b>	<b>44</b>
4.1	The Multiple Access Channel . . . . .	46
4.1.1	Orthogonal Schemes . . . . .	48
4.1.2	Non-Orthogonal Schemes . . . . .	49
4.2	Proposed CDMA-like Access Scheme . . . . .	51
4.2.1	Analog Joint Source Channel Coding using the proposed CDMA-like scheme . . . . .	56
4.2.1.1	Uncoded Transmission ( $M = 1$ ) . . . . .	57
4.2.1.2	2:1 Bandwidth Reduction ( $M = 2$ ) . . . . .	58
4.3	A Hybrid Analog-Digital System for the MAC . . . . .	59
4.3.1	Theoretical Analysis . . . . .	59
4.3.2	Practical Implementation . . . . .	61
4.3.2.1	Analog Encoder . . . . .	61
4.3.2.2	Digital Encoder . . . . .	62
4.4	Extension to more than two users . . . . .	62

4.5	Simulation Results . . . . .	64
4.5.1	Pure analog CDMA-like scheme . . . . .	64
4.5.2	Hybrid Analog-Digital Scheme . . . . .	65
4.6	Conclusion . . . . .	67
<b>5</b>	<b>ANALOG JSCC FOR THE BROADCAST CHANNEL . . . . .</b>	<b>69</b>
5.1	Introduction . . . . .	69
5.2	The Broadcast Channel . . . . .	70
5.2.1	Formal Characterization of the Discrete Broadcast Channel . . . . .	72
5.2.2	Broadcasting Gaussian sources over the Gaussian Broadcast Channel . . . . .	74
5.3	Separation Based solutions . . . . .	77
5.4	Analog Mappings for The Broadcast Channel . . . . .	79
5.5	Rationale of AS-SQLC . . . . .	86
5.6	Distortion Analysis and Optimal Decoder . . . . .	89
5.7	AS-SQLC Generalization to Correlated Sources . . . . .	92
5.7.1	Distortion Analysis and Decoder Design . . . . .	94
5.7.2	Optimal Decoders . . . . .	96
5.8	Simulation Results . . . . .	99
5.9	Conclusion . . . . .	105
<b>6</b>	<b>CONCLUSION AND FUTURE WORK . . . . .</b>	<b>106</b>
	<b>BIBLIOGRAPHY . . . . .</b>	<b>108</b>
	<b>Appendix</b>	
<b>A</b>	<b>POWER ALLOCATION . . . . .</b>	<b>115</b>
<b>B</b>	<b>SIMPLE SCHEMES FOR THE BROADCAST CHANNEL . . . . .</b>	<b>116</b>

## LIST OF TABLES

3.1	Specific system parameters obtained from [46] . . . . .	25
-----	---	----

## LIST OF FIGURES

1.1	Canonical Digital Communications systems based on the separation principle vs Analog JSCC systems. . . . .	2
1.2	Different configurations of the general multi terminal communications problem: (a) Multiple Access Channel; (b) the Broadcast Channel; (c) Interference Channel (d) Relay Channel; and, (e) Two Way Channel.	4
2.1	Bit Mapping to 16 QAM. . . . .	12
2.2	Canonical Digital Communications Systems based on the separation principle vs Analog JSCC systems. . . . .	12
2.3	PCCPVQ codebook for the 2:1 Bandwidth compression case for SNRs of 0, 10, 20, and 50 dB (taken from [31]) . . . . .	13
2.4	Example of space filling curve: Archimedean spiral with $\Delta = 1$ , and $\Delta = 0.4$ . The positive branch is when $\theta > 0$ and the negative branch when $\theta \leq 0$ . . . . .	15
2.5	Robustness of digital systems vs analog systems. <i>SDR</i> is a performance metric and will be formally defined in subsection 2.3.3.	17
2.6	SDR as a function of the compression rate for uniform and optimal scalar quantization of i.i.d. Gaussian samples. . . . .	19
2.7	OPTA graph (in dB) for $\kappa = 4,2,1,0.5$ (top to bottom), when transmitting i.i.d Gaussian samples over AWGN channels . . . . .	21
3.1	Propagation loss of electromagnetic waves in water as a function of the distance and frequency (taken from [44]). . . . .	23
3.2	System diagram of an encoder based on the 2:1 Archimedean spiral.	24

3.3	End-to-end channel model including the non-linear amplifier transfer function at the transmitter, the attenuation profile and the impulse response of the ISI channel. . . . .	25
3.4	Capacity achieving distribution for the simplified channel when the separation between the transmitter and receiver, $d$ , is 2 Km. CSNR = 18.5 dB (left) and 11 dB (right). . . . .	28
3.5	Capacity of the AWGN linear channel, and the simplified non-linear channel obtained using the Blahut-Arimoto algorithm. . . . .	29
3.6	System used to postulate a bound for the capacity of the end-to-end underwater channel. . . . .	30
3.7	Value of $C_B = \sum_i C_d(\frac{ H_i ^2 \gamma_d P_i}{\sigma_{n^2}^i})$ for the end-to-end non-linear channel for $d = 0.5, 1, 2$ and 4 Km. The capacity of the same channel assuming an ideal linear amplifier is also shown. . . . .	33
3.8	Rate of change, $C'$ , for $C_d(\frac{P \gamma_d}{\sigma_{n^2}})$ for the simplified non-linear channel and the AWGN channel for $d = 1$ Km. . . . .	34
3.9	Optimal power allocation vs allocation obtained by the heuristic (modified water-filling-like) algorithm for the end-to-end non-linear ISI channel, when the communication distance is 1 Km, for CSNR = 9.3 and CSNR = 22.1 dB. The number of parallel channels is $N = 1024$ . . . . .	35
3.10	Overall system model of the transmitter. . . . .	36
3.11	The histogram matching block modifies the distribution of the input data. The distance between transmitter and receiver is 1 Km, CSNR = 27 dB, and the optimized parameters are $(\epsilon_1 = 0.2, \beta = 2, \sigma = 5, \epsilon_2 = 0, \epsilon_3 = 0)$ . . . . .	38
3.12	DFE structure . . . . .	39
3.13	Simulation results for the simplified non-linear channel (no ISI) when the distance between the transmitter and receiver is 0.5, 1, 2 and 4 Km. . . . .	41

3.14	Simulation results for the end-to-end channel (including non-linearity and ISI). The distance between the transmitter and receiver is 0.5, 1, 2 and 4 Km and the ISI channel response is shown in Figure 3.3. . . . .	43
4.1	General multi-terminal network. Notice that each transmitter has a set of sources and that have to be communicated to a subset of the receivers with a given fidelity. The desired fidelity level could be different for each receiver. . . . .	45
4.2	The Multiple Access Channel with $N$ users. . . . .	46
4.3	Capacity region for the 2-user AWGN Multiple Access Channel. . . . .	47
4.4	The codebook $C_{K \times K}$ is obtained by scaling the Hadamard matrix columns corresponding to user $i$ by the factor $\eta_i = \frac{1}{\sqrt{m_i}}$ . The $K \times K$ access codebook is partitioned into $N$ sub matrices, $C_{K \times m_i}$ with $1 \leq i \leq N$ , where $C_{K \times m_i}$ is the access code for user $i$ . . . . .	51
4.5	Proposed scheme for two users ( $N = 2$ ) with $K = 8$ , $m_1 = 3$ and $m_2 = 5$ . The upper branch corresponds to user 1 and the lower to user 2. Note the data of each user $x_j^i$ is fixed for all the signaling times $1 \leq k \leq 8$ . . . . .	52
4.6	$8 \times 8$ Hadamard matrix. Here $K = 8$ , $m_1 = 3$ and $m_2 = 5$ . To generate the matrix $\mathbf{C}_{8 \times 8}$ , the first 3 columns are assigned to user 1 and then scaled by $\frac{1}{\sqrt{3}}$ . The remaining 5 columns are assigned to user 2 and scaled by $\frac{1}{\sqrt{5}}$ . . . . .	53
4.7	Equivalent CDMA system corresponding to Figure 4.5. The first $m_1 = 3$ equivalent users correspond to the 3 different symbols of user 1 in our proposed scheme, while the next $m_2 = 5$ equivalent users correspond to the 5 different symbols of user 2. . . . .	53
4.8	MAC capacity and the proposed scheme capacity for $P_1 = 200$ , $P_2 = 400$ and codebook size $K = 32$ . Each point of the curve is obtained from (4.25) and (4.26) by sweeping $m_1$ from 0 to 32. . . . .	55
4.9	Theoretical limit for the hybrid scheme: The lower curve is obtained by using the CDMA-like access scheme and sweeping $m$ from 0 to 32. The middle curve represents the achievable rates by the combination of the CDMA-like access scheme and the digital code used by user 2. . . . .	61
4.10	Proposed analog-digital coding scheme for two users. . . . .	62

4.11	System performance for $M = 1$ and different values of $m_i$ (using optimal power allocation) when $K = 16$ . Note that irrespectively of the values of $m_i$ , the scheme achieves the OPTA exactly for the two and three user cases. . . . .	64
4.12	System performance for $M = 2$ and different values of $m_i$ s (using optimal power allocation) when $K = 16$ . Notice that irrespectively of the values of $m_i$ s, the achieved SDR is only 1 dB away from the OPTA. . . . .	65
4.13	Performance of the hybrid analog-digital scheme using a digital code of rate $\kappa$ for user 2, and an uncoded analog system ( $M = 1$ ). . . . .	66
4.14	Performance of the hybrid analog-digital scheme using an optimal digital code and an uncoded analog system ( $M = 1$ ). Note that the performance is tangent to the MAC capacity meaning it is optimal for that specific rate pair. . . . .	67
4.15	Performance of the analog-digital scheme for three users ( $N = 3$ ) when transmitting uncoded analog sources ( $M = 1$ ). Note that the performance is tangent to the MAC capacity meaning it is optimal for that specific rate pair. . . . .	68
5.1	General framework for the Broadcast channel. There is one transmitter which has a set of messages or sources. The transmitter wishes to communicate each message to a subset of the receivers with a given fidelity. The desired fidelity level may be different for each receiver. . . . .	70
5.2	Different orderings of four messages in a four time slot communication system. Each order represents a message from a codebook. . . . .	72
5.3	Bivariate Gaussian probability density function for $\rho^2 = 0$ (left) and $\rho^2 = 0.9$ (right). . . . .	75
5.4	Broadcasting a Bivariate Gaussian source over the Gaussian Broadcast Channel. . . . .	75
5.5	Optimal coding schemes and associated regions as described in [13]. Note that the maximum distortion incurred can not be larger than 1 because we are working with sources of variance 1. . . . .	77

5.6	Different Separation Based schemes for different values of $\rho$ . Notice that the optimal separation based scheme is equivalent to Scheme C.	80
5.7	Encoder for an AS-SQLC system.	82
5.8	The decoder of AS-SQLC systems. There are two instances of the decoder, one at each user site. The decoder is parametrized by the received noise variance, $N_i$ .	83
5.9	Space filling curve corresponding to the proposed SQLC system. Source symbols $(s_1, s_2)$ are projected onto the curve to produce $(v_1, v_2)$ .	84
5.10	Space filling curve for AS-SQLC. The two sources $(s_1, s_2)$ are projected onto the curve and the resulting pair is transmitted as indicated in the text. Notice the <i>continuity</i> of the curve, eliminating the threshold effect.	85
5.11	Complete system diagram of the AS-SQLC system.	86
5.12	Distribution of $\hat{v}_2$ , when $v_2 = 1.5$ . (a) SQLC; (b) AS-SQLC. Notice the disappearance of the threshold effect in 5.12(b).	87
5.13	Distribution of $\mathbf{V}_2$ for two different values of $\alpha$ . Increasing $\alpha$ makes the distribution more uniform but increases the percentage of data that gets clipped.	88
5.14	Information rates obtained by the SQLC and the AS-SQLC systems.	88
5.15	Optimal detector function $\Psi$ vs the suboptimal function in [13]. (a) SNR= 8 dB, $\Delta = 1.0, \alpha = 1.2$ ; (b) SNR= 20 dB, $\Delta = 1.0, \alpha = 1.0$ .	92
5.16	Complete system diagram of the generalized AS-SQLC system for transmitting correlated sources.	93
5.17	Complete system diagram of the AS-SQLC system with optimal decoders.	97
5.18	Optimal decoders for $P = 1, N_1 = 0.04, N_2 = 10N_1, \rho^2 = 0, \mathbf{H} = \mathbf{I}$ . (a) uses $\Delta = 1.5$ and $\alpha = 1.2$ as encoding parameters, while (b) uses $\Delta = 2.0$ and $\alpha = 1.5$ .	97

5.19	Optimal decoders for $P = 1, N_1 = 0.04, N_2 = 10N_1, \rho^2 = 0.9$ . <a href="#">5.19(a)</a> uses the identity matrix as the precoding matrix $\mathbf{H}$ , while <a href="#">5.19(b)</a> uses $[1 \ 0; -1 \ 1]$ as $\mathbf{H}$ . . . . .	98
5.20	Optimal decoders for $P = 1, \rho^2 = 0.4, \Delta = 1, \mathbf{H} = [1 \ 0; -0.9 \ 1]$ . (a) considers $N_1 = N_2 = 0.01$ , while for (b) considers $N_1 = N_2 = 0.1$ . . . . .	99
5.21	Optimal decoders for $P = 1, N_1 = N_2 = 0.1, \Delta = 1$ . (a) has a source correlation, $\rho^2 = 0.4$ , while (b) has a source correlation $\rho^2 = 0.9$ . Notice that the second source $\hat{s}^2$ in <a href="#">5.21(b)</a> closely follows the decoded values of $\hat{x}_1$ has $\rho^2 = 0.9$ . . . . .	100
5.22	System performance under different conditions: (a) $\rho^2 = 0.8, N_1 = 0.004, N_2 = 10N_1, P = 1$ , (b) $\rho^2 = 0.4, N_1 = 0.004, N_2 = 4N_1, P = 1$ . . . . .	101
5.23	System performance under different conditions: (a) $\rho^2 = 0.7, N_1 = 0.008, N_2 = 20N_1, P = 1$ , (b) $\rho^2 = 0.2, N_1 = 0.002, N_2 = 20N_1, P = 1$ . . . . .	102
5.24	System performance under different conditions: (a) $\rho^2 = 0, N_1 = 0.01, N_2 = N_1, P = 1$ , (b) $\rho^2 = 0, N_1 = 0.01, N_2 = 2N_1, P = 1$ . . . . .	103
B.1	Smart time sharing: <a href="#">(a)</a> shows the case when $\zeta = \frac{1}{3}$ and, <a href="#">(b)</a> shows the case when $\zeta = \frac{1}{4}$ . . . . .	117
B.2	OPTA curves for $P = 1, N_1 = 0.002, N_2 = 10N_1$ and $\rho = 0$ : <a href="#">(a)</a> depicts the log scale; and, <a href="#">(b)</a> depicts the linear scale. . . . .	118

## ABSTRACT

This dissertation discusses various problems in analog Joint Source Channel Coding (JSCC). Analog JSCC is an attractive communication scheme due to its encoding/decoding simplicity, and its ability to achieve near-optimal performance using very short code lengths. JSCC systems have received a renewed interest in recent years due to, among other factors, the sub-optimality of separation based schemes in many situations in multi-terminal communications. Different from traditional digital communication systems which utilize a quantizer followed by a source code and a channel code, analog JSCC systems combine source and channel coding into a single block and deal with real numbers.

We present original work on the application of space filling curves, a common scheme in analog coding, to different communication scenarios. We begin by examining how to extend the use of space filling curves to non-linear channels with Inter-Symbol Interference (ISI). This type of channel arises when considering acoustic communications in the underwater environment, where the power amplifier used for communication is highly non-linear, and multi-path propagation causes ISI. We first study a simplified version of the acoustic channel assuming a frequency flat (no ISI) response, developing a scheme to adapt space filling curves to the simplified channel and studying its theoretical limits. Then, we extend our work to the complete end-to-end acoustic channel (including ISI), presenting a communication system for the end-to-end channel.

We then investigate the problem of transmitting independent sources over the Gaussian Multiple Access Channel (MAC). The Gaussian MAC consists of two or more users communicating information to a central receiver over a shared noisy physical channel. We introduce an analog CDMA-like access scheme that allows users to transmit at different rates over the MAC. The developed access scheme is suitable for

the transmission of analog JSCC encoded sources. The CDMA-like access scheme will be proven to be optimal for a particular case when the channel degrees of freedom are assigned amongst the users in a particular way. We will then present a hybrid analog-digital scheme which is an extension of the analog CDMA-like access scheme. The hybrid scheme uses analog and digital codes, designed for the point-to-point channel, and will be proven to be optimal for the entire region of the MAC.

Finally, the dissertation introduces a new communication scheme for the two-user Gaussian Broadcast channel. The channel consists of a common transmitter wishing to communicate information to two receivers over a noisy Gaussian channel. The broadcast channel is an interesting case, since in general separation based schemes cannot achieve the theoretical limits. The new developed scheme is a variant of Scalar Quantizer Linear Coder (SQLC) systems, and is suitable for transmitting correlated Bivariate Gaussian sources. The scheme will be analyzed and shown to outperform the best known separation based schemes.

## Chapter 1

### INTRODUCTION

The use of digital communications systems based on the Shannon separation principle between source and channel coding [1] has led to ubiquitous communications in our society. In this framework, continuous signals are first acquired and source encoded. Then, capacity approaching channel codes are utilized. It is well known that this approach is optimal provided that there are no constraints in terms of complexity and delays. However, long block lengths are required, and these separated systems are not very robust to changes in the channel parameters.

Recently, systems based on analog joint source-channel coding have been discussed in the literature [2, 3, 4, 5]. In this approach, the concatenation of the (vector) quantizer, source encoder and channel encoder characteristic of digital systems is substituted by an end-to-end analog encoder. This discrete-time, continuous-amplitude system directly processes the acquired samples using a non-linear transformation, whose output is transmitted directly through the channel after proper modulation. A schematic diagram of canonical digital communication vs analog JSCC systems is depicted in Figure 1.1. For the same performance, these schemes may present more robustness and require less encoding/decoding complexity than traditional digital systems. A more detailed discussion about analog joint source channel coding will be given in Chapter 2.

Analog JSCC systems, typically, have much simpler encoders and decoders as compared to their digital counterparts, which leads to a power efficient encoder and decoder [6]. Recently, there has emerged a class of wireless communications systems termed “energy harvesting systems” where the decoder harvests the energy of the transmitted data as well as other sources in the electromagnetic spectrum and use

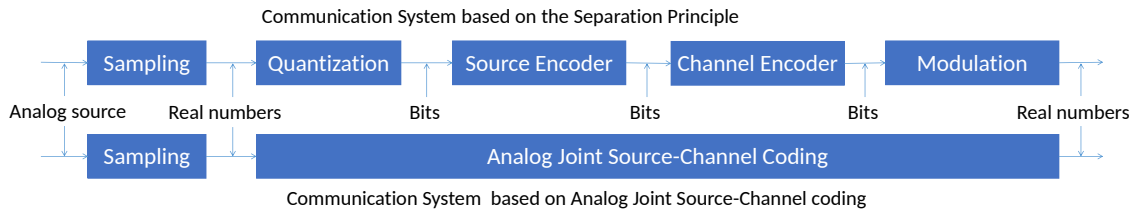


Figure 1.1: Canonical Digital Communications systems based on the separation principle vs Analog JSCC systems.

that energy to help in the decoding process [7]. Although we will not be discussing energy harvesting systems in this dissertation, we give this example to demonstrate the importance that energy efficiency plays in the design of communication systems. This will be more true in the future as more Internet of Things (IOT)-type devices enter the market and become ubiquitous. These devices typically send small data rates to a smart hub, and have a limited battery, making energy efficiency paramount for these devices [8]. This casts analog JSCC systems in a very positive light owing to their encoding/decoding simplicity.

Designing an optimal digital (separated) system is a complex process. For each desired communication rate, a vector quantizer, a source code, a channel code and a modulation scheme must all be designed in an optimal manner as shown in Figure 1.1. For certain channel classes, if each individual component in the system is optimal, then the end-to-end system is also optimal<sup>1</sup>. The use of separated systems for transmitting Gaussian Sources over the AWGN channel was proven optimal by Shannon in his seminal paper [1]. An interesting remark for such separation based digital system is that if an optimal scalar quantizer were used (instead of the optimal vector quantizer), with all remaining system modules optimal, then the system will operate at a 1.6 dB loss from the optimal system predicted by the theoretical limits [6].

Analog JSCC have also been successfully applied to problems in multi-terminal

---

<sup>1</sup> It is optimal in the asymptotic sense when the code block length goes to  $\infty$ , in practice however the system modules must be tested to ensure that the system is not catastrophic, meaning, for example, that a small error in the coded bits does not produce total failure/error for the source decoder.

communications such as communication over the Multiple Access Channel [9, 10, 11, 12], over the Broadcast channel [13, 14], and for OFDM and MIMO channels [15, 16, 17]. Although multi-terminal communications and Information Theory are relatively old fields<sup>2</sup>, they have recently received a great deal of interest from the industry. This interest comes primarily from the wireless community, where the rapid proliferation of cell phones along with the limited bandwidth (bandwidth crunch), particularly in dense metropolitan areas, has motivated the industry to actively investigate the theoretical limits of the underlying wireless channel. Several other factors have helped the acceleration of this trend, as more powerful hardware at the user's equipment and at the base stations allow for implementation of more complicated algorithms and techniques. The emergence of commercial Software Defined Radio (SDR) and Software Defined Networks (SDNs) solutions have allowed the wireless network providers great flexibility to experiment and prototype different access techniques [22].

Current research efforts typically in Network Information Theory focus on special configuration for the general multi-user problem as Figure 1.2 shows, such as Multiple Access Channels, Broadcast Channels, Relay Channels, Interference Channels, and the Two Way Channel. In the multiple access channel, there are several (two or more) users communicating data (possibly correlated) to a central receiver. This is analogous to the uplink scenario for cellular networks where different users (UE) communicate and send their data to the base station (eNB). In the broadcast channel, there is one transmitter communicating data to several receivers. Again, in the cellular setting this corresponds to the downlink where the eNB transmits data to several UEs. In the relay channel, there is a relay (or several relays) that receive(s) the data from the transmitter and forward it (after possibly some manipulation) to the receiver. The receiver also receives the original transmitted data of the transmitter, as well as the information sent by the relay. In the Interference Channel, there are two or more users transmitting the information only to their respective receiver, i.e. receiver  $i$  is

---

<sup>2</sup> The Capacity region of the Gaussian multiple access channel as well as the Broadcast channel were found between 1971-1974 [18, 19, 20, 21]

only interested in the information of transmitter  $i$  and nothing else. The Interference channel can be considered a hybrid between the MAC and broadcast channels. Finally, there is the two way channel where there are two users wishing to communicate to each other *in both directions*. Generally, the communication network topology could be a combination of any of the above configurations.

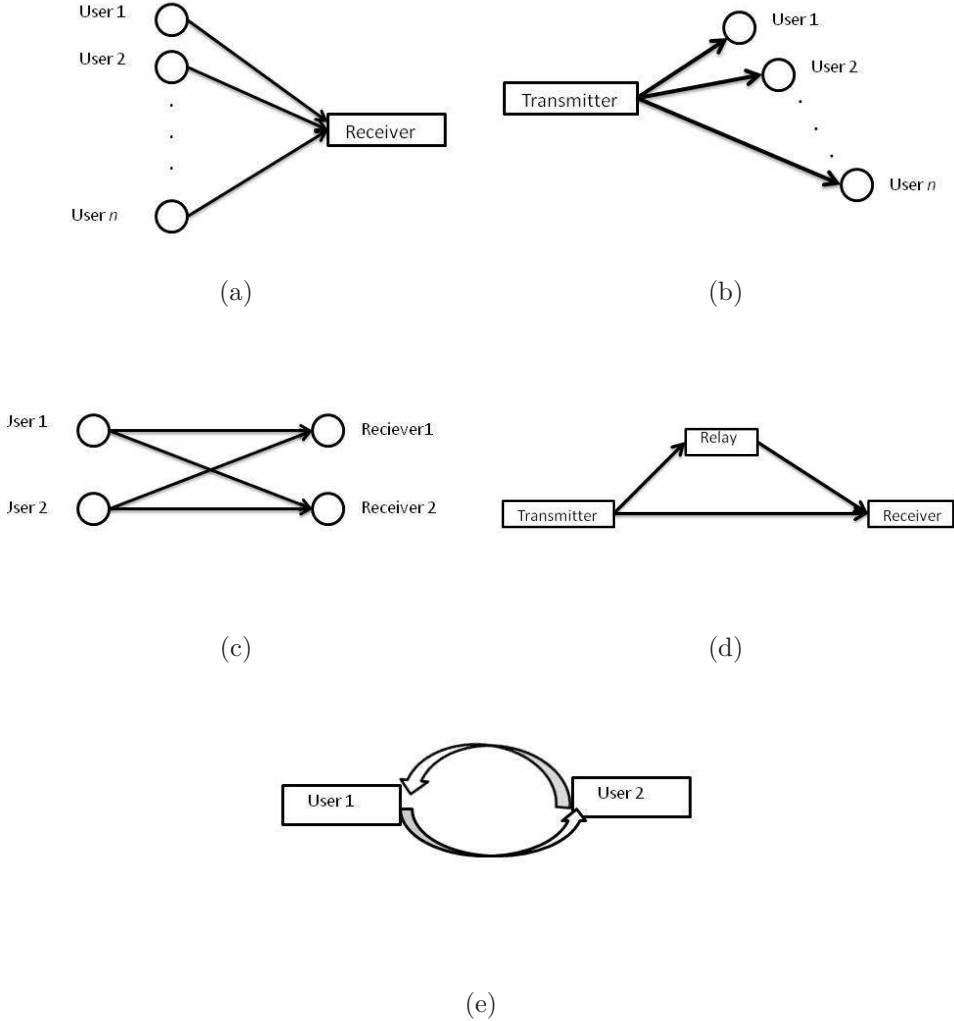


Figure 1.2: Different configurations of the general multi terminal communications problem: (a) Multiple Access Channel; (b) the Broadcast Channel; (c) Interference Channel (d) Relay Channel; and, (e) Two Way Channel.

This dissertation will present original work on the applications of analog JSCC to various communications scenarios. Chapter 2 begins by giving an overview and

comparison of digital and analog communication systems. In Chapter 3, we will discuss the problem of data transmission over the underwater acoustic channel, where the communication channel is highly non-linear and experiences ISI. We will develop a system that adapts space filling curves for use in the acoustic channel. The proposed scheme is an example of the flexibility of JSCC systems, and of the simplicity they provide in the design of encoding/decoding systems. When evaluating the performance of our proposed JSCC scheme, we are faced with the problem of calculating the Shannon capacity of channel. For non-standard channels we have to calculate the capacity via a version of the Blahut-Arimoto algorithm. We first apply the algorithm to obtain the capacity of a simplified version of the channel that does not include the ISI. We then extend the analysis and provide a capacity bound for the end-to-end channel (including the non-linearity and ISI).

In Chapter 4, we propose a hybrid analog-digital scheme for the  $N$ -user Multiple Access Channel that allows the transmission of independent user's information over the MAC. The proposed scheme is suitable for any number of users, and for any source to channel bandwidth ratio. The analog component of the scheme is an orthogonal CDMA-like access scheme, which will be proven optimal for particular non-trivial channel conditions. However, the analog component alone cannot be used optimally to achieve any desired point in the capacity region. The hybrid scheme combines traditional analog digital codes designed for the point-to-point channel in an optimal manner, and will be shown to achieve any point in the convex hull of the capacity region of the MAC.

In Chapter 5, we consider the two user Gaussian Broadcast Channel. We will discuss a new class of analog coders named Alternating Sign Scalar Quantizer Linear Coder (AS-SQLC), suitable for the transmission of Bivariate Gaussian sources over the two-user degraded broadcast channel. We will improve on our previous work in [13], where we developed a zero delay (block length equal to one symbol) communication system that operates very close to the theoretical limits of the channel. The work in [13] made several simplifications in the design of the system decoder, which led to

sub-optimal performance. Here, we provide a mathematical analysis of the AS-SQLC system, and derive the optimal decoder for the proposed system, demonstrating the performance gain by Monte-Carlo simulations. Finally, we will conclude the dissertation and discuss future research directions in Chapter 6.

## Chapter 2

### ANALOG JOINT SOURCE CHANNEL CODING SYSTEMS

Telecommunications play a pivotal role in our lives today. Telecommunications was the heart of the first great transformations of the early twentieth century. The first Radio communication was consummated by Marconi in 1895, and the first general public radio service commenced in Pittsburgh in 1920 [23]. From that point onward, many great innovations came to fruition in a relatively short time-frame, such as public television broadcast, inter-continental public communications, and satellite communications. The second great revolution that Telecommunications has spurred was in the 1990s. These were considered by many the golden times (the dot com bubble) of the telecommunication industry. The World Wide Web was growing exponentially, and second generation digital cellular phones were ubiquitous. The problem that took communication engineers almost fifty years to solve had also been solved in that decade. The problem was finding practical channel codes with the power to communicate sufficiently close to the channel capacity, something that had been theorized by Shannon in his landmark paper in 1948 [1]. The solution to that problem turned out to be the use of random-like codes such as Turbo codes and LDPC codes. Although Gallager invented Low Density Parity Check Codes in his thesis in 1963 [24], Turbo codes were recognized first as the solution to the problem. The invention of Turbo codes and the rediscovery of LDPC codes would not have been very interesting events in their own right (although they were for many academics in the field), had it not been for the rapid growth of Integrated Circuits, which enabled fast efficient implementations of the capacity achieving codes at progressively cheaper cost and better performance.

In digital communication systems, the data is first sampled and quantized (if it is a continuous-time, continuous-amplitude waveform such as voice) into a discrete set.

The resulting bits are input to a source encoder to remove the redundancy, and then passed to a channel encoder, which adds redundancy to combat the noise introduced by the transmission medium. This framework has several advantages. First it was proven asymptotically optimal by Shannon in [1] for point to point AWGN channels. Second, it decouples system design into individual independent modules. In this way, if an optimal source code<sup>1</sup> is designed, we are able to use it with another optimal channel code that a different designer has perfected<sup>2</sup>.

Digital communication systems would not have been that ubiquitous without great advances in DSP and IC technologies. Up until the early 1980s, Digital communications was thought to be too complex to merit implementation against pure analog baseband communications [25]. It was Moore’s law that was the enabler of such digital implementations, which not only outperformed the analog schemes, but did so using less transistors. One of the many reasons that analog communications faded was that they lacked a comprehensive “framework” for system design. Most designs were ad-hoc and there was no clear concept of source/channel codes. There were modulation schemes such as FM and AM, and although FM did provide noise protection, it did so at the expense of a larger communication bandwidth, typically much larger than the original baseband signal to be transmitted. Although in FM systems the source/channel bandwidth ratio can be controlled via the modulation index parameter  $\beta$  [26], analog systems do not have the notion of “error free” communications. As a matter of fact, this was one of the ground breaking promises of Shannon paper’s in 1948 [1]: error free communication at a non-zero information rate with bounded power. This will be laid out in detail in the following section.

---

<sup>1</sup> In this context, code means an encoder/decoder pair.

<sup>2</sup> The source-channel separation theorem holds for infinite block length codes. The combination of certain practical source/channel codes may lead to “catastrophic” errors, in which a small number of errors in the channel decoder leads to many errors after source decoding in the original uncoded bits.

## 2.1 Framework for Digital Communications

Our model for the point to point channel will be that of a Gaussian Source,  $\mathbf{S}$ , emitting i.i.d (independent identically distributed) source symbols with zero mean and unity variance, that is  $\mathbf{S} \sim N(0, 1)$ . The ultimate goal is to communicate the source to a receiver while maintaining some metric of source “goodness” or fidelity at the receiver. Digital communication systems typically achieve this by first feeding the Gaussian source into a quantizer, typically a Vector Quantizer where a block of  $k_{symbol}$  source symbols is fed to the quantizer and a block of  $k_{source} = \eta_1 k_{symbol}$  binary bits are produced. In this framework  $\eta_1$  is average number of bits per source symbol. The uniform quantizer is the simplest, with a uniform quantization step [27]. Then there is the optimal (in the Mean Squared Error sense) scalar Quantizer. And finally, the optimal MSE vector quantizer, which achieves the best performance [28]. We will discuss quantization in more detail in 2.3.1.

After quantization, source coding is performed. There are typically two options for source coding, depending if the system designer chooses to implement a lossless or a lossy compression scheme. The best lossless compression scheme is to use entropy coding such as Huffman codes or other powerful practical entropy coding schemes. The designer might also choose to implement a lossy compression scheme<sup>3</sup>. Lossy source coding schemes include the much-celebrated JPEG format, which uses wavelets as the basis of the lossy transformation. Layer 3 of MPEG is also a well known lossy compression scheme for audio signals. Even though lossy compression schemes incur information loss, they are still used because that loss does not significantly affect the overall picture look or the way audio sounds. These compression schemes exploit the human visual and auditory sensitivities and limitations to encode a lossy version that looks almost indistinguishable from the original. In general, lossy compression is used when certain fidelity needs to be maintained in the reconstructed data. Consider, for

---

<sup>3</sup> Lossy compression may be preferable in certain scenarios. It might seem strange for a lossy compression scheme to be preferable over a lossless one. However (finite) quantization is always lossy for most kinds of sources. Hence, the system designer has the choice of where to *insert* and control distortion. Lossy compression is among those tools.

example, a temperature sensor producing a temperature reading, accurate to the 4<sup>th</sup> decimal digit. The user might only care about accuracy to within one decimal digit and the loss of information of the 3 digits can be tolerated. This is of course a simplified example and a simple arithmetic rounding function should produce the desired effect.

Source coding takes a block of  $k_{source}$  bits and produces a block of  $k_{channel} = \eta_2 k_{source}$  bits, where  $\eta_2$  is the average number of bits per source bit. Notice that for an uncoded system,  $\eta_2 = 1$ . Also, for a lossless system  $\eta_2$  is upper-bounded by the entropy rate of the source. The purpose of source coding is to remove unnecessary or redundant information in the bit stream.

After source coding, channel coding is performed with the purpose of combating the noise in the communication channel. Different from source coding, which aims to remove redundancy, channel codes introduce *controlled* redundancy in the data stream. This redundancy is what allows the channel decoder at the receiver to successfully recover the original uncoded data from the corrupted data received at the receiver site. The channel encoder takes  $k_{channel}$  bits and produces  $\eta_3 k_{channel}$  channel bits. Prior to Turbo codes, which appeared in 1993 [29], all practical channel codes such as convolutional codes or Reed-Solomon Block codes operated at a 3-4 dB margin of the capacity [25]. With the invention of Turbo codes and the rediscovery of Low Density Parity Check (LDPC) codes, the gap to capacity for the AWGN channel was practically closed [30]. LDPC and Turbo codes belong to a general class of codes termed “pseudo-random” codes, which are easily decodable via iterative message passing algorithms.

The last step in digital communication systems is channel modulation. Modulation is the process of mapping the bit stream to channel symbols. The most commonly used modulation scheme is Quadrature Amplitude Modulation (QAM), where the bit stream is mapped to a rectangular grid as shown in Figure 2.1. QAM mapping is the de-facto channel mapper used in communication systems due to its robust performance and easy implementation. QAM by itself is not the optimal solution to maximize the channel throughput. However, when combined with a powerful channel code (such as LDPC or Turbo Codes), the performance is excellent. For a QAM system, the input

is a block of  $\eta_4$  bits and the output is one channel symbol. A common configuration for modulation is “Bit Interleaved Coded Modulation” or BICM. In BICM, the output of the channel encoder is interleaved and then passed to the QAM mapper. Another common code type of modulation is combining channel coding and modulation into a single block, as in Trellis Coded Modulation (TCM). TCM is similar to Binary Convolutional Codes, but with the difference that the alphabet itself is non-binary. TCM codes have good performance but can be computationally expensive to decode.

In summary, the combination of quantization, source coding, channel coding and modulation is required for a digital communication system to convert a stream of source symbols  $S_t$ ,  $t = 1, 2, \dots, \infty$ , into a stream of channel symbols. For each source symbol there is on average  $\kappa = \eta_1 \eta_2 \eta_3 \eta_4$  channel symbols. The value of  $\kappa$  determines whether the system is a bandwidth compression system ( $\kappa > 1$ ), which means there are less channel symbols than source symbols, a bandwidth expansion system ( $\kappa < 1$ ), or simply a matched source-channel system ( $\kappa = 1$ ). Note that for a matched system, the designer might choose to simply transmit the data directly (uncoded) or to perform some processing. This will be elaborated later in this chapter.

Notice that the system designer has four parameters to adjust ( $\eta_1, \eta_2, \eta_3, \eta_4$ ). Shannon proved that if the individual components of the system are optimally designed, then the entire system is optimal<sup>4</sup>. This provides some relief for the designer, but again, it does not address how the the individual components of the system have to be designed.

## 2.2 Analog JSCC Systems

Section 2.1 introduced digital communication systems and presented the four major components (quantization, source coding, channel coding and modulation). These four blocks can be replaced by a single analog processing block as shown in Figure 2.2.

---

<sup>4</sup> Asymptotically, and Shannon only proved this for the point to point channel.

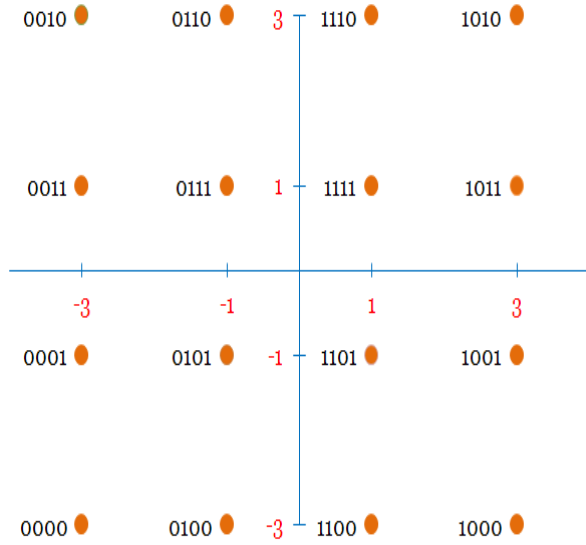


Figure 2.1: Bit Mapping to 16 QAM.

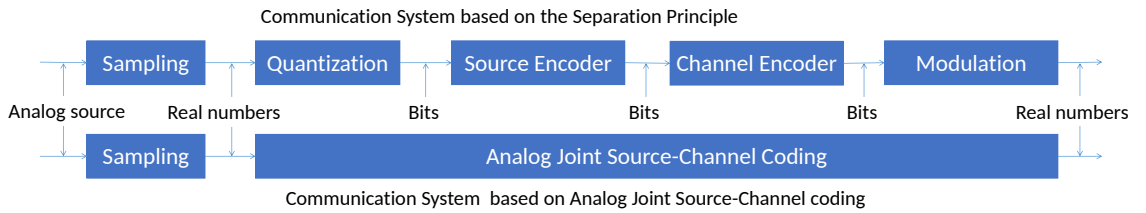


Figure 2.2: Canonical Digital Communications Systems based on the separation principle vs Analog JSCC systems.

An Analog JSCC system can be described by a function,  $f$ , which takes  $M$  source symbols and produces  $N$  symbols to be transmitted, that is

$$f : \mathbb{R}^M \mapsto \mathbb{R}^N. \quad (2.1)$$

The design of an optimal encoding function,  $f$ , and the corresponding decoder, for general values of  $M, N$  is still an open question<sup>5</sup>. Here,  $\kappa = \frac{M}{N} = \eta_1\eta_2\eta_3\eta_4$

<sup>5</sup> In the non-asymptotic sense. If the ratio of  $\frac{M}{N}$  is kept constant, and letting  $M, N \rightarrow \infty$ , we can use the digital systems design tools, as explained in Section 2.1.

Several approaches have been considered to obtain good mappings. These include the use of Power Constrained channel optimized vector quantization (PCCOVQ), which is an extension of the Generalized Lloyd Max Algorithm. PCCOVQ was studied extensively in [31, 32] for Bandwidth expansion and compression, and an example of PCCOVQ codebook is shown in Figure 2.3. PCCOVQ is very computationally intensive, and training does not guarantee a global optimum. Moreover, decoding is very expensive as it typically requires searching over the entire codebook or a large subset of it. Although there are techniques to simplify decoding, they generally do not work well for higher dimensions of  $M$  and  $N$ .

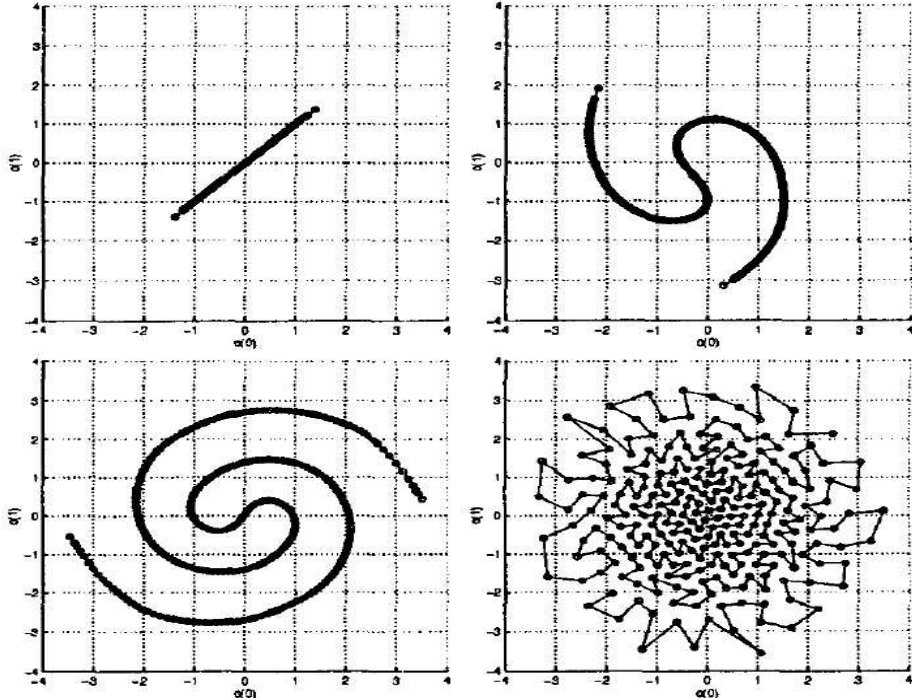


Figure 2.3: PCCPVQ codebook for the 2:1 Bandwidth compression case for SNRs of 0, 10, 20, and 50 dB (taken from [31])

### 2.2.1 Linear Analog Systems

A natural choice for the encoding function  $f$  in (2.1) could be an  $M \times N$  matrix. Linear systems were studied in [33] and it was demonstrated that for general  $M$  and  $N$  they perform well in the low SNR regime, but their performance saturates rapidly as

the SNR increases. It is interesting to note that when  $M = N$ , uncoded transmission of a Gaussian source is *optimal* over the AWGN channel [34].

### 2.2.2 Space filling curves

Space filling curves are another category of analog coding systems. In space filling curves, the codebook or encoding function is specified by a deterministic algebraic function. Figure 2.4 shows an example of two such curves for a 2:1 bandwidth reduction system,  $M = 2, N = 1$ . These curves can also be the basis for bandwidth expansion ( $M = 1, N = 2$ ). Systems based on the use of space filling curves were proposed independently by Shannon and Kotelnikov [35, 36]

As the name suggests, the curve tries to fill the space in such a way that any source point  $\mathbf{x} \in \mathbb{R}^M$  is very close to the curve (in terms of some metric, typically the  $\mathbb{L}_1$  or  $\mathbb{L}_2$  norm). This reduces what is typically called the “encoding distortion”. Moreover, the second objective is to try to separate the encoded data  $\mathbf{y} \in \mathbb{R}^N$  as far as possible so that the channel noise does not distort the original transmitted symbol too much (this is typically called the channel distortion), while at the same time meeting a certain power constraint  $P$ . The different types of distortion and their effect on the system performance were analyzed in [32]. Another type of error that occurs in certain systems based on space filling curves is when a small channel noise leads to significant degradation in the signal fidelity. This type of error is typically called “spurious errors” or the “threshold effect”. It is similar to catastrophic errors in digital systems. The encoding distortion and channel distortion are present in every space filling curve communication system, and they are in a sense an inherent system property. Encoding distortion is conceptually similar to quantization in digital systems, while the channel distortion is similar to channel decoding errors in digital systems.

We will focus our attention on the Archimedean spiral, shown in Figure 2.4 and

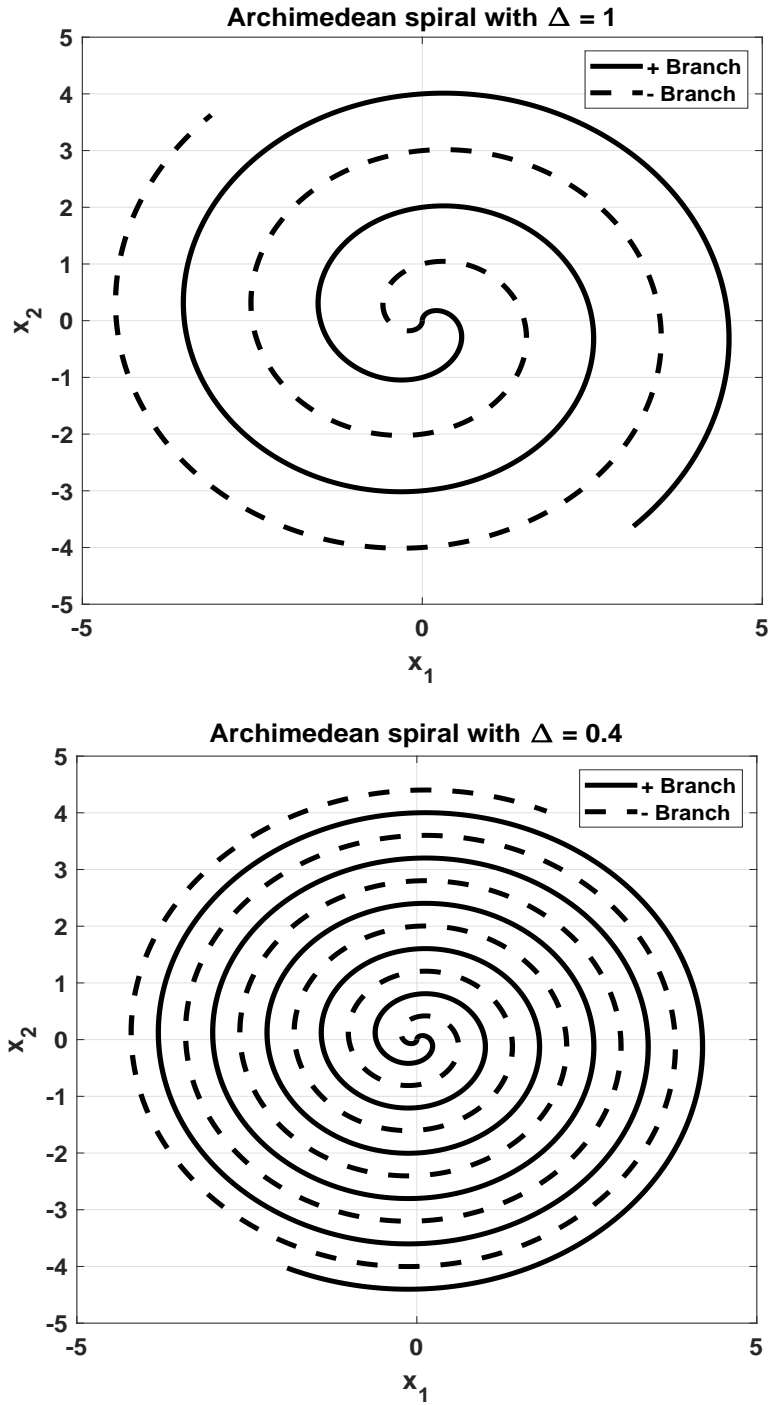


Figure 2.4: Example of space filling curve: Archimedean spiral with  $\Delta = 1$ , and  $\Delta = 0.4$ . The positive branch is when  $\theta > 0$  and the negative branch when  $\theta \leq 0$ .

defined parametrically as

$$\begin{cases} x_1 = \frac{\Delta}{\pi} \theta \sin \theta \\ x_2 = \frac{\Delta}{\pi} \theta \cos \theta \end{cases} \text{ for } \theta \geq 0, \quad \begin{cases} x_1 = -\frac{\Delta}{\pi} \theta \sin \theta \\ x_2 = \frac{\Delta}{\pi} \theta \cos \theta \end{cases} \text{ for } \theta < 0, \quad (2.2)$$

where  $\Delta$  is the distance between two neighboring spiral arms and  $\theta$  is the angle from the origin to the point  $(x, y)$  on the curve. Figure 2.4 shows two cases when  $\Delta = 1$  and 0.4. The Archimedean spiral is studied in detail in [37, 38].  $\Delta$  controls the “circumference” or length of the curve in a given square. Decreasing  $\Delta$  makes the curve more dense as shown in Figure 2.4. The encoding distortion will be made smaller when  $\Delta$  is small, as the curve fills the space better and in fact to achieve better performance at high SNRs, a smaller  $\Delta$  is used [38]. The Archimedean spiral can be used both for bandwidth expansion and compression systems. In this dissertation, we will focus on bandwidth compression systems, mainly on 2:1 systems. Note that the Archimedean Spiral shape is very similar to that of the optimal PCCOVQ shown in Figure 2.3 for a wide range of SNRs.

### 2.2.3 Analog vs Digital Tradeoff

Other than the observation that digital systems are ubiquitous, they do offer some advantages over their analog JSCC counterparts. For instance, we can easily design practical digital systems that approach capacity [30]. This would require an involved system design with different parameters, as explained in Section 2.1. Analog systems on the other hand lack a unifying framework, and every new problem has to be studied practically from the grounds-up. Although some analog codes, such as those based on space filling curves, have been well studied, it is far from the richness that digital codes offer to the system designer. It should also be mentioned that practical digital systems spend a non negligible portion of the channel degrees of freedom in channel estimation, and when designed to operate at a near capacity limit, they become “inelastic” and rigid. In other words, any degradation in the channel conditions (e.g, SNR), lead to a system breakdown, and the bit error rate would diverge from the designed point. On the other hand, if the SNR does improve, no higher data rate or better signal fidelity is achieved (unless the system parameters are re-calibrated). Figure 2.5 illustrates this idea: Both the digital and analog systems are designed to operate at  $SNR = A$ . When the SNR deviates from that, the digital system either

breaks or does not perform better. On the other hand, the analog system is *robust* and performs well at different SNRs, but not as well as analog systems designed specifically for that target SNR.

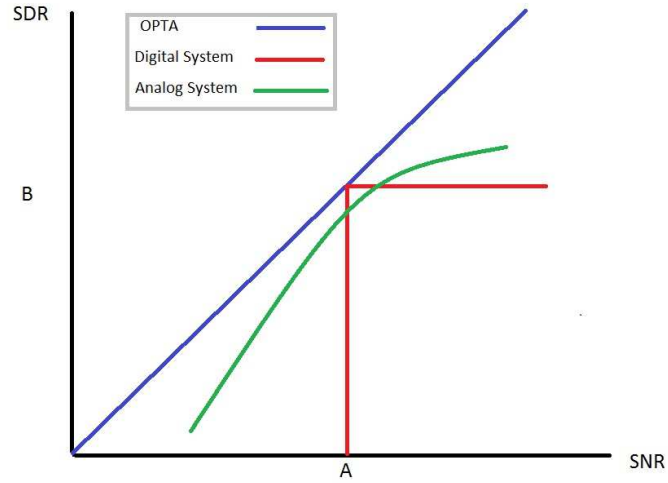


Figure 2.5: Robustness of digital systems vs analog systems.  $SDR$  is a performance metric and will be formally defined in subsection 2.3.3.

As mentioned above, it is possible to design the digital system optimally in a strict SNR vs SDR sense. However, Figure 2.5 does not show the power required for encoding and decoding the transmitted messages. Determining the power consumed by a particular algorithm is not obvious, since IC fabrication technologies changes every couple of years. In [6], the number of operations for encoding/decoding the Archimedean spiral was considered and compared with an equivalent all-digital system. The superiority of the analog approach was shown in terms of encoding and decoding complexity. Furthermore, the delay (latency) is not represented in Figure 2.5, since a large block length is typically used for digital systems.

### 2.3 Theoretical Limits

The theoretical limit of the channel is a fundamental property and does not change whether an analog or digital system is used. In analog JSCC we are interested in the end-to-end system performance in terms of distortion that can be achieved for

a given Signal to Noise Ratio, SNR. This theoretical limit is calculated from the rate distortion function and the channel capacity.

### 2.3.1 Rate Distortion Function

Continuous sources take uncountably many values and they cannot be reproduced faithfully by a countable number of bits. The Rate Distortion function provides the minimum number of bits required to represent a given symbol under a given distortion criteria. The most commonly used criterion for distortion is the Mean Squared Error (MSE), which is the  $\mathbb{L}_2$  norm. Shannon characterized the Rate Distortion theory for Gaussian sources under the mean squared error criterion in [1]. For a Gaussian source  $S \sim \mathcal{N}(0, \sigma_s^2)$ , and a target distortion  $D = E(S - \hat{S})^2$ , where  $\hat{S}$  is the recovered source, the rate distortion function is given by

$$R(D) = \frac{1}{2} \log_2 \frac{\sigma_s^2}{D} \text{ bits.} \quad (2.3)$$

Going from a discrete-time continuous-value symbols to discrete-time discrete-value symbols is called Quantization and it is typically a lossy process. There are different types of Quantizers, A scalar quantizer operates on just one source symbol, while a vector quantizer operates on a vector of source symbols. A uniform quantizer is one in which the quantization step is uniform (constant), and it is the easiest to implement. [27] gives an overview of the different types of quantizers. Figure 2.6 shows a plot of the SDR<sup>6</sup> achieved by a uniform scalar quantizer for i.i.d. Gaussian samples [27]. Notice that the performance of scalar quantization improves by adding more bits, but the gap to the Rate Distortion function gets larger.

The results for the optimal scalar quantizer in Figure 2.6 were obtained using the Lloyd-Max Algorithm [27]. As can be seen in Figure 2.6, adding 1 more bit to the scalar quantizer gains about 4 dB in performance, yet the gap to the rate distortion

---

<sup>6</sup> The SDR is the Signal to Distortion Ratio. It is a logarithmic measure of the signal fidelity and is given by  $SDR = 10 \log_{10}(\frac{\sigma_s^2}{D})$ .

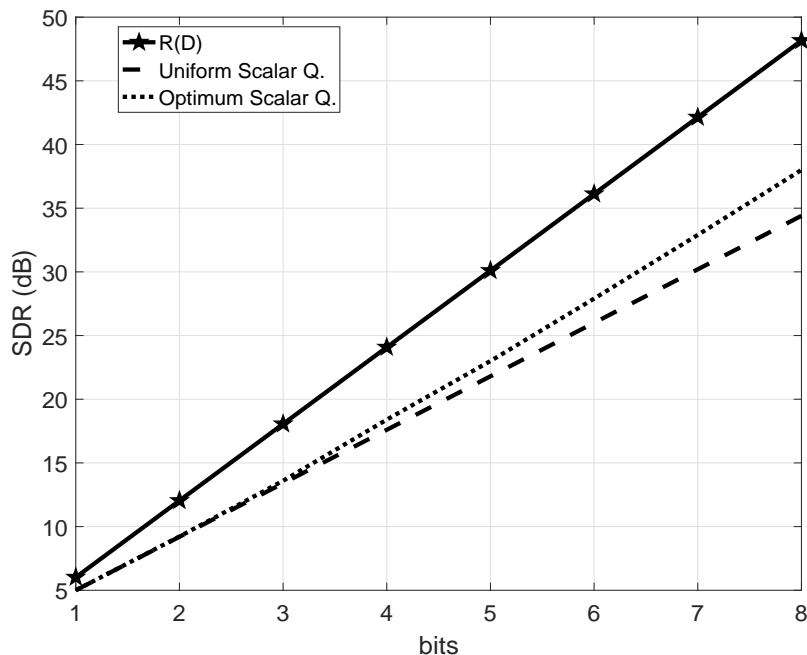


Figure 2.6: SDR as a function of the compression rate for uniform and optimal scalar quantization of i.i.d. Gaussian samples.

limit gets larger. An interesting observation is that if everything in the system is designed optimally and an optimal scalar quantizer (but not the optimal VQ) is used, then the system operates 3 dB away from  $R(D)$  if, for example, the quantizer has a bit of rate of 2.

### 2.3.2 Channel Capacity

Channel Capacity is a term first coined by Claude Shannon in the paper that founded the era of digital communications [1]. Prior to Shannon, telecommunication engineers relied on analog communications techniques such as AM, FM and their variants. It was a held belief that to improve the fidelity of the transmitted signal, one had to increase the operating power or sacrifice bandwidth. In his seminal paper, Shannon showed that error free communications at a finite power and finite bandwidth with an information rate  $R$  is feasible, as long as such rate was below a fundamental parameter of the channel, called channel capacity.

For an AWGN channel, with an average power constraint of  $P$ , and noise variance  $\sigma_n^2$ , it is easy to show that the capacity is given by [40]

$$C(P) = \frac{1}{2} \log_2 \left( 1 + \frac{P}{\sigma_n^2} \right) \text{ bits.} \quad (2.4)$$

### 2.3.3 Optimal Performance Theoretically Attainable

The Optimal Performance Theoretically Attainable (OPTA) connects source and channel coding to form a complete end-to-end characterization of the system performance. Assume  $M$  source symbols are to be communicated over an AWGN channel, under an average power constraint  $P$ . We can use the channel  $N$  times to convey our  $M$  source symbols. The question to be answered is: What is the best signal fidelity,  $D$ , that the system can achieve? The answer is provided by the equation

$$MR(D) \leq NC(P), \quad (2.5)$$

where  $C(P)$  is the capacity of the channel and  $R(D)$  is the rate distortion function of the source. If we further assume that we wish to transmit a Gaussian Source  $S$  with zero mean and variance  $\sigma_s^2$ , that is  $S \sim N(0, \sigma_s^2)$  over an AWGN channel with noise variance  $\sigma_n^2$  and using an average power of  $P$  to communicate, then (2.5) reduces to

$$\frac{M}{2} \log \frac{\sigma_s^2}{D} \leq \frac{N}{2} \log \left( 1 + \frac{P}{\sigma_n^2} \right) \quad (2.6)$$

Equation (2.6) defines a region where communication is feasible. A system operating at the boundary (when equality is achieved in (2.6)) of this region is optimal and we typically say that the system achieves the OPTA. Replacing  $\leq$  with equality, and massaging (2.6) yields

$$\text{SDR}_{OPTA} = \left( 1 + \text{SNR}_{OPTA} \right)^{\frac{M}{N}}, \quad (2.7)$$

where SDR is the Signal to Distortion Ratio. Notice that we are seeking to minimize the distortion,  $D$ . SDR, on the other hand, is the inverse of  $D$ . Hence the larger the

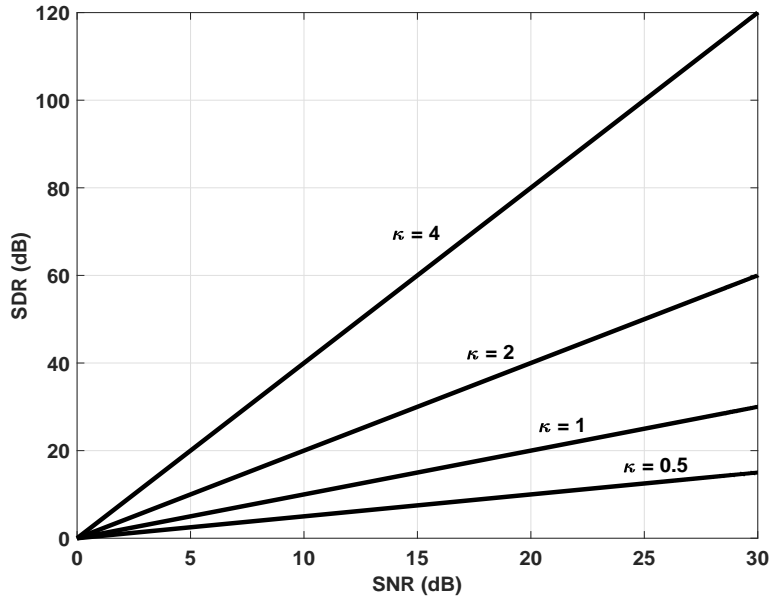


Figure 2.7: OPTA graph (in dB) for  $\kappa = 4, 2, 1, 0.5$  (top to bottom), when transmitting i.i.d Gaussian samples over AWGN channels

SDR, the closer the reconstructed source is to the original. Defining  $\kappa = \frac{M}{N}$  to be the channel use ratio, we have a bandwidth compression system if  $\kappa > 1$ . If  $\kappa < 1$ , we have a bandwidth expansion system, and  $\kappa = 1$  is the matched bandwidth case.

Converting (2.7) into the log domain and assuming that  $\log(1+x) \approx \log(x)$  for large  $x$ , yields

$$\text{SDR}_{OPTA} \text{ (dB)} \approx \kappa \text{SNR}_{OPTA} \text{ (dB)} \quad (2.8)$$

Notice, that  $\text{SDR}_{OPTA}$  (dB) is almost a linear function of the  $\text{SNR}_{OPTA}$  (dB), and the slope is determined by the channel expansion ratio.

So far we have discussed OPTA for the point-to-point AWGN channel when transmitting i.i.d Gaussian sources. Similar analysis can be performed for general correlated and distributed sources, such as the case for the Multiple Access Channel. We will address OPTA for general channels in the coming chapters.

## Chapter 3

### ANALOG JSCC FOR UNDERWATER COMMUNICATIONS

#### 3.1 Introduction

##### 3.1.1 Introduction to Underwater channels

Underwater communications is an old field that has many civilian and military applications. It is a challenging field for several reasons. First, communications via Electromagnetic (EM) waves is extremely difficult at sufficiently large distances (more than 1 Kilometer) because of immense attenuation [41], as Figure 3.1 shows. For example at a frequency of 100 kHz, the attenuation when communicating at a distance of 1 Km is about 8000 dB. This renders acoustic communications a very attractive feasible alternative to EM waves. Acoustic communications uses sound waves and the typical bandwidth is  $|0-50 \text{ kHz}|$ , much smaller than in typical wireless communication systems [42].

Traditional techniques developed in wireless communications to combat ISI and Doppler spread are generally not applicable here. For instance, Orthogonal Frequency Division Multiplexing (OFDM) assumes linearity of the channel response to effectively utilize the DFT. However in the underwater channel, as we will see shortly, the acoustic power amplifier is severely non-linear, making direct application of OFDM techniques infeasible [43].

In the remainder of this section, we introduce the space filling curves system used for the underwater acoustic channel, defining the model for the end-to-end channel that we will use in this chapter. In Section 3.2, we develop a theoretical analysis of a simplified version of the acoustic channel that does not incorporate the ISI, and postulate a bound for the end-to-end acoustic channel. Section 3.3 discusses different

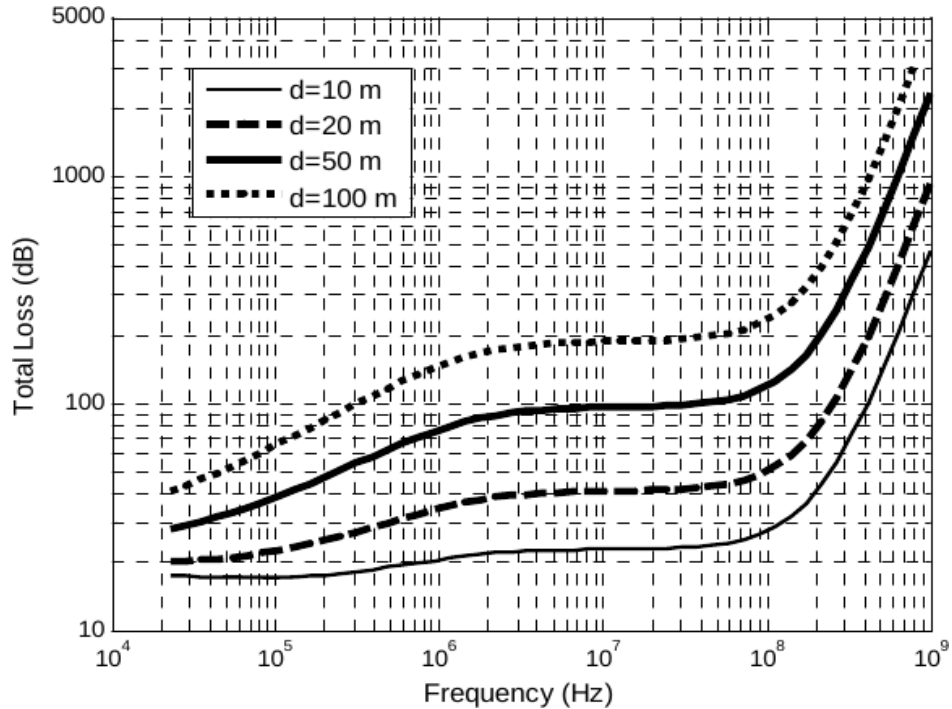


Figure 3.1: Propagation loss of electromagnetic waves in water as a function of the distance and frequency (taken from [44]).

power allocation methods necessary in obtaining the bound for the end-to-end acoustic channel. Section 3.4 focuses on designing an analog JSCC communication scheme suitable for the non-linear channels under consideration. Simulation results are presented in Section 4.5. Finally, Section 4.6 concludes the chapter.

### 3.1.2 Space Filling Curves

The encoding system used in this paper is based on the Shannon Kotelnikov mappings [35, 36]. In particular, we will utilize the Archimedean Spiral, discussed in Section 2.2.2 and studied in detail in [37].

The mapping function  $M_{\Delta}(x', y')$  takes any source pair  $(x', y')$  and projects it to the closest point on the spiral, that is

$$\hat{\theta} = M_{\Delta}(x', y') = \arg \min_{\theta} \left\{ \left( x' \pm \frac{\Delta}{\pi} \theta \sin \theta \right)^2 + \left( y' - \frac{\Delta}{\pi} \theta \cos \theta \right)^2 \right\}. \quad (3.1)$$

Then,  $\hat{\theta}$  is processed by the function  $T_\alpha(\hat{\theta}) = \hat{\theta}^\alpha$ . Both parameters  $(\Delta, \alpha)$  are optimized according to the channel signal to noise ratio,  $CSNR$ <sup>1</sup>[38]. The system diagram of the encoder is depicted in Figure 3.2.

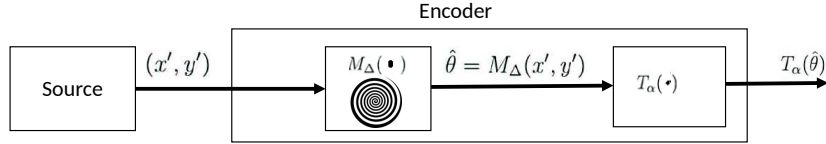


Figure 3.2: System diagram of an encoder based on the 2:1 Archimedean spiral.

### 3.1.3 Overall Channel Model

The complete system diagram of the end-to-end underwater acoustic channel studied here is shown in Figure 3.3. As shown in the figure, the first channel block is the transmit non-linear power amplifier, with gain  $g$  in the linear region, which exhibits saturation effects at the extremes and also near the origin. Then, the output of the amplifier is sent through the underwater channel, which presents ISI<sup>2</sup> and introduces attenuation,  $\gamma_d$ , which depends on the distance,  $d$ , between the transmitter and the receiver. The receiver introduces zero mean Gaussian noise,  $\mathbf{Z}$ , with fixed variance,  $\sigma_n^2$ , independent of the distance between the transmitter and receiver. Note that, as shown later, due to the non-linear nature of the system, the attenuation has to be considered in its own right and can not be absorbed into the noise variance. Table 3.1 summarizes the specific system parameters obtained from real measurements in [46].

---

<sup>1</sup>  $CSNR$  will be formally defined later in (3.2).

<sup>2</sup> The specific Channel Impulse Response (CIR) shown in Figure 3.3 was obtained by actual measurements of the underwater acoustic channels considered in [46]. The CIR for underwater channels is dynamic and changes during the course of the day with temperature, salinity, water speed, and other factors. In this paper, we only consider one realization of the CIR as shown in Figure 3.3.

We will use these parameters throughout the chapter. We define the Channel Signal to Noise Ratio,  $CSNR$ , as measured at the *receiver* side, as

$$CSNR = \frac{P \times \gamma_d}{\sigma_n^2}, \quad (3.2)$$

where  $P$  is the transmitted power.

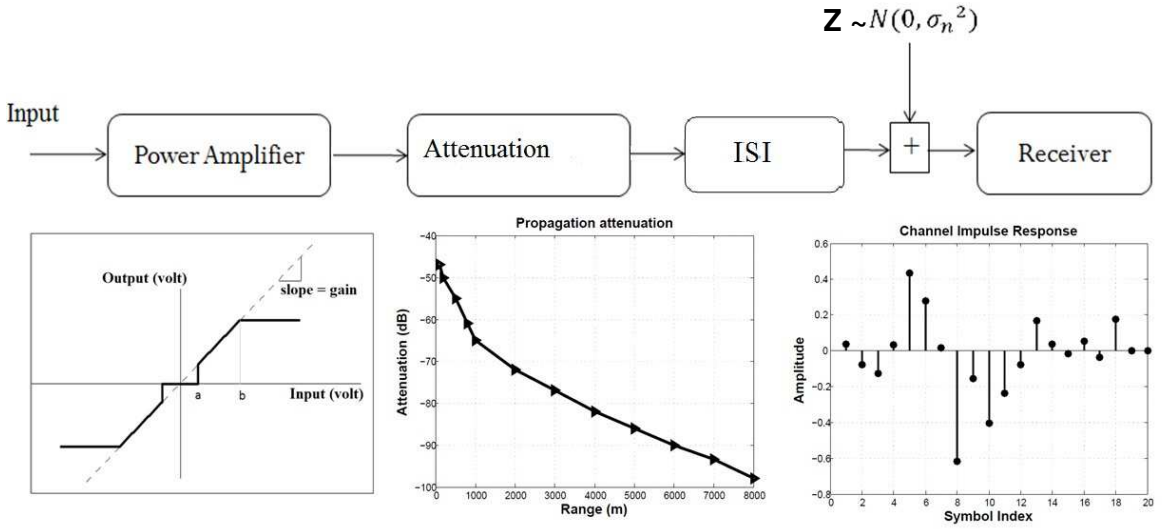


Figure 3.3: End-to-end channel model including the non-linear amplifier transfer function at the transmitter, the attenuation profile and the impulse response of the ISI channel.

Table 3.1: Specific system parameters obtained from [46]

$a$ (amplifier low cutoff)	$b$ (amplifier high cutoff)	$g$ (amplifier gain)	$\sigma_n^2$ (noise variance)
2	20	$\frac{1}{20} \sqrt{2 \cdot 10^{19}}$	$10^{8.87}$ (87.7 dBm)

We will first derive the theoretical limits for a simplified non-linear channel which does not consider the ISI. We will later study the end-to-end channel comprising the non-linear amplifier as well as the ISI channel.

## 3.2 Theoretical Analysis

### 3.2.1 Simplified Non-linear Channel (No ISI)

In this section we will first consider the simplified non-linear channel (*without* the ISI). We calculate the capacity of this continuous-amplitude non-linear channel using a modified version of the Blahut-Arimoto algorithm, which was originally designed for a discrete channel with a finite number of inputs [47], but can be extended to continuous-amplitude channels. The channel capacity  $C$  is defined as  $C = \max_{p(x)} I(X; Y)$ , where  $I(X; Y)$  is the mutual information between  $X$ , the input alphabet to the channel, and  $Y$ , the output alphabet. The maximization is performed over all probability mass functions  $p(x)$  of the input. Notice that the capacity can be rewritten as [40]

$$C = \max_{q(x|y)} \max_{r(x)} \sum_{x,y} r(x)p(y|x) \log \left( \frac{q(x|y)}{r(x)} \right), \quad (3.3)$$

where  $r(x)$  is chosen to minimize  $D(p(y)q(x|y) || p(y)r(x))$ ,  $D(\cdot || \cdot)$  is the relative entropy between two probability distributions, and  $p(y|x)$  is the conditional probability of  $y$  given  $x$ . Similarly,  $q(x|y)$  is the conditional probability of  $x$  given  $y$ .

The Blahut-Arimoto algorithm proceeds in an iterative manner searching over two spaces, the space of pdfs  $r(x)$  and the space of pdfs  $q(x|y)$ . The algorithm starts with an initial  $r(x)$  and calculates  $q(x|y)$ , then recalculates  $r(x)$  using  $q(x|y)$  and keeps alternating the calculation between  $r(x)$  and  $q(x|y)$ . Since for a fixed  $r(x)$  (3.3) is convex in  $q(x|y)$ , and for a fixed  $q(x|y)$  (3.3) is also convex in  $r(x)$  [40], it is easy to show that this algorithm converges to the global maximum [48]. The algorithm derives simple upper and lower bounds on the mutual information obtained at each iteration, and it stops once the upper and lower bounds are within the tolerance specified (for example 0.001 information bits).

The Blahut-Arimoto algorithm can take into account constraints imposed on the input distribution of  $X$ . Let  $f_1, f_2, \dots, f_n$  be functions defined on  $X$  and let the constraints be defined as  $f_i(X) \leq K_i$ ,  $i = 1, 2, \dots, n$ . Then, the second maximization in (3.3) becomes  $\max_{r(x)}(\cdot)$  such that  $r(x)$  satisfies each one of the constraints,  $f_i$ .

In our specific system we have two constraints. First the amplitude constraint, due to the non-linear nature of the transmit amplifier, is given by  $f_1(X) = \int B(x)f_X(x)dx \leq \omega$ , where  $f_X(x)$  is the pdf of  $X$ ,  $\omega$  is any positive real number different from  $\infty$ , and  $B(x)$  is defined as

$$B(x) = \left\{ \begin{array}{ll} \infty & \text{when } |x| > b \\ \infty & \text{when } |x| < a \text{ except at } x = 0. \\ 0 & \text{otherwise} \end{array} \right\}.$$

The second constraint is for the transmitted power,  $P$ , and is given by  $f_2(X) = E(X^2) = \int x^2 f_X(x)dx \leq P$ , where  $E(\cdot)$  is the expected value operator and  $P$  is the average transmitted power per channel use.

The Blahut-Arimoto algorithm can be extended to continuous channels [49]. The main idea is to discretize the continuous input/output alphabet and then apply the algorithm on the discrete ‘‘samples’’ of the original continuous pdfs. It is known that for amplitude constrained Gaussian channels the capacity achieving distribution is discrete. This was proved in [50] and discussed through simulations in [51]. However, the Blahut-Arimoto algorithm converges rather slowly since the complexity is  $O(|X|^3)$ , where  $|X|$  is the cardinality of the input alphabet symbols, and our channel is continuous and has to be finely sampled to guarantee convergence [49]. If the stopping criteria is relaxed to 0.1 bits, the algorithm converges much faster and the distribution obtained is at most 0.1 information bits away from the actual (discrete) capacity achieving distribution.

For a communication range of  $d$ , an average transmission power of  $P$  and receiver noise variance of  $\sigma_{n^2}$ <sup>3</sup>, the Blahut-Arimoto algorithm allows us to calculate the capacity,  $C_d(\frac{P}{\sigma_{n^2}})$ , as well as the capacity achieving distribution of the simplified channel. Figure 3.4 depicts the capacity achieving distribution (within 0.1 information bits accuracy) for two different values of CSNRs when the separation between the transmitter and receiver,  $d$ , is 2 Km, and the non-linear amplifier is defined as in Table 3.1.

Notice that for  $x = 0$  there is no signal in the saturated regions ( $|x| > b$  or

---

<sup>3</sup>  $\sigma_{n^2}$  is fixed for our system

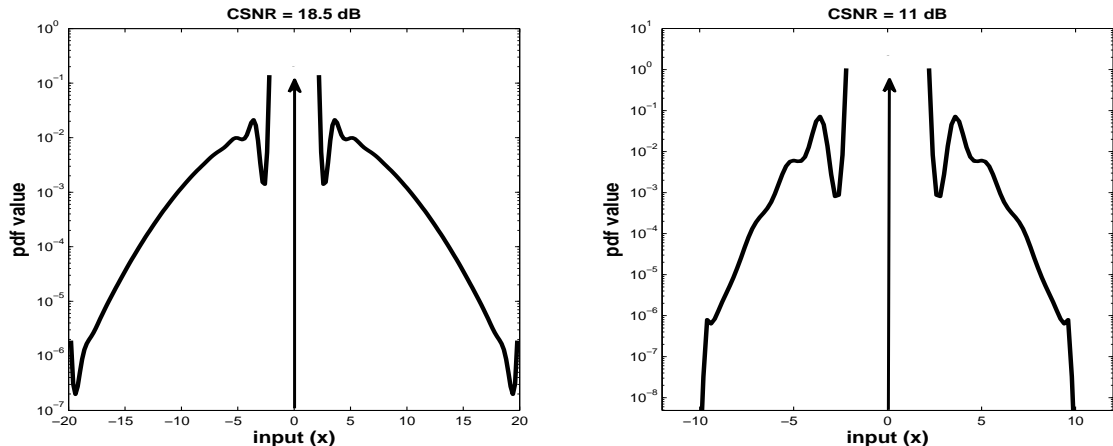


Figure 3.4: Capacity achieving distribution for the simplified channel when the separation between the transmitter and receiver,  $d$ , is 2 Km. CSNR = 18.5 dB (left) and 11 dB (right).

$x < a$ ), reflecting our first constraint that inputs in these regions lead to a waste of energy. It is interesting to note that the fraction of symbols that get mapped to zero depends on the CSNR under consideration: The less power available, the more zeros are transmitted. The shape of the pdf in the linear region ( $a < |x| < b$ ) also depends on the CSNR, getting narrower as the CSNR decreases. Figure 3.5 shows the capacity, obtained by the Blahut-Arimoto algorithm, of the simplified non-linear channel when  $d = 1$  Km.

### 3.2.2 End-to-end Channel (with ISI)

For the case of the end-to-end channel in which, in addition to the non-linearity, ISI is considered, calculating the capacity via the Blahut-Arimoto algorithm is not feasible, since this algorithm only works for memoryless channels<sup>4</sup>. A possible approach to calculate the capacity of the end-to-end channel would be to develop an end-to-end channel model (e.g. a hidden Markov Model) and calculate the capacity of this model. In this way, we would get rid of the growing exponential complexity of the problem in  $n$ . However, developing good models is not an easy endeavor and we will not pursue this

---

<sup>4</sup> We could consider a block channel of length  $n$  as the input to the algorithm, and let  $n \rightarrow \infty$ . However, this solution is intractable and has exponential complexity in  $n$ .

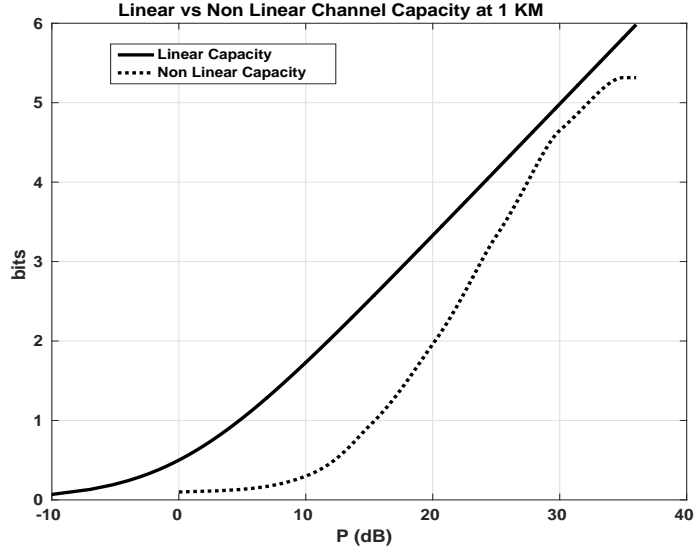


Figure 3.5: Capacity of the AWGN linear channel, and the simplified non-linear channel obtained using the Blahut-Arimoto algorithm.

path in this paper. Rather, we focus on obtaining an approximation to bound the end-to-end channel capacity as explained below. In order to obtain the approximation, we introduce a set of parallel channels  $\mathbf{X}^N = \{\mathbf{X}_1, \mathbf{X}_2 \dots \mathbf{X}_k\}$  as depicted in Figure 3.6, where  $\mathbf{X}_i$  and  $\mathbf{Y}_i$  are the sequences corresponding to the  $i$ -th frequency band of  $\mathbf{X}$  and  $\mathbf{Y}$ , respectively. Specifically:  $\mathbf{X}_i = F^{-1}\{\Pi_i F\{\mathbf{X}\}\}$  and  $\mathbf{Y}_i = F^{-1}\{\Pi_i F\{\mathbf{Y}\}\}$ , where  $\Pi_i$  is an ideal bandpass filter, and  $F$  and  $F^{-1}$  are the Fourier Transform and Inverse Fourier Transform, respectively. We assume that each sub-channel has a flat frequency response of  $H_i$ , which approximates the original end-to-end channel frequency response,  $\mathbf{H}$ , at that particular frequency band. The fidelity of the approximation improves as the number of sub-channels  $N$  increases<sup>5</sup>.

Consider now the transmission of  $\mathbf{X} = [\mathbf{X}_1 \dots \mathbf{X}_N]$  through the system in Figure 3.6 in such a way that the system is used  $N$  times, and at each time  $i$ , the  $i^{\text{th}}$  frequency component of  $\mathbf{X}$ ,  $\mathbf{X}^i = [\mathbf{0} \ \mathbf{X}_i \ \dots \ \mathbf{0}]$ , is transmitted so that

$$\mathbf{Y}_i = f_i(\mathbf{X}_i) + \mathbf{Z}_i, \quad (3.4)$$

---

<sup>5</sup> In the limit as  $N \rightarrow \infty$ , the formulation is exact.

where  $f_i$  is a non-linear function that depends on the parameters of the end-to-end channel. We postulate that the capacity of this scheme<sup>6</sup>,  $C_B$ , is higher than the capacity of the original end-to-end channel, and more specifically that an upper bound of the capacity of the end-to-end channel can be obtained as

$$C_B = \sum_{i=1}^N C_d\left(\frac{P_i \gamma_d |H_i|^2}{\sigma_n^2}\right), \quad (3.5)$$

so that each sub-channel in (3.4) has power  $P_i$  ( $\sum_i P_i = P$ , where  $P$  is the transmission power of the end-to-end channel) and experiences a frequency response of  $H_i$ . This brings us to the question of optimal power allocation amongst the  $N$  parallel channels to maximize  $C_B = \sum_i C_d\left(\frac{|H_i|^2 \gamma_d P_i}{\sigma_n^2}\right)$ , where  $C_d(\cdot)$  is the capacity of the simplified non-linear channel (without ISI), calculated using the Blahut-Arimoto algorithm as explained in Section 3.2.1.

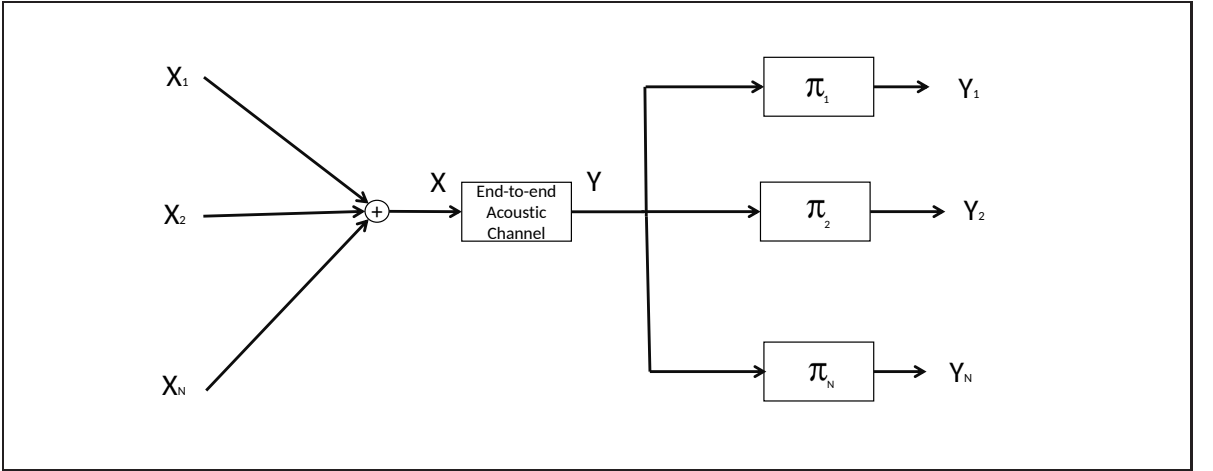


Figure 3.6: System used to postulate a bound for the capacity of the end-to-end underwater channel.

---

<sup>6</sup> Notice that if  $\mathbf{X} = [\mathbf{X}_1 \cdots \mathbf{X}_N]$  is transmitted, the channel non-linearity would induce leakage between inputs  $X_j$  and outputs  $Y_k$ , for  $j \neq k$ . Intuitively, this would lead to performance degradation.

### 3.3 Power Allocation for the End-to-end Channel

#### 3.3.1 Optimal Power Allocation Scheme for $C_B$

We can obtain the optimal power allocation,  $P$ , that maximizes  $C_B = \sum_i C_d(\frac{|H_i|^2 \gamma_d P_i}{\sigma_n^2})$  by using Lagrange multipliers. First, we form the functional

$$J(P_1, P_2 \dots, P_k) = \sum C_d(\frac{P_i \gamma_d |H_i|^2}{\sigma_n^2}) + \lambda(\sum P_i). \quad (3.6)$$

In order to obtain the optimal power allocation, we differentiate w.r.t  $P_i$  in (3.6) and set the result to zero to obtain

$$\frac{\gamma_d |H_i|^2}{\sigma_n^2} C'_d(\frac{P_i \gamma_d |H_i|^2}{\sigma_n^2}) = -\lambda = \text{constant}. \quad (3.7)$$

The constant  $\lambda$  acts as a parameter that needs to be adjusted to satisfy the total power constraint of the channel. This can be thought of as a necessary condition to achieve optimality, but it does not give us direct computational steps to come up with the optimal power allocation. Next, we develop an iterative algorithm that aims at finding the optimal power allocation for (3.6). The algorithm starts by choosing a random power allocation  $(P_1^1, \dots, P_N^1)$ , where the superscript denotes iteration number, such that  $\sum_i P_i^j = P$ . After each iteration  $j$ , we evaluate

$$\begin{aligned} \lambda_i^j &= \frac{\gamma_d |H_i|^2}{\sigma_n^2} C'_d(\frac{P_i^j \gamma_d |H_i|^2}{\sigma_n^2}) \\ \hat{\lambda}_i^j &= \lambda_i^j - \sum_{i=1}^N \frac{\lambda_i^j}{N}. \end{aligned} \quad (3.8)$$

$\hat{\lambda}_i^j$  in (3.8) is the deviation from the mean for sub-channel  $i$  at iteration  $j$ . From (3.7), we know that the optimal power allocation would make all  $\lambda_i^j$ 's equal to a constant number. We then use a strategy based on  $\hat{\lambda}_i^j$  to adjust the power at the next iteration. A simple strategy would change the power for each sub-channel  $i$ , by a constant amount

$(\Delta P)$ , depending on the sign of  $\hat{\lambda}_i^j$ , i.e.,

$$P_i^{j+1} = c_i^j \times (P_i^j - \Delta P \text{sign}(\hat{\lambda}_i^j))^{\oplus}, \quad (3.9)$$

where  $(\oplus)$  forces the power to lie between the power amplifier limits,  $[a^2, b^2]$  and is given by

$$(x)^{\oplus} = \begin{cases} a^2 & x < a^2 \\ x & a^2 < x < b^2 \\ b^2 & x > b^2 \end{cases}. \quad (3.10)$$

The term  $c_i^j$  in (3.9) is a normalization parameter to ensure that the power constraint  $\sum P_i = P$  is met in each iteration. We run this algorithm for a fixed large number of iterations or until the difference in the objective function between two successive iterations is below a desired tolerance  $\Delta C$ . For faster convergence, we could adopt more elaborate strategies, such as making the increment/decrement in power,  $\Delta P_i$ , vary depending on how divergent from the mean  $\hat{\lambda}_i^j$  is. It is interesting to note that the above algorithm is a variant of gradient descent, and we see in Appendix A that the function  $C_B = \sum_i C_d(\frac{|H_i|^2 \gamma_d P_i}{\sigma_{n^2}^i})$  is concave and does indeed have a global maximum which can be reached by gradient descent.

Note that the larger the number of channels  $N$ , the better approximation to the original channel. We have run the above algorithm for  $N = 512, 1024, 2048, 4096$  and found out empirically that  $N = 1024$  gives a fairly accurate approximation of the channel (further increases do not change the results up to four significant digits). Hence  $N$  will be chosen as 1024 in the sequel. Figure 3.7 shows the value of  $C_B = \sum_i C_d(\frac{|H_i|^2 \gamma_d P_i}{\sigma_{n^2}^i})$  for the end-to-end non-linear ISI channel using the aforementioned power allocation technique for a communication distance of 0.5, 1, 2 and 4 Km.

### 3.3.2 Heuristic Power Allocation Scheme for $C_B$

We now describe a much simpler heuristic algorithm for power allocation, which is a modified version of the water filling solution. The water filling solution is the

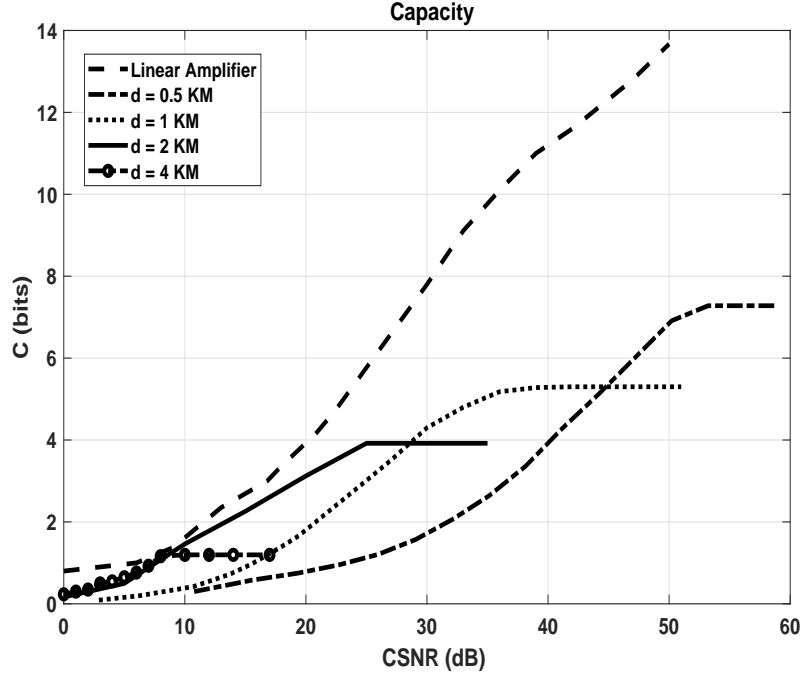


Figure 3.7: Value of  $C_B = \sum_i C_d(\frac{|H_i|^2 \gamma_d P_i}{\sigma_n^2})$  for the end-to-end non-linear channel for  $d = 0.5, 1, 2$  and  $4$  Km. The capacity of the same channel assuming an ideal linear amplifier is also shown.

technique used to obtain the optimal power allocation in the case of linear ISI channels [40]. The non-linear power amplifier has a zero response for any  $x$ , where  $|x| < a$ . Hence, it is not possible to have a non-zero information rate with a transmission power smaller than  $a^2$ . Moreover, the power amplifier has a maximum range of  $|b|$ , and no extra information can be communicated at  $P > b^2$ . Hence the Kuhn-Tucker conditions are modified<sup>7</sup> to be  $\sqrt{(x^2)^\oplus}$ , where  $\oplus$  was defined in (3.10). Interestingly, the results in (3.7) reflect that, since for  $P \cong b^2$ ,  $C_d(\cdot)$  plateaus and  $C'_d$  goes quickly to zero as shown in Figure 3.8. Accordingly the optimal strategy does not allocate any power when  $P > b^2$ . Figure 3.9 shows, for  $CSNR = 9.38$  dB and  $CSNR = 22.1$  dB, the resulting power allocation when running the optimal algorithm and compares it with the power allocation using the heuristic water-filling-like simplified technique, when the distance between the transmitter and receiver,  $d$ , is 1 Km. It is interesting to note that the

<sup>7</sup> For linear channels, the condition is  $(x)^+ = \max(x, 0)$

gains from the optimal power allocation are 0.1 and 0.3 dB. The gain is particularly small when the overall transmission power is in the middle region of  $[a^2, b^2]$ . This can be explained by Figure 3.8, as in this case  $C'$  is almost identical for both the linear AWGN channel and the non linear end-to-end acoustic channel.

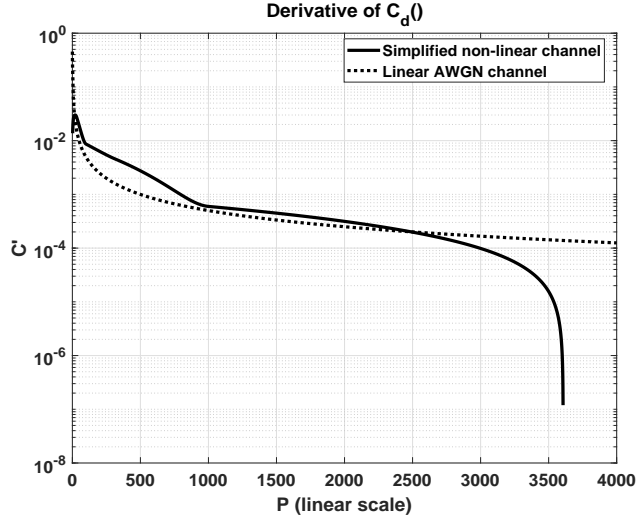


Figure 3.8: Rate of change,  $C'$ , for  $C_d(\frac{P\gamma_d}{\sigma_n^2})$  for the simplified non-linear channel and the AWGN channel for  $d = 1$  Km.

It is interesting to note that for the channel defined in Figure 3.3, the performance gain obtained by optimal power allocation (rather than simply uniform power allocation) is negligible, in particular at high SNRs. This observation holds for both the linear ISI channel and the non-linear end-to-end ISI channel. For example, for the case of 2 Km, the gain at  $CSNR = 4$  dB is just 0.4 dB for the non-linear end-to-end ISI channel, and only 0.06 dB for the linear ISI channel. The diminishing return of optimal water-filling allocation was reported in [52] for MIMO channels under different channel conditions.

We should note that the modified Kuhn-Tucker conditions, along with (3.7) might not be satisfiable for all  $P$ , in particular if  $P$  is too small or too large. This is not surprising given the shape of the power amplifier transfer function. As Figure 3.9 shows, using the heuristic power allocation scheme leads to minor losses in terms of

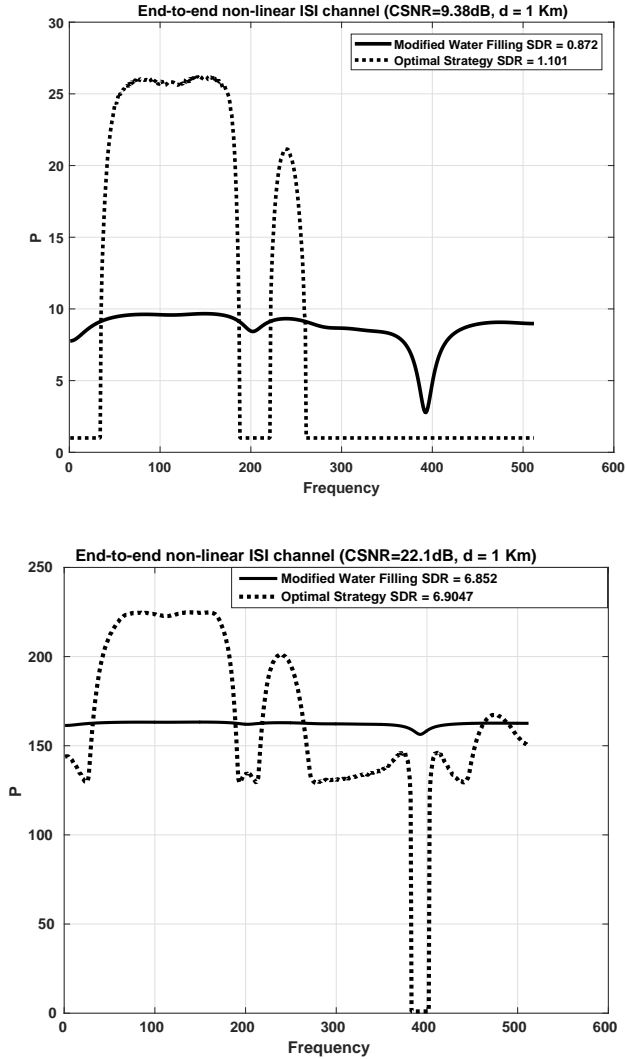


Figure 3.9: Optimal power allocation vs allocation obtained by the heuristic (modified water-filling-like) algorithm for the end-to-end non-linear ISI channel, when the communication distance is 1 Km, for CSNR = 9.3 and CSNR = 22.1 dB. The number of parallel channels is  $N = 1024$ .

performance, yet it does not require the iterative algorithm described earlier.

### 3.4 Proposed System

Given the non-linear characteristics of the channel, the direct use of the standard space-filling curves described in Section 3.1.2 will not lead to good performance. The reason is that standard curves allocate much of the energy in regions close to the origin, while the non-linear amplifier maps all data points  $x$  such that  $|x| < a$  (an

important fraction of the data, since we assume that the mean of the source is zero) to zero, and thus those points would suffer severe distortion. Hence, it is necessary to utilize novel transformations so that the channel input follows a distribution close to the capacity achieving distribution obtained in Section 3.2. We will do this by still utilizing standard space-filling curves, but changing the shape of the distribution by applying a Histogram Matching block, a novel transformation that matches the output of the space-filling encoder to the existing non-linearity.

Figure 3.10 shows the proposed encoder. We assume that the source emits zero-mean Gaussian i.i.d samples which are encoded by the 2:1 spiral mapping and the shaping function  $T_\alpha(\hat{\theta}) = \hat{\theta}^\alpha$ , as defined in Section 3.1.2. Then, the output is passed through a Histogram Matching block  $F(x)$ , which transforms the pdf of the input to match the channel statistics, aiming at obtaining a distribution for the channel input close to that discussed in Section 3.2 for the simplified channel. Finally, the output of the Histogram Matching block is passed through the non-linear amplifier and sent through the channel.

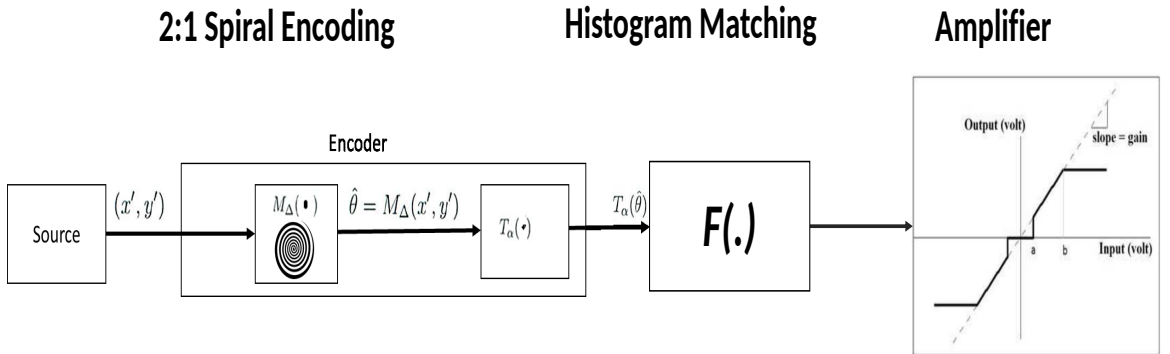


Figure 3.10: Overall system model of the transmitter.

It is important to remark that for the end-to-end channel we use the capacity achieving distribution of the simplified channel. The rationale is that we do not know the capacity achieving distribution of the end-to-end channel, but, intuitively, the non-linearity has a much more constraining effect on the capacity than the ISI (e.g., if the

information is transmitted in the saturated regions of the non-linear amplifier, most of it will be lost).

In order to implement the histogram matching block, we will use the well known fact that given an input pdf  $g(x)$  and a required output pdf  $h(x)$ , then the function  $F$  that transforms the pdf of the input from  $g(x)$  to  $h(x)$  is given by  $F(x) = H^{-1}(G(x))$ , where  $G(r) = \int_{-\infty}^r g(x)dx$  and  $H(r) = \int_{-\infty}^r h(x)dx$  are the Cumulative Distribution Functions of  $g(x)$  and  $h(x)$ , respectively. Following the discussion in Section 3.2, we postulate the following family of distributions as  $h(x)$

$$h(x) = \left\{ \begin{array}{ll} \epsilon_1 \delta(x) & x = 0 \\ c \cdot e^{-\frac{(x-a)^\beta}{2\sigma^2}} & a < x < b \\ c \cdot e^{-\frac{(x+a)^\beta}{2\sigma^2}} & -b < x < -a \\ \epsilon_2 \delta(|x| - b) & |x| = b \\ \epsilon_3 \delta(|x| - a) & |x| = a \\ 0 & \text{otherwise} \end{array} \right\}. \quad (3.11)$$

Notice that in addition to  $\Delta$  and  $\alpha$ , we have to optimize over five different parameters  $(\epsilon_1, \beta, \sigma, \epsilon_2, \epsilon_3)$  to obtain the distribution  $h(x)$  that achieves the highest SDR for a given CSNR ( $c$  is a normalization constant so that  $\int h(x)dx = 1$ , and  $\delta(\cdot)$  is the Dirac delta function). The first line in (3.11) reflects the fact that we have a degree of freedom to use at  $x = 0$ . Lines 2 and 3 describe the equation of a generalized Gaussian with mean  $a$  and  $-a$ , respectively, parameter  $\beta$  and variance  $\sigma^2$ . Lines 4 and 5 accommodate the possibility of a Dirac delta at the amplifier extremities. Line 6 reflects that we do not send any symbol in the saturated regions of the amplifier, as that would be a waste of energy for the transmitter. Figure 3.11 shows the histogram of the channel input obtained after we perform the optimization, as well as the histogram of the output of the space-filling curve, when the distance between the transmitter and receiver is 1 Km for CSNR = 27 dB.

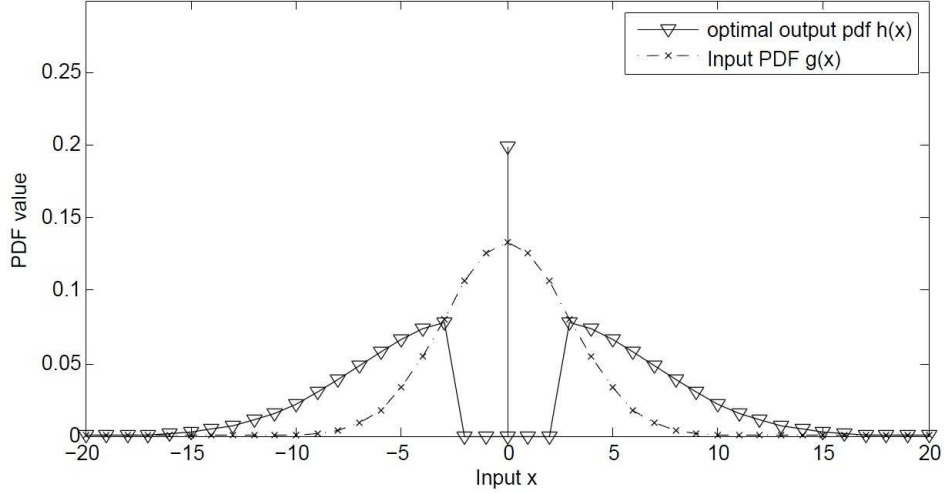


Figure 3.11: The histogram matching block modifies the distribution of the input data. The distance between transmitter and receiver is 1 Km, CSNR = 27 dB, and the optimized parameters are  $(\epsilon_1 = 0.2, \beta = 2, \sigma = 5, \epsilon_2 = 0, \epsilon_3 = 0)$ .

### 3.4.1 Decoder Structure

The decoder for the proposed system for the end-to-end channel is composed of two main components. First, an inner equalizer that deals with the ISI by performing MMSE detection. Then, an outer decoder that takes the estimate from the equalizer as input and performs ML decoding on the histogram matching block, followed by ML decoding of the 2:1 spiral mapping. This two stage decoder is similar to the one proposed for linear channels in [53], where it was shown to achieve excellent performance. Obviously, only the outer decoder is required if there is no ISI (simplified channel). Given the estimate,  $r$ , produced by the equalizer, the ML estimate at the outer decoder is obtained by first calculating

$$\hat{\theta}_{ML} = T_{\alpha}^{-1}\left(F^{-1}\left(\frac{r}{g \times \gamma_d}\right)\right), \quad (3.12)$$

where  $g$  is the amplifier gain and  $\gamma_d$  is the channel attenuation as defined in Figure 3.3,  $F$  is the transfer function of the histogram matching block defined earlier, and  $T_{\alpha}$  is defined in Figure 3.2. Then, we perform the inverse mapping on  $\hat{\theta}_{ML}$  to obtain the ML estimates of the original transmitted source pair  $(x', y')$ .

As inner equalizer, we consider a Time Domain Equalizer, performing either MMLS Linear Equalization (MMSE-LE) or MMSE Decision Feedback Equalization (MMSE-DFE). We assume that the channel impulse response and the noise variance are known at the receiver. Given the transmitted symbols  $\mathbf{x}_k$  and the received symbols  $\mathbf{d}_k$ , the Linear MMSE equalizer  $W$  is obtained as [54]

$$\hat{W}_{LE} = \arg \min_W E \|(\mathbf{x}_k - \mathbf{W}^H * \mathbf{d}_k)\|^2, \quad (3.13)$$

where  $*$  is the convolution operator. Then, the output of the equalizer,  $\mathbf{r}_k = \mathbf{W}^H * \mathbf{d}_k$ , is passed to the inner decoder discussed above.

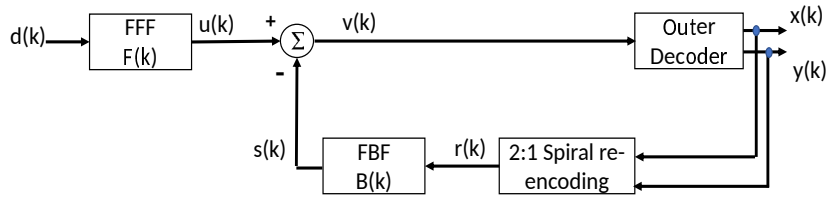


Figure 3.12: DFE structure

As shown in Figure 3.12, the DFE equalizer is composed of two filters: the Feed-Forward Filter (FFF) and the Feed-Back filter (FBF). The FFF removes the precursor ISI (i.e., the ISI before the transmitted symbol) and the FBF deals with the postcursor ISI. The DFE uses the previous symbol estimates  $r(k)$  and subtracts their effect from the current symbol  $u(k)$ . Note that in digital communication systems there is a threshold operation that is used to produce one of the (finite) symbols of the constellation. However, in the proposed discrete-time analog processing system, the number of possible points in the constellation is not finite, and the only possibility to obtain the source pair estimate  $(x, y)$  is to “clean” the estimate  $v(k)$ . This is done by utilizing the outer decoder block to obtain a source pair  $(x, y)$  from  $v(k)$ . Then we re-encode the pair  $(x, y)$  utilizing the spiral curve to obtain  $r(k)$ . The filters  $F, B$  are designed so as to minimize the MSE between the transmitted symbols  $\mathbf{x}_k$  and the input to the

outer decoder  $\mathbf{v}_k$  [54], i.e.,

$$\langle \hat{F}, \hat{B} \rangle_{MMSE} = \arg \min_{F, B} E \|\mathbf{x}_k - \mathbf{v}_k\|^2. \quad (3.14)$$

### 3.5 Simulation Results

In this section we first present simulation results for the simplified channel (i.e., no ISI). Then, we take the ISI into consideration and present the results for the end-to-end system. The benchmark we use to evaluate our system is the Optimum Performance Theoretically Attainable (OPTA), as defined in section 2.3.3.

#### 3.5.1 Simplified non-linear Channel (no ISI)

In this section we first present simulation results for the simplified non-linear channel (without considering the ISI). In our simulations we focus on the transmission of memoryless Gaussian sources using the proposed system specified in Section 3.4. We simulated the system for four different separation distances between the transmitter and receiver (0.5, 1, 2 and 4 Km), and for a wide range of CSNRs (0 to 60 dB). For each CSNR, we calculated the parameters defined in (2.2), (3.1) as well as (3.11) to optimize for the SDR, and corroborated, as shown in Figure 3.13, that for a wide range of CSNRs, the system achieves a performance very close to the OPTA (curve labeled “OPTA for the simplified non-linear channel”). In particular, the system is only 2 dB away from the OPTA for all ranges except for very high CSNRs, where it plateaus earlier than the OPTA. This pattern occurs independently of the separation distance between the transmitter and receiver, and is caused by the saturation at the extreme ends of the amplifier where  $|x| > b$  (see Figure 3.3). Thus, the maximum throughput supported by the simplified non-linear channel is bounded.

The OPTA for the AWGN channel (i.e. without the non-linear amplifier) is also depicted in Figure 3.13 for illustration purposes. As shown in the figures, when CSNR is not very high the gap between the OPTA for the AWGN channel and the OPTA for the simplified non-linear channel decreases as the CSNR increases, reflecting

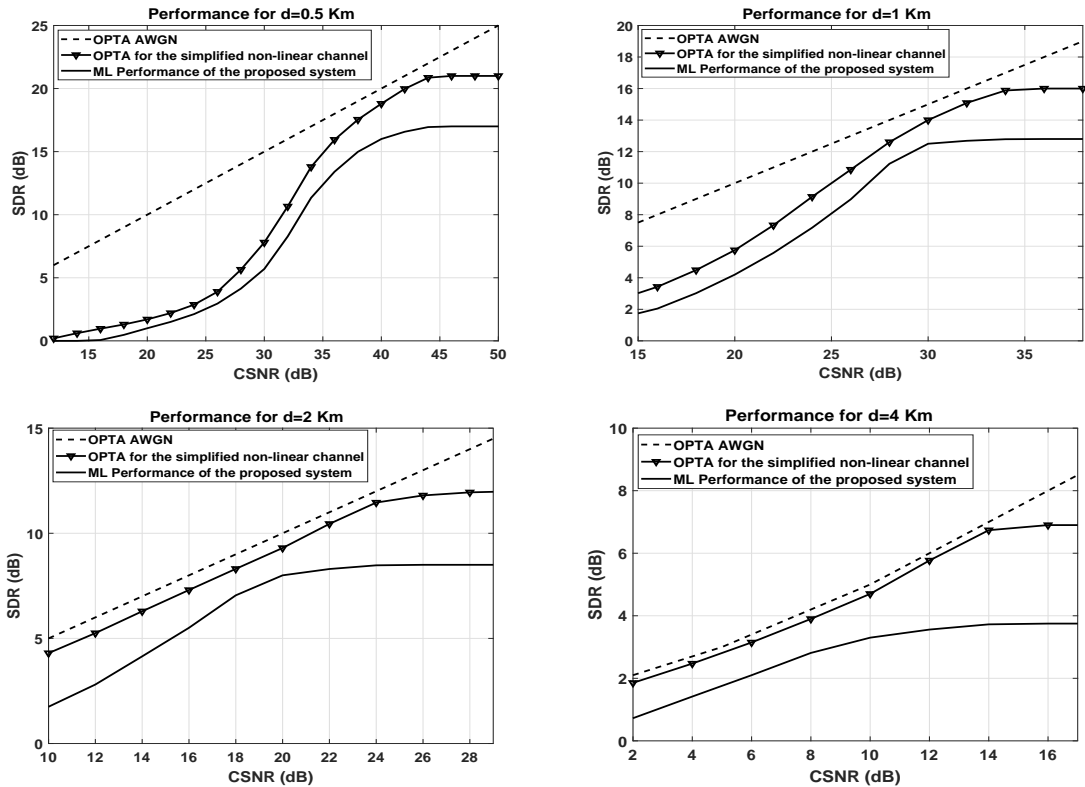


Figure 3.13: Simulation results for the simplified non-linear channel (no ISI) when the distance between the transmitter and receiver is 0.5, 1, 2 and 4 Km.

the fact that there is a strong non-linearity near zero which adversely affects the low CSNR regime. Notice, however, that as we increase the separation distance between the transmitter and receiver, the performance loss due to the non-linearity becomes less and less pronounced. The reason is that since the noise variance at the receiver is fixed, for a given CSNR the energy at the transmitter increases as the attenuation increases, and thus the region in the non-linear amplifier around 0 has less influence.

### 3.5.2 End-to-end non-linear ISI Channel

Figure 3.14 presents the results for the end-to-end channel (including ISI and non-linearity) defined in Figure 3.3. We designed the system as discussed in Section 3.4, for the simplified channel without ISI<sup>8</sup>. Then, we applied the resulting system to the end-to-end channel defined in Figure 3.3 and compared the results obtained

<sup>8</sup> As explained before, the main constraint in terms of end-to-end system performance is the non-linear amplifier. This means that the amplifier non-linearity is the main driving factor in system design.

using MMSE-LE equalization with those of an MMSE-DFE equalizer. The length of the MMSE-LE equalizer is 10 times the length of channel impulse response shown in Figure 3.3, which is also the length of the FFF in the MMSE-DFE equalizer. The length of the FBF is 18. The resulting performance when the distance between the transmitter and receiver is 0.5, 1, 2 and 4 Km is shown in Figure 3.14. Notice that the performance obtained with the DFE equalizer is a little bit better than that of the LE equalizer. In addition to these results, four bounds are also depicted in the figures: i) the theoretical bound (OPTA) for a pure AWGN channel, ii) the OPTA for the system in Figure 3.3 when only the ISI is considered (i.e., without considering the non-linearity), iii) the OPTA for the system in Figure 3.3 when only the non-linearity is considered (i.e., without considering the ISI), and iv) the postulated upper bound for the OPTA of the end-to-end non-linear ISI channel in Figure 3.3 (i.e., considering both the non-linearity and the ISI). It is important to remark that the postulated bound of the end-to-end system is very close to the OPTA considering only the non-linearity, and both are far away from the OPTA obtained when the non-linearity is not considered. This reaffirms the usefulness of designing the system for the simplified channel (i.e., considering only the non-linearity but not the ISI channel.)

### 3.6 Conclusion

We have extended the use of analog joint source-channel coding techniques based on spiral-like space filling curves to non-linear channels of the type encountered in underwater acoustic communications. We first considered the simplified case of non-linear channels with no ISI. Then we extended our approach to end-to-end underwater channels, incorporating the ISI and the amplifier non-linearity. For the simplified non-linear channel, the capacity is calculated extending the Blahut-Arimoto algorithm, while for the end-to-end channel we postulated a capacity bound. Optimal and suboptimal power allocation schemes were discussed. We concluded the paper by presenting simulation results for the complete communication system. The resulting performance was shown to be very close to the theoretical limits for a wide range of CSNRs and

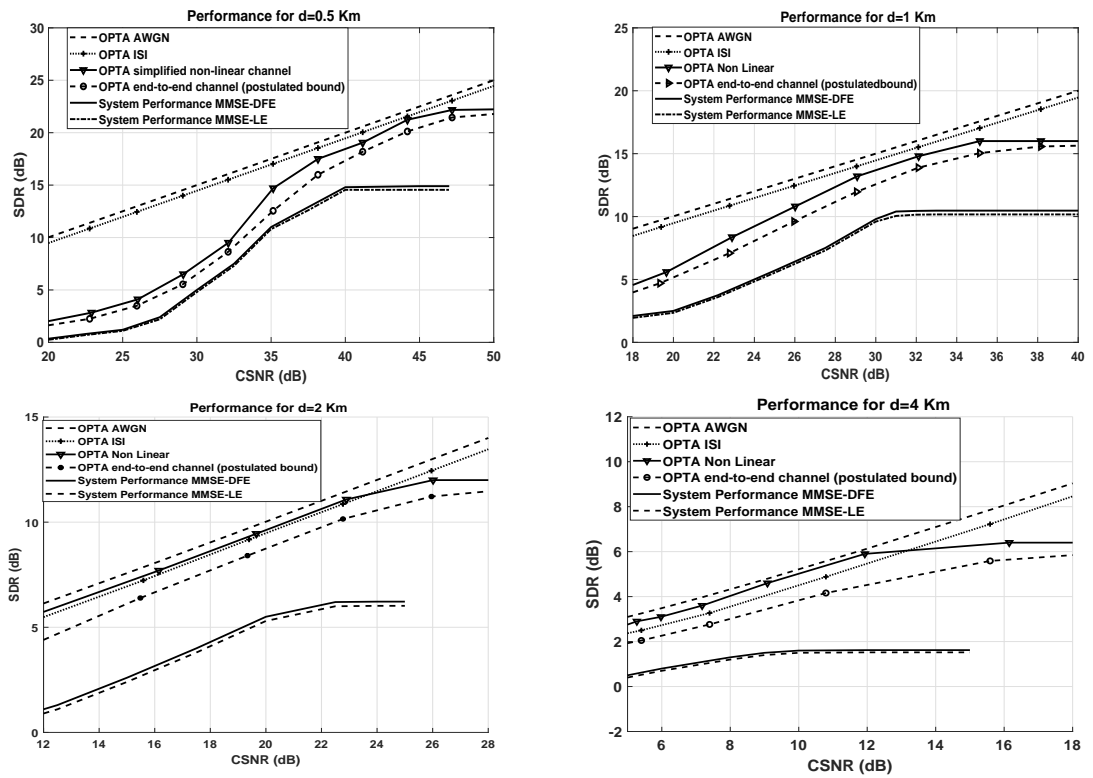


Figure 3.14: Simulation results for the end-to-end channel (including non-linearity and ISI). The distance between the transmitter and receiver is 0.5, 1, 2 and 4 Km and the ISI channel response is shown in Figure 3.3.

communication ranges.

## Chapter 4

### ANALOG JSCC FOR THE MULTIPLE ACCESS CHANNEL

So far we have discussed techniques of analog coding for the point to point channel. Multi-Network channels consist of one or more transmitters and one or more receivers as shown in Figure 4.1. Each transmitter  $i \in M$ , has a set of  $K_i$  sources or messages,  $S_{ik_j}$ , that have to be communicated to one or more receivers. Moreover, the transmitter seeks to guarantee a certain fidelity for each (message, receiver) pair. The sources being transmitted could in general be independent or correlated (amongst the same transmitter or across multiple transmitters). The channel transition function between the transmitters and receivers is also another variable in the characterization. The problem has many variables and neither the capacity region nor a general well-performing communication scheme is known.

This chapter discusses the application of analog JSCC systems to the Multiple Access Channel (MAC), where there are multiple transmitters wishing to communicate to a common receiver over a shared communication medium. Previous work on analog joint source-channel coding for the MAC has focused on the two user case and includes the work in [57], which extends the Nested Quantization digital technique proposed in [58] to transmitting Multi-variate Gaussian sources over the  $N$ -user MAC. A hybrid digital-analog scheme was proposed in [59] for the transmission of Bivariate Gaussian sources over the fading MAC. In [60, 61] the authors design an optimal mapping for transmitting Bivariate Gaussian sources over the MAC and other channels using variational methods. In this Chapter, we propose a novel hybrid digital analog scheme that combines an analog CDMA-like access scheme with traditional digital codes. Different from previous works, our scheme utilizes standard analog and digital mappings which are designed for point-to-point communications (such as space filling curves [2]

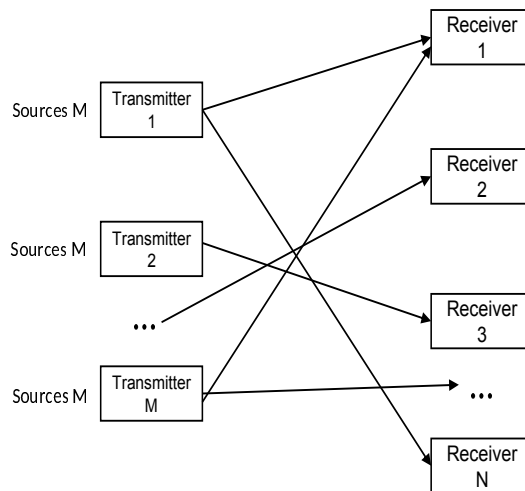


Figure 4.1: General multi-terminal network. Notice that each transmitter has a set of sources and that have to be communicated to a subset of the receivers with a given fidelity. The desired fidelity level could be different for each receiver.

and LDPC codes). The proposed hybrid scheme is suitable both for the symmetric and asymmetric distortions case (where each user in the MAC targets a different distortion), for different source-channel ratios, and for two or more users. The resulting performance is very close to the theoretical limits.

This chapter is organized as follows: Section 4.1 introduces the Multiple Access Channel and discusses the general communication techniques used. Section 4.2 first presents the analog component of the hybrid scheme: an orthogonal CDMA-like access scheme suitable for the transmission of analog JSCC systems. Analysis is performed and the optimality of the purely-analog scheme is proved for several cases of interest. Section 4.3 builds on Section 4.2 and presents the complete hybrid analog-digital scheme, particularizing the presentation for two users. We will then discuss extensions of the Hybrid scheme to more than two users in Section 4.4. In Section 4.5, we will present the simulation results for the case of two and three users, first considering the purely analog system, and then the complete hybrid analog-digital scheme. We

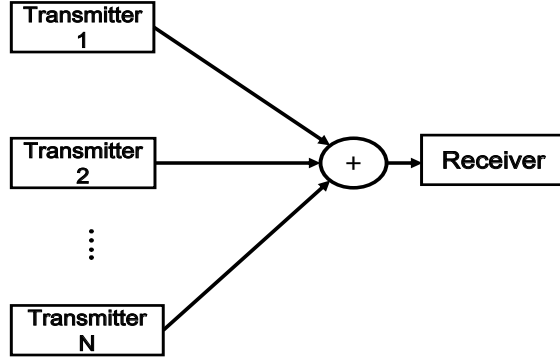


Figure 4.2: The Multiple Access Channel with  $N$  users.

will demonstrate the advantages of the hybrid scheme and show that it can achieve optimality for any point in the capacity region. Finally, Section 4.6 concludes the chapter.

#### 4.1 The Multiple Access Channel

The  $N$ -user Multiple Access Channel is a channel with  $N$  users, each wishing to transmit data to a common receiver as shown in Figure 4.2. A typical example of this channel is cell phones communicating to a common base station. This Chapter deals with the AWGN MAC, where each user  $i$  produces information  $X_i = [x_{i1} \ x_{i2} \ \cdots]$  from an alphabet  $\mathcal{X}_i$  and sends that over the channel under an average power constraint  $P_i$

$$\lim_{\Omega \rightarrow \infty} \frac{1}{\Omega} \sum_{j=0}^{\Omega} x_{ij}^2 \leq P_i \quad i = 1, 2, \dots, N \quad (4.1)$$

At the receiver, a noise with variance  $\sigma_n^2$  (without loss of generality, we assume  $\sigma_n^2 = 1$  in the sequel) is added to the received data, so that at time  $j$ , the receiver sees  $y_j = \sum_{i=1}^N x_{ij} + n_j$ . For such a channel, the maximum rate of communication is given by [40]

$$\sum_J R_i \leq \frac{1}{2} \log_2(1 + \sum_J P_i) \quad \forall i \in J, \quad \forall J \subset \mathcal{P}(\{1, 2, \dots, N\}), \quad (4.2)$$

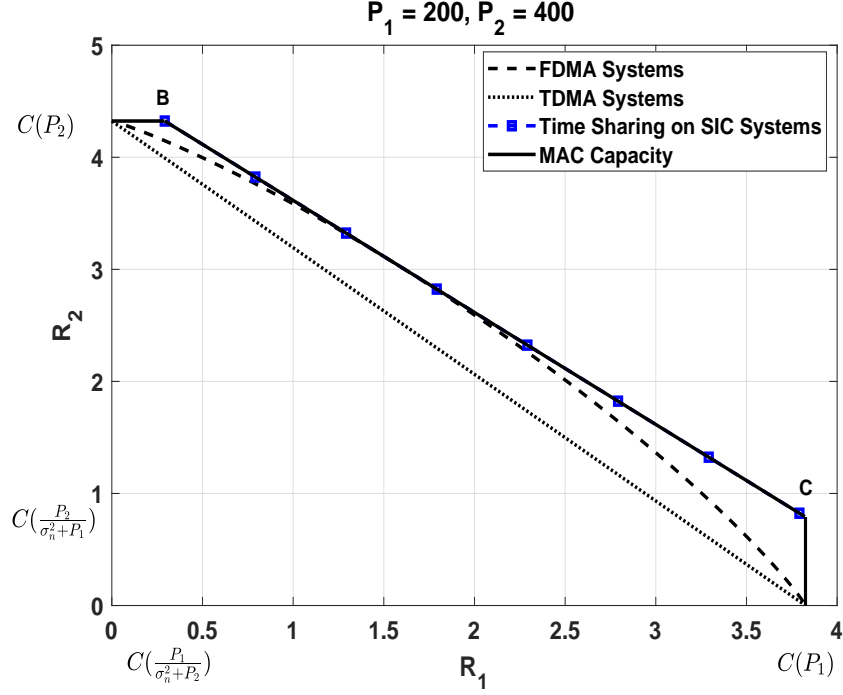


Figure 4.3: Capacity region for the 2-user AWGN Multiple Access Channel.

where  $\mathcal{P}(\cdot)$  is the power set [40].

Equation (4.2) defines a polyhedron in  $N$  dimensions, and each inequality in (4.2) defines an edge of the polyhedron. Figure 4.3 shows the capacity region for the two user case. The *maximum* sum rate is

$$\sum_{i=1}^N R_i \leq C_{MAC} = \frac{1}{2} \log_2 \left( 1 + \sum_{i=1}^N P_i \right). \quad (4.3)$$

Schemes used for communications over the MAC can be broken down into two main categories: Orthogonal schemes such as Time Division Multiple Access (TDMA), Frequency Division Multiple Access (FDMA), and Code Division Multiple Access (CDMA), and non-orthogonal schemes. Among the non-orthogonal schemes, we will discuss those that are commonly called Successive Interference Cancellation (SIC) schemes. SIC is being used in 5G systems under the name NOMA (Non-orthogonal Multiple Access) [62].

### 4.1.1 Orthogonal Schemes

TDMA is the most intuitive solution for the MAC. User  $i$  fully utilizes the channel and transmits for a fraction  $\lambda_i$  of the time, while the remaining  $N - 1$  users stay quiet, with  $\sum_{i=1}^N \lambda_i = 1$ . The TDMA achievable rates are

$$R_i = \lambda_i C_i, \quad (4.4)$$

$$C_i = \frac{1}{2} \log(1 + P_i). \quad (4.5)$$

In FDMA schemes, the two users share the channel degrees of freedoms by partitioning the channel into into  $N$  non over-lapping frequency sub-bands and letting each user use the allotted sub-band to send data. If user  $i$  is allocated  $\lambda_i 2\pi$  rads<sup>1</sup>, such that  $\sum_{i=1}^N \lambda_i = 1$  then the rate achieved by each user is given by

$$R_i = \lambda_i \log\left(1 + \frac{P_i}{\lambda_i}\right). \quad (4.6)$$

Figure 4.3 demonstrates Time and Frequency Division systems for the two user case ( $N = 2$ ). It is clear from Figure 4.3 that TMDA is optimal only at the two extrema of the Capacity region, while FDMA is also optimal at the point where the channel degrees of freedom are proportionally allocated to the users power, ( $\frac{\lambda_1}{\lambda_2} = \frac{P_1}{P_2}$ ) [40].

Unlike FDMA and TDMA, CDMA does not separate the users based on time or frequency, but on code. Similar to FDMA and TDMA, any two CDMA code-words are also orthogonal. The scheme we use here will be based on Direct Sequence (DS) CDMA, where an orthogonal matrix is chosen, such as the Walsh-Hadmark matrix<sup>2</sup>

---

<sup>1</sup> Note that since this is a discrete time system, we are dealing with units of rads and the full spectrum is contained to  $2\pi$  rads.

<sup>2</sup> Any Hermitian matrix can be used as a basis for CDMA, like the Fast Fourier Transform (FFT) and Discrete Cosine Transofrm (DCT).

which is defined recursively by

$$H_1 = [1] \quad (4.7)$$

$$H_{i+1} = \begin{bmatrix} H_i & H_i \\ -H_i & H_i \end{bmatrix} \quad \text{for } i = 2, 3, \dots \quad (4.8)$$

The matrix is Hermitian (Orthogonal), that is  $\mathbf{H}\mathbf{H}^T = \lambda\mathbf{I}$ , where  $\mathbf{I}$  is the identity matrix. In the absence of noise, this allows us to transmit and receive  $K$  symbols, where  $K$  is the cardinality of  $\mathbf{H}$ , over  $K$  time samples. Each symbol is modulated by a row of the matrix  $\mathbf{H}$ , and is reconstructed by a filter matched to the modulating code. In matrix notation, if the  $K$  symbols we wish to transmit are  $\mathbf{x}$ , the channel output over  $K$  time samples  $\mathbf{y}$ <sup>3</sup> is given by  $\mathbf{y} = \mathbf{H}\mathbf{x}$ . To reconstruct  $\mathbf{x}$ , we use the matched filter to  $\mathbf{H}$ , which in the absence of noise is  $\mathbf{G} = \mathbf{H}^{-1}$ , so that the reconstructed  $\hat{\mathbf{x}}$  is given by  $\hat{\mathbf{x}} = \mathbf{H}^{-1}\mathbf{y} = \mathbf{x}$ .

#### 4.1.2 Non-Orthogonal Schemes

Orthogonal schemes lack the ability to achieve any arbitrary point on the capacity region, as shown in Figure 4.3. On the other hand, SIC is able to achieve *any* point in the capacity region. For example, to achieve point  $B$  in Figure 4.3, user 1 sends information at the full rate  $R_1$  using a capacity achieving code. The decoder decodes the information treating the second source transmission as noise, hence the effective SNR is  $\frac{P_1}{\sigma_n^2 + P_2}$ <sup>4</sup>. Having decoded user 1 perfectly, the decoder re-encodes the data of user 1 using the code used by user 1 and *subtracts* (or *cancels*) that from the noisy received signal,  $y$ , effectively achieving an SNR of  $\frac{P_2}{\sigma_n^2}$  for the second user. The following equations summarize how to achieve point  $B$  in Figure 4.3.  $f_1, f_2$  are capacity

---

<sup>3</sup> Both  $\mathbf{x}$  and  $\mathbf{y}$  are  $K \times 1$  vectors

<sup>4</sup> This assumes that  $P_2$  follows a Gaussian distribution which indeed does when the capacity achieving distribution is used

achieving channel codes, and  $g_1, g_2$  are the corresponding decoders.

$$x_1 \xrightarrow[\text{designed for } \frac{P_1}{P_2 + \sigma_n^2}]{f_1(\cdot)} y_1 \quad \text{user 1 transmission} \quad (4.9)$$

$$x_2 \xrightarrow[\text{designed for } \frac{P_2}{\sigma_n^2}]{f_2(\cdot)} y_2 \quad \text{user 2 transmission} \quad (4.10)$$

$$z = y_1 + y_2 + n \quad \text{data at the receiver} \quad (4.11)$$

$$z = y_1 + \boxed{y_2 + n} \quad \text{User 1 treats } y_2 \text{ as noise and decodes} \quad (4.12)$$

$$\hat{x}_1 = g_1(z) = x_1 \quad \text{By the noisy channel coding theorem} \quad (4.13)$$

$$z^* = z - f_1(\hat{x}) = z - y_1 \quad (4.14)$$

$$z^* = y_2 + n \quad \text{User 2 decodes} \quad (4.15)$$

$$\hat{x}_2 = g_2(z^*) = x_2 \quad (4.16)$$

Similarly, point C in Figure 4.3 can be achieved by reversing the roles of users 1 and 2 in (4.9) above. Hence, these two SIC systems allow us to achieve the extreme points (B,C) on the capacity region. Time sharing can then be used on these two systems to achieve any point in the capacity outer bound, as shown in Figure 4.3. This demonstrates that there is a great advantage for SIC systems over orthogonal systems, namely the ability to achieve any point on the MAC capacity region, while orthogonal systems are only optimal for one point when the channel degrees of freedom are allocated in proportion to each user available transmission power. In practice, CDMA has advantages of its own, as it is robust against decoding errors. The reason is that if the decoding step fails in SIC systems for the digitally encoded data (or if there are decoding errors), the subsequent decoding steps will fail. This is particularly more pronounced for SIC systems with a large number of users (system generalizations for more than two users will be discussed in Section 4.4), where the probability of decoding failure increases. Moreover, CDMA systems are easier to encode and decode.

## 4.2 Proposed CDMA-like Access Scheme

In this section, we introduce the analog component of the proposed hybrid scheme. For the  $N$  users to transmit over the MAC, we propose the utilization of a  $K \times K$  orthogonal codebook,  $\mathbf{C}_{K \times K}$ , with  $K \geq N$ . To that end, we start off with an orthogonal matrix of size  $K$ , such as the Hadamard matrix, and assign  $m_i$  columns to user  $i$  so that  $\sum_{i=1}^N m_i = K$ . We then scale each user's columns by  $\eta_i = \frac{1}{\sqrt{m_i}}$ . The scaled columns assigned to user  $i$  are denoted by  $\underline{\mu}_1^i \ \underline{\mu}_2^i \ \cdots \ \underline{\mu}_{m_i}^i$ . As shown in (4.17), we group the columns assigned to user  $i$  into one submatrix denoted by  $\mathbf{C}_{K \times m_i} = [\underline{\mu}_1^i \ \underline{\mu}_2^i \ \cdots \ \underline{\mu}_{m_i}^i]$ , which is the access codebook that user  $i$  uses to send the data. Specifically,

$$\mathbf{C}_{K \times K} = [\mathbf{C}_{K \times m_1} | \mathbf{C}_{K \times m_2} \cdots | \mathbf{C}_{K \times m_N}],$$

with (4.17)

$$\begin{aligned} \mathbf{C}_{K \times m_i} &= [\underline{\mu}_1^i \ \underline{\mu}_2^i \ \cdots \ \underline{\mu}_{m_i}^i] \\ &= \begin{bmatrix} \underline{\mathbf{c}}_1^i \\ \underline{\mathbf{c}}_2^i \\ \vdots \\ \underline{\mathbf{c}}_K^i \end{bmatrix} = \begin{bmatrix} c_1^i(1) & c_1^i(2) & \cdots & c_1^i(m_i) \\ c_2^i(1) & c_2^i(2) & \cdots & c_2^i(m_i) \\ \vdots & \vdots & \cdots & \vdots \\ c_K^i(1) & c_K^i(2) & \cdots & c_K^i(m_i) \end{bmatrix} \end{aligned} \quad (4.18)$$

Figure 4.4: The codebook  $\mathbf{C}_{K \times K}$  is obtained by scaling the Hadamard matrix columns corresponding to user  $i$  by the factor  $\eta_i = \frac{1}{\sqrt{m_i}}$ . The  $K \times K$  access codebook is partitioned into  $N$  sub matrices,  $\mathbf{C}_{K \times m_i}$  with  $1 \leq i \leq N$ , where  $\mathbf{C}_{K \times m_i}$  is the access code for user  $i$ .

In the proposed scheme, each user makes use of  $K$  time intervals (with  $K \geq N$ ) to send its information. The data user  $i$  transmits over this time frame is  $\underline{\mathbf{x}}^i = [x_1^i \ x_2^i \ \cdots \ x_{m_i}^i]$ . Note that in general different users may have different channel data rates  $\frac{m_i}{K}$ . At time  $1 \leq k \leq K$ , user  $i$  utilizes code  $\underline{\mathbf{c}}_k^i = [c_k^i(1) \ c_k^i(2) \ \cdots \ c_k^i(m_i)]$ , the  $k^{th}$  row of  $\mathbf{C}_{K \times m_i}$ , and

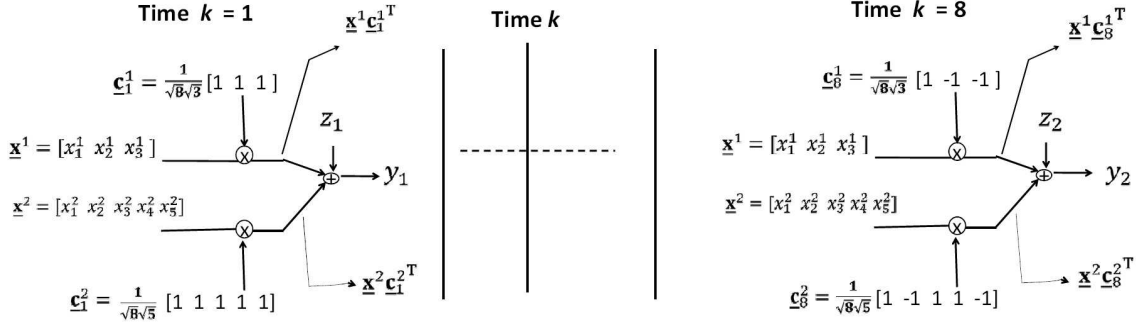


Figure 4.5: Proposed scheme for two users ( $N = 2$ ) with  $K = 8$ ,  $m_1 = 3$  and  $m_2 = 5$ . The upper branch corresponds to user 1 and the lower to user 2. Note the data of each user  $x_j^i$  is fixed for all the signaling times  $1 \leq k \leq 8$ .

transmits  $\underline{\mathbf{x}}^i \mathbf{c}_k^i \mathbf{T}$ , so that the received signal  $\underline{\mathbf{y}} = [y_1 \ y_2 \ \cdots \ y_K]$  is given by

$$y_k = \sum_{i=1}^N \underline{\mathbf{x}}^i \mathbf{c}_k^i \mathbf{T} + z_k = \sum_{i=1}^N \sum_{j=1}^{m_i} x_j^i c_k^i(j) + z_k, \quad 1 \leq k \leq K. \quad (4.19)$$

As noted before, the data to be sent by user  $i$ ,  $\underline{\mathbf{x}}^i$ , is *repeated* during the  $K$  signaling times. Therefore, the overall power received by each user is  $K P_i$ . Figure 4.5 illustrates the proposed scheme for a two user case ( $N = 2$ ) with  $m_1 = 3$  and  $m_2 = 5$ , using the Hadamard matrix in Figure 4.6 to construct the access codes.

Notice that since the input source samples are i.i.d, the proposed scheme is equivalent to a CDMA system with  $K$  users and  $K$  spread sequences (the columns of the matrix  $\mathbf{C}_{K \times K}$ ), with the first  $m_1$  users of the equivalent scheme corresponding to the  $m_1$  symbols of user 1, the next  $m_2$  users of the equivalent scheme corresponding to the  $m_2$  symbols of user 2, and so on. Figure 4.7 shows the equivalent CDMA system corresponding to Figure 4.5.

Note that the off diagonal entries of  $\mathbf{C}_{K \times K} \mathbf{C}_{K \times K} \mathbf{T}$  are zero because each  $\underline{\mu}_j^i$  is a scaled column of an orthogonal matrix. Hence  $\mathbf{C}_{K \times K} \mathbf{C}_{K \times K} \mathbf{T} = \mathbf{D}$  is a  $K \times K$

$$\mathbf{H}_{8 \times 8} = \frac{1}{\sqrt{8}} \begin{bmatrix} 1 & 1 & 1 & 1 & 1 & 1 & 1 & 1 \\ 1 & -1 & 1 & -1 & 1 & -1 & 1 & -1 \\ 1 & 1 & -1 & -1 & 1 & 1 & -1 & -1 \\ 1 & -1 & -1 & 1 & 1 & -1 & -1 & 1 \\ 1 & 1 & 1 & 1 & -1 & -1 & -1 & -1 \\ 1 & -1 & 1 & -1 & -1 & 1 & -1 & 1 \\ 1 & 1 & -1 & -1 & -1 & -1 & 1 & 1 \\ 1 & -1 & -1 & 1 & -1 & 1 & 1 & -1 \end{bmatrix} \quad (4.20)$$

Figure 4.6:  $8 \times 8$  Hadamard matrix. Here  $K = 8$ ,  $m_1 = 3$  and  $m_2 = 5$ . To generate the matrix  $\mathbf{C}_{8 \times 8}$ , the first 3 columns are assigned to user 1 and then scaled by  $\frac{1}{\sqrt{3}}$ . The remaining 5 columns are assigned to user 2 and scaled by  $\frac{1}{\sqrt{5}}$ .

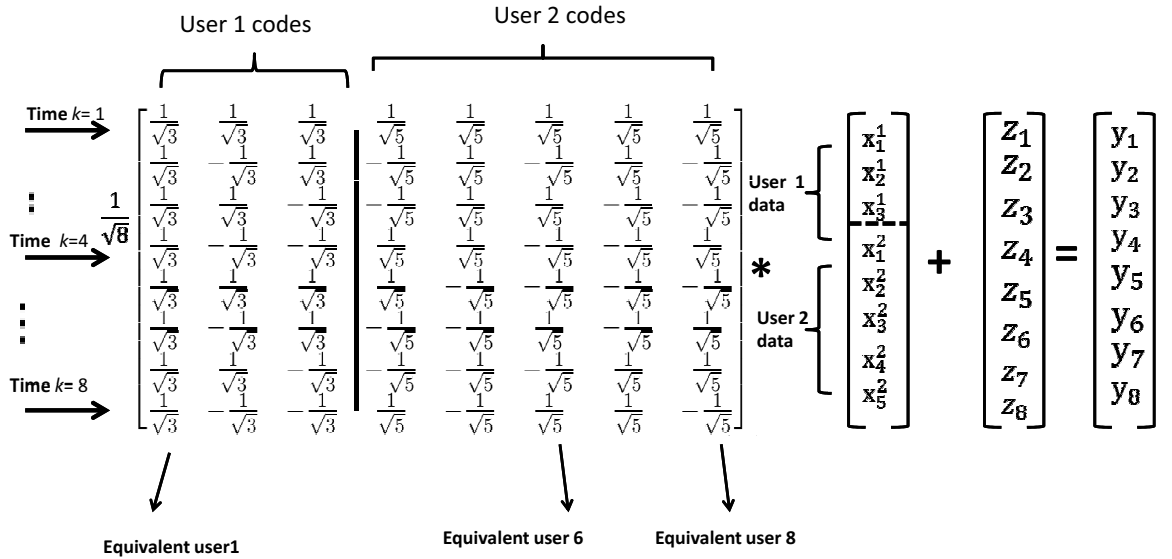


Figure 4.7: Equivalent CDMA system corresponding to Figure 4.5. The first  $m_1 = 3$  equivalent users correspond to the 3 different symbols of user 1 in our proposed scheme, while the next  $m_2 = 5$  equivalent users correspond to the 5 different symbols of user 2.

diagonal matrix with  $N$  distinct values ( $m_i$  entries of value  $\frac{1}{m_i}$ , where  $1 \leq i \leq N$ ). Thus, the proposed scheme is equivalent to  $K$  orthogonal Single-Input Single-Output (SISO) channels and its sum rate, in terms of bits per channel use, is

$$R_{scheme} = \frac{1}{K} \left[ \sum_{i=1}^N \sum_{j=1}^{m_i} \left( \frac{1}{2} \log_2 \left( 1 + \frac{K P_i}{m_i} \right) \right) \right], \quad (4.21)$$

where we have divided by  $K$  because the proposed system uses the MAC  $K$  times. Note that the power of each parallel SISO channel is the power of the spreading sequence  $\underline{\mu}_j^i \underline{\mu}_j^i = \frac{1}{m_i}$  times the overall power  $K P_i$  received from user  $i$ .

From (4.3), the maximum sum rate is

$$C_{MAC} = \frac{1}{2} \log_2 \left( 1 + \sum_{i=1}^N P_i \right) = \frac{1}{2} \log_2 \left[ 1 + \sum_{i=1}^N \sum_{j=1}^{m_i} \left( \frac{P_i}{m_i} \right) \right]. \quad (4.22)$$

Using the log sum inequality, it can be easily shown that  $R_{scheme}$  and  $C_{MAC}$  are equal if and only if

$$\frac{P_i}{m_i} = \frac{P_j}{m_j} \quad \forall j \neq i \text{ with } 1 \leq i, j \leq N. \quad (4.23)$$

This result is not surprising since the equivalent CDMA scheme achieves the MAC capacity when all the  $K$  equivalent users have the same power.

Particularizing the above result for the two-user case ( $N = 2$ ) gives the optimal  $m_1$  and  $m_2$ :  $\frac{P_1}{m_1^*} = \frac{P_2}{m_2^*}$ , such that  $m_1^* + m_2^* = K$ . Solving for the optimal  $m_i$ ,  $i = 1, 2$  yields

$$m_i^* = \frac{K P_i}{P_1 + P_2} \quad i = 1, 2. \quad (4.24)$$

Since  $m_i$  is the number of columns assigned to user  $i$ , it should be an integer. Even though the  $m_i^*$ 's may not be integers, if the code size  $K$  is chosen large enough ( $m_1, m_2$ ) can be chosen as close to the optimal ( $m_1^*, m_2^*$ ) as desired.

We can break up (4.21) to obtain the rate achieved by each user. For example,

for the two user case,  $N = 2$ , we have

$$R_1 = \frac{1}{K} \left( \sum_{j=1}^{m_1} \frac{1}{2} \log_2 \left( 1 + \frac{K P_1}{m_1} \right) \right) \quad (4.25)$$

$$R_2 = \frac{1}{K} \left( \sum_{j=m_1+1}^K \frac{1}{2} \log_2 \left( 1 + \frac{K P_2}{m_2} \right) \right). \quad (4.26)$$

Figure 4.8 shows the maximal rates achieved by each user for the two user case when  $P_1 = 200$  and  $P_2 = 400$ . The MAC capacity region is obtained from (4.2). In the Figure, we choose  $K = 32$ . As indicated in (4.23), there exists a point in the graph in which the proposed scheme achieves the MAC capacity.

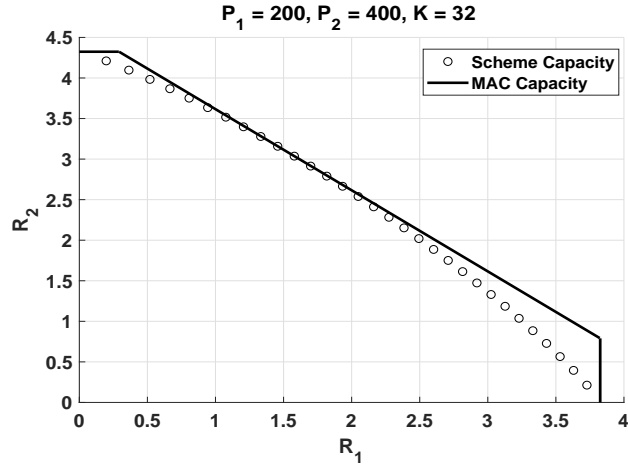


Figure 4.8: MAC capacity and the proposed scheme capacity for  $P_1 = 200$ ,  $P_2 = 400$  and codebook size  $K = 32$ . Each point of the curve is obtained from (4.25) and (4.26) by sweeping  $m_1$  from 0 to 32.

Note that Figure 4.8 is similar to the one obtained with an orthogonal FDMA system. However, the proposed scheme has the advantage of ease of analysis and design, and the potential to be extended to situations where the users are correlated. We also note that TDMA or FDMA systems would require the use of different rates in the analog joint source-channel encoder for each user, while here the rate is incorporated into the access scheme itself, which facilitates the design.

#### 4.2.1 Analog Joint Source Channel Coding using the proposed CDMA-like scheme

The  $N$  users are each transmitting an i.i.d Gaussian source,  $S_i$ , each having zero mean and a variance of  $\sigma_S^2$ . Previous to the access scheme, we assume each user processes its source using an  $M : 1$  analog joint source channel encoder. To simplify the analysis we assume that the source-channel communication ratio,  $M$ , is common to all users, although the proposed scheme can be easily generalized for different user ratios. When  $M = 1$ , the source samples,  $s_j^i$ ,  $j = 1, \dots, m_i$  are input directly to the access scheme so that  $x_j^i = \sqrt{\frac{P_i}{\sigma_S^2}} s_j^i$ ,  $j = 1, \dots, m_i$ , while for  $M = 2$  two consecutive source symbols  $(s_{2j}^i, s_{2j+1}^i)$  are encoded by a space-filling curve to generate the channel symbol  $x_j^i$ .

Under the Mean Squared Error (MSE) distortion criteria, the rate distortion function of any of the aforementioned sources is given by [40]

$$R(D_i) = \begin{cases} \frac{1}{2} \log_2\left(\frac{\sigma_S^2}{D_i}\right) & \text{for } D_i < \sigma_S^2, \\ 0 & \text{otherwise} \end{cases} \quad (4.27)$$

where  $D_i$  is average MSE distortion incurred by user  $i$ .

Considering optimal power allocation for each of the users as given by (4.23), the optimal theoretical limit (OPTA) for this problem is given by

$$M \left[ \frac{m_1}{K} \log\left(\frac{\sigma_S^2}{D_1}\right) + \dots + \frac{m_N}{K} \log\left(\frac{\sigma_S^2}{D_N}\right) \right] < \frac{1}{2} \log(1 + P_1 + \dots + P_N). \quad (4.28)$$

By defining

$$\overline{SDR} = \frac{m_1}{K} \log_{10}\left(\frac{\sigma_S^2}{D_1}\right) + \dots + \frac{m_N}{K} \log_{10}\left(\frac{\sigma_S^2}{D_N}\right), \quad (4.29)$$

(4.28) can be re-written as

$$\overline{SDR} < \frac{5}{M} \log_{10}(1 + P_1 + \dots + P_N). \quad (4.30)$$

Notice the change in the base of the logarithm.

Again, it is important to remark that (4.30) does not hold for all combinations of  $(P_1, P_2, \dots, P_N)$ , but it does when the power allocation for each user is optimized according to (4.23). Notice that (4.30) represents the minimum “average” distortion incurred by the system when user  $i$  performs bandwidth compression by a factor of  $M$  and utilizes  $m_i$  access codes. We will use (4.30) to represent the Optimum Performance Theoretically Attainable (OPTA) in terms of  $\overline{SDR}$  vs  $SNR = 10 \log_{10}(P_1 + \dots + P_N)$ , and compare this optimal performance with simulation results obtained from the proposed system when, for each  $SNR$  value, the power allocation for each user,  $SNR_i = 10 \log_{10} P_i$ , is optimized following (4.23).

#### 4.2.1.1 Uncoded Transmission ( $M = 1$ )

As explained before, the source samples,  $s_j^i, j = 1, \dots, m_i$ , are input directly to the access scheme so that  $x_j^i = \sqrt{\frac{P_i}{\sigma_s^2}} s_j^i, j = 1, \dots, m_i$ . Notice that with this scheme user  $i$  transmits  $m_i$  source symbols using  $K$  signaling intervals.

At the receiver site, we perform MMSE decoding on the received vector  $\underline{\mathbf{y}}$  to obtain the MMSE estimate of the transmitted vector  $\mathbf{s}$  comprising user 1 and user 2 data. We observe that the received vector  $\underline{\mathbf{y}}$  can be expressed as  $\underline{\mathbf{y}} = \mathbf{H}\mathbf{\Gamma}\mathbf{s} + \mathbf{z}$ , where  $\mathbf{\Gamma}$  is a diagonal scaling matrix containing either  $\sqrt{\frac{P_1}{\sigma_s^2}}$  or  $\sqrt{\frac{P_2}{\sigma_s^2}}$ . The MMSE estimate of the transmitted data is given by

$$\hat{\underline{\mathbf{s}}} = ((\mathbf{H}\mathbf{\Gamma})^T \mathbf{H}\mathbf{\Gamma} + 2\mathbf{I})^{-1} (\mathbf{H}\mathbf{\Gamma})^T \underline{\mathbf{y}}. \quad (4.31)$$

Since  $\mathbf{H}^T \mathbf{H} = \mathbf{I}$ , (4.31) reduces to

$$\hat{\underline{\mathbf{s}}} = (\mathbf{\Gamma}^T \mathbf{\Gamma} + 2\mathbf{I})^{-1} (\mathbf{H}\mathbf{\Gamma})^T \underline{\mathbf{y}}, \quad (4.32)$$

which, given the orthogonalization produced by the CDMA-like access scheme, is just the result of applying a matched filter.

#### 4.2.1.2 2:1 Bandwidth Reduction ( $M = 2$ )

For the 2:1 Bandwidth reduction case, each user utilizes a space-filling curve to encode two consecutive source symbols  $(s_{2j}^i, s_{2j+1}^i)$  into symbol  $x_j^i$ . Therefore, user  $i$  transmits  $2m_i$  source symbols over the  $K$  signaling intervals. As analog encoders, we will utilize the non-linear Archimedean spiral [37, 38] defined parametrically as

$$\begin{cases} u = \frac{\Delta_i}{\pi}\theta \sin \theta \\ v = \frac{\Delta_i}{\pi}\theta \cos \theta \end{cases} \text{ for } \theta \geq 0, \quad \begin{cases} u = -\frac{\Delta_i}{\pi}\theta \sin \theta \\ v = \frac{\Delta_i}{\pi}\theta \cos \theta \end{cases} \text{ for } \theta < 0, \quad (4.33)$$

where  $\Delta_i$  is the distance between two neighboring spiral arms in the curve corresponding to user  $i$  and  $\theta$  is the angle from the origin to the point  $(u, v)$  on the curve. The mapping function  $M_{\Delta_i}(s_{2j}^i, s_{2j+1}^i)$  takes any source pair  $(s_{2j}^i, s_{2j+1}^i)$  and projects it to the closest point on the spiral, that is

$$\begin{aligned} \hat{\theta}_j^i &= M_{\Delta_i}(s_{2j}^i, s_{2j+1}^i) = \\ &\arg \min_{\theta} \left\{ (s_{2j}^i \pm \frac{\Delta_i}{\pi}\theta \sin \theta)^2 + (s_{2j+1}^i - \frac{\Delta_i}{\pi}\theta \cos \theta)^2 \right\}. \end{aligned} \quad (4.34)$$

After the mapping,  $\hat{\theta}_j^i$  is processed by the function  $T_{\alpha_i}(\hat{\theta}_j^i) = (\hat{\theta}_j^i)^{\alpha_i}$  to produce  $x_j^i$ . For each user, both parameters  $(\Delta_i, \alpha_i)$  are optimized according to the corresponding power allocation  $P_i$  [38], where, for each SNR,  $P_i$ , the optimal power allocation, is chosen according to (4.23).

The decoder is composed of two main components. First, the MMSE outer detector (similar to the MMSE detector that was used in (4.31)) that decouples the two users data. Second, the inner decoder after the MIMO detector, which performs Maximum Likelihood (ML) decoding on the 2:1 spiral compression system. Given the received vector  $\mathbf{y}$ , the MMSE estimate of the transmitted vector  $\mathbf{x}$  is obtained as in (4.31). Then, the ML estimate of  $\theta$  for user  $i$  is calculated by inverting the transformation  $T_{\alpha_i}(\cdot)$

$$(\hat{\theta}_j^i)_{ML} = T_{\alpha_i}^{-1}(\hat{x}_j^i). \quad (4.35)$$

Finally, we perform the inverse mapping on  $(\hat{\theta}_j^i)_{ML}$  according to (4.33) to obtain the ML estimates of the original transmitted source pair  $(\hat{s}_{2j}^i, \hat{s}_{2j+1}^i)$  of each user.

### 4.3 A Hybrid Analog-Digital System for the MAC

As we have discussed in Section 4.1.2, orthogonal systems such as FDMA, TDMA or the CDMA-based access scheme only achieve capacity at three points on the convex hull of the capacity region (and two of them are trivial points as shown in Figure 4.3). Analog codes are readily usable with such orthogonal schemes, as we have shown in Section 4.2, but not with SIC because the transmitted waveform of one of the users must be reproduced exactly as it was transmitted. This is to allow the decoder to subtract that waveform from the noisy received waveform before proceeding to decode the second user information. This is possible with digital codes because they take values from a finite set of possibilities. However, analog codes are continuous in amplitude and the range they can take is infinite. Hence, the analog waveform cannot be reproduced faithfully at the decoder and SIC cannot be used with analog codes. In this section, we build on the work of Section 4.2 and present the complete hybrid analog-digital system.

#### 4.3.1 Theoretical Analysis

The proposed hybrid analog-digital scheme works by having both users use an orthogonal access scheme to transmit data, and then having one of the users superimpose a digital code to transmit the remaining data. At the receiver, the digital code is decoded first and subtracted from the received waveform. Then, we proceed to decode the remaining data stemming from the orthogonal scheme as if the orthogonal scheme had been used alone from the beginning. We will demonstrate that the combination of the orthogonal CDMA-access scheme and the superimposed digital code can be used to achieve any point in the convex hull of the capacity region.

Our examples in this Section will focus on the two user case ( $N = 2$ ), but the hybrid scheme can be extended for  $N > 2$ , as we show later in Section 4.4. For the

two users to transmit over the MAC, we utilize the same orthogonal CDMA-based access scheme of Section 4.2, except that we do not allocate the full power  $P_2$  to user 2. Instead, user 2 uses a power of  $(P_2 - \Delta P_2)$  to communicate over the MAC. Hence, when the aforementioned orthogonal scheme is used with power  $P_1$  for user 1 and power  $P_2 - \Delta P_2$  for user 2, where  $0 \leq \Delta P_2 \leq P_2$ , the sum rate is given by

$$R_{Orth} = R_1 + R_2 = \frac{m}{K} \frac{1}{2} \log_2 \left( 1 + \frac{K P_1}{m} \right) + \frac{K-m}{K} \frac{1}{2} \log_2 \left( 1 + \frac{K(P_2 - \Delta P_2)}{K-m} \right) \quad (4.36)$$

The above equation is illustrated in Figure 4.9. By choosing  $K = 32$ , the different points of the orthogonal scheme are plotted by sweeping  $m$  from 0 to 32. User 2 would then use a digital code with the remaining power  $\Delta P_2$  to transmit at a rate of  $R_{Digital}$ . The maximum rate of this scheme is given by

$$R_{Digital} = \frac{1}{2} \log_2 \left( 1 + \frac{\Delta P_2}{1 + P_1 + P_2 - \Delta P_2} \right). \quad (4.37)$$

We note that the above rate for the digital code treats the orthogonal transmissions with power  $P_1$  and  $P_2 - \Delta P_2$  as *noise* (along with the channel noise itself, of course). Equation (4.37) also assumes that the overall noise distribution that the digital system sees is Gaussian. This is exactly the case here, since a necessary condition for the analog component to achieve (4.36) is to have a Gaussian distribution for each of the  $K$  orthogonal sub-channels.

If  $m$  is chosen so that  $\frac{m}{P_1} = \frac{K-m}{P_2 - \Delta P_2}$ , then it can be easily shown by the log sum inequality that  $R_{Orth} = \frac{1}{2} \log_2(1 + P_1 + P_2 - \Delta P_2)$ . Then, the total information rates that user 1 and user 2 can achieve,  $R_{Sum}$ , is given by

$$R_{Sum} = R_{Orth} + R_{Digital} = \frac{1}{2} \log_2(1 + P_1 + P_2) = C_{MAC}, \quad (4.38)$$

This means that this particular decomposition of the channel does not lose capacity. Moreover, we can achieve any point on the convex hull of the capacity simply by varying

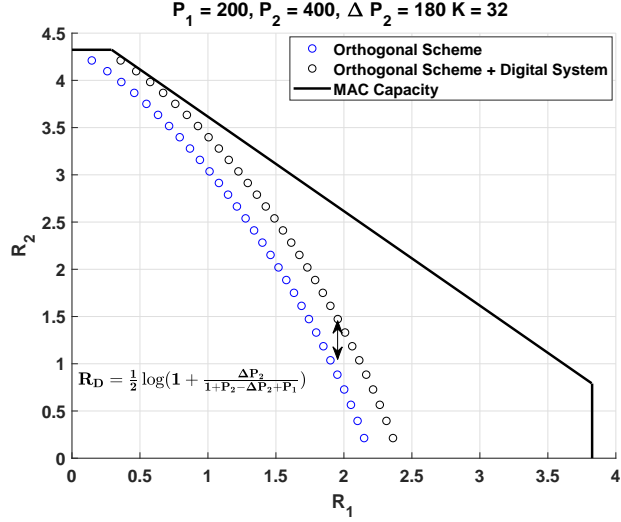


Figure 4.9: Theoretical limit for the hybrid scheme: The lower curve is obtained by using the CDMA-like access scheme and sweeping  $m$  from 0 to 32. The middle curve represents the achievable rates by the combination of the CDMA-like access scheme and the digital code used by user 2.

$\Delta P_2$  from  $[0, P_2]$ .

### 4.3.2 Practical Implementation

Note that for the digital part of the system, the Channel Coding theorem states that as long as the information rate is less than  $R_{digital}$ , error free communication is feasible. Hence, to implement the proposed scheme we use a powerful channel code to transmit at or near the capacity of the channel, and at the decoder we subtract the waveform that was transmitted. Then, we proceed to decode the orthogonal scheme data, encoded as described in Section 4.2. Note that the equations in (4.36) are still valid because the orthogonal scheme is not affected by the digital code since we subtract the digital code at the decoder. The system diagram of the overall scheme is shown in Figure 4.10.

#### 4.3.2.1 Analog Encoder

For the analog part of the system, we use the analog coding scheme described in subsection 4.2.1.1. In particular, we focus here on the uncoded analog scheme ( $M = 1$ ),

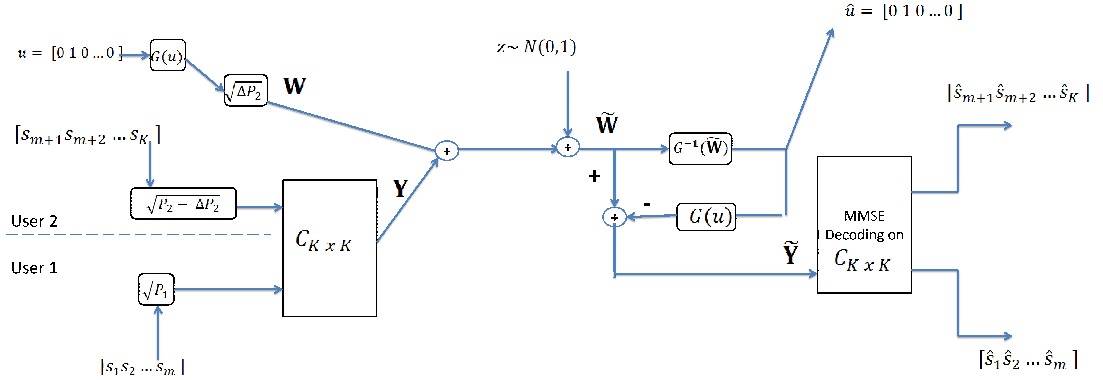


Figure 4.10: Proposed analog-digital coding scheme for two users.

although the scheme can be extended to general channel bandwidth ratios.

#### 4.3.2.2 Digital Encoder

For the digital part of the system, we use the family irregular of LDPC codes with a code length of 64,800 bits in the DVB-S2 standard [63]. The reason for this choice is that this standard supports different code rates (ranging from  $\frac{1}{4}$  to  $\frac{9}{10}$ ), and the parity matrices for this family of codes are readily available in MATLAB <sup>®</sup>. For our simulations, we use an orthogonal codebook size of  $K = 1024$ . Since we have to decode the digital code first and subtract it from the received waveforms, we have to wait at least 64,800 channel realizations before we decode the orthogonal component of the system (which corresponds to  $\lceil \frac{64,800}{1024} \rceil = 64$  blocks of the orthogonal scheme.)

#### 4.4 Extension to more than two users

In this section, we demonstrate that both the orthogonal CDMA-based access scheme and the Hybrid analog digital system are well suited for AWGN Multiple Access Channels with more than two users. First, we recall the capacity of a general  $N$ -user

AWGN MAC [40]

$$\sum_{i \in S} R_i \leq C\left(\sum_{i \in J} P_i\right). \quad (4.39)$$

Here,  $J$  is the power set of  $(1, 2, \dots, N)$ . The capacity region is a polyhedron in  $N$  dimensions. It has a shape similar to that of Figure 4.3, but expanded in  $N$  dimensions instead of two. For the case of pure analog communication, the orthogonal access scheme proposed in Section 4.2 is optimal when the channel access codes are allocated in proportion to each user's power, that is  $\frac{P_i}{m_i} = \frac{P_j}{m_j} \forall i, j \in [1, N]$ . In order to achieve any point in the capacity region of (4.39), the hybrid scheme in Section 4.3 can be extended for  $N$  users. First all users should utilize the orthogonal access scheme with powers  $(P_1, P_2 - \Delta P_2, P_3 - \Delta P_3, \dots, P_n - \Delta P_n)$ , with each user being allocated a proportional number of access codes according to its power, as described earlier. Then, users 2 to  $N$ , each utilize a capacity-achieving digital code with their remaining  $\Delta P_i$  transmission power. Each code is designed to operate at an SNR of

$$\text{SNR}_i = \frac{\Delta P_i}{N_0 + P_{\text{analog}} + \sum_{j=i+1}^N \Delta P_j}. \quad (4.40)$$

By applying the log sum inequality, it can be shown that by properly choosing the number of channel access codes,  $m_i$ , and the power for the digital source components ( $\Delta P_i$ ), any point in the capacity region can be achieved. The order of decoding is important here: first we decode the digital component of user  $N$ , treating everything else as noise. Then, we subtract the re-encoded version from the received waveform to decode the digital component of user  $N - 1$ , treating everything else as noise. We repeat the process until all digital codes of all users have been decoded. Then, we decode the analog component of each user, as shown in Section 4.2.

## 4.5 Simulation Results

### 4.5.1 Pure analog CDMA-like scheme

We first consider the purely analog scheme with no digital component. We begin by presenting the results for different values of  $m_i$  when  $K = 16$  and the source symbols of each user are transmitted either directly ( $M = 1$ ) or using a 2:1 spiral curve ( $M = 2$ ). As described before, in our simulations we utilize the optimal power allocation as given in (4.23) for an overall system power specification  $SNR = 10 \log_{10}(P_1 + \dots + P_N)$ , and compare the “average” distortion  $\overline{SDR}$  as defined in (4.29) with the theoretical limit obtained in (4.30). Notice that this limit does not depend on the specific values of  $m_i$ . The results for  $M = 1$  and different values of  $m_i$  are shown in Figure 4.11. Notice that the proposed scheme is *optimal*, i.e. it achieves the distortion bound for all SNRs, irrespectively of the values of  $m_i$  (when  $P_i$  are chosen optimally according to (4.23)).

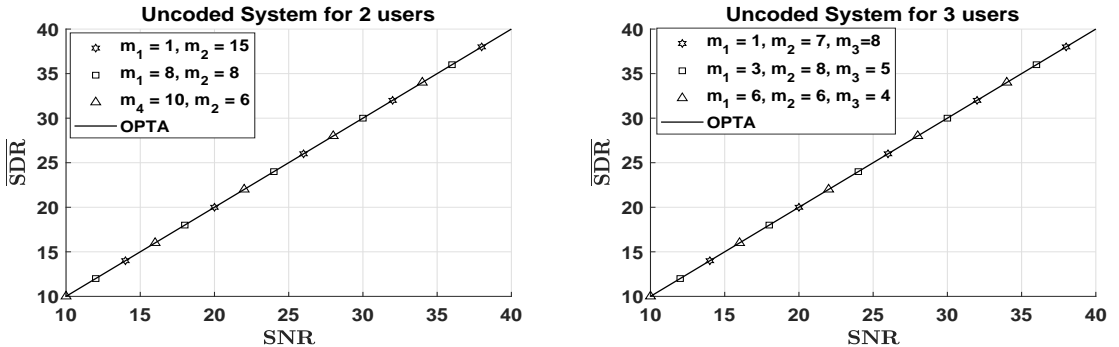


Figure 4.11: System performance for  $M = 1$  and different values of  $m_i$  (using optimal power allocation) when  $K = 16$ . Note that irrespectively of the values of  $m_i$ , the scheme achieves the OPTA exactly for the two and three user cases.

The above result is very interesting indeed. It was shown by Gobblick [34] that for point-to-point communications, uncoded transmission of Gaussian sources through Gaussian channels is optimal when one source symbol is transmitted per channel use. The use of the access codes converts the MAC channel into  $K$  orthogonal parallel SISO channels, as (4.21) demonstrates, and the system achieves optimal performance over the MAC when the  $P_i$ 's are chosen according to (4.23).

Simulation results for the  $M = 2$  case and different values of  $m_i$  (using optimal power allocation), with  $K = 16$ , are shown in Figure 4.12. Notice that irrespectively of the values of  $m_1$  and  $m_2$ , our system is only about 1 dB away from the OPTA for a wide range of SNRs.

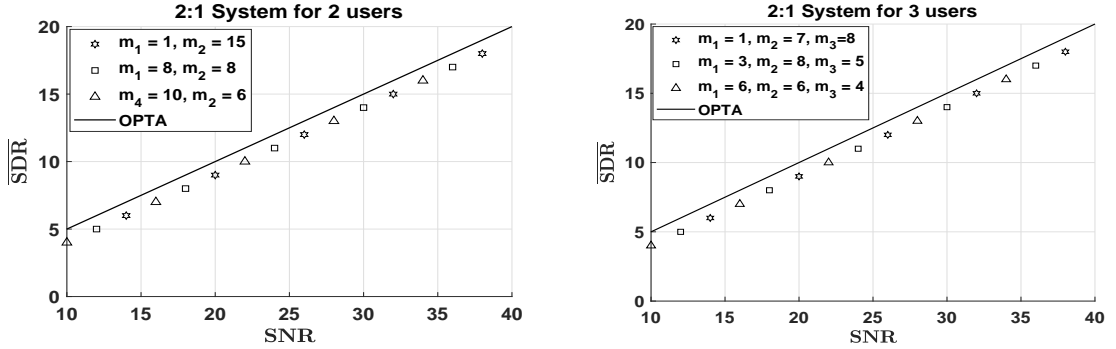


Figure 4.12: System performance for  $M = 2$  and different values of  $m_i$ s (using optimal power allocation) when  $K = 16$ . Notice that irrespectively of the values of  $m_i$ s, the achieved SDR is only 1 dB away from the OPTA.

#### 4.5.2 Hybrid Analog-Digital Scheme

Second, we present the results of the hybrid scheme described in Section 4.3. For the analog part, we use the CDMA-like scheme to transmit uncoded ( $M = 1$ ) zero mean Gaussian sources with unity variance. The first and second user transmit  $m$  and  $K - m$  source symbols, respectively, over  $K$  signaling times. Then, the second user utilizes one of the LPDC digital codes of the DVB-S2 family to transmit an equiprobable binary sequence (Bernoulli with  $p = \frac{1}{2}$ ) at an information rate of  $\kappa$ <sup>5</sup>. Note that the performance of digital systems is typically measured by the Bit Error Rate (BER) achieved at a particular SNR, while for analog JSCC systems the average distortion (or SDR) of the source being transmitted is typically measured, as we defined in sub-section 4.2.1. To measure the performance of the hybrid system, we use the *equivalent* rate that the analog scheme achieves based on the resulting distortion, which is captured

<sup>5</sup> Note that  $\kappa$  above is not necessarily one of the code rates supported by the DVB-S2 standard. We use puncturing of the nearest lower code rate supported in the standard to get the desired  $\kappa$ .

by the rate distortion function. For the digital part of the scheme, we use the digital code rate,  $\kappa$ , at a BER of  $10^{-7}$ , which is a BER typical for digital systems. Hence the hybrid scheme achieved rates are given by

$$\begin{aligned} R_1 &= \frac{m}{2K} \log_2\left(\frac{1}{D_1}\right) \\ R_2 &= \frac{K-m}{2K} \log_2\left(\frac{1}{D_2}\right) + \kappa \end{aligned} \quad (4.41)$$

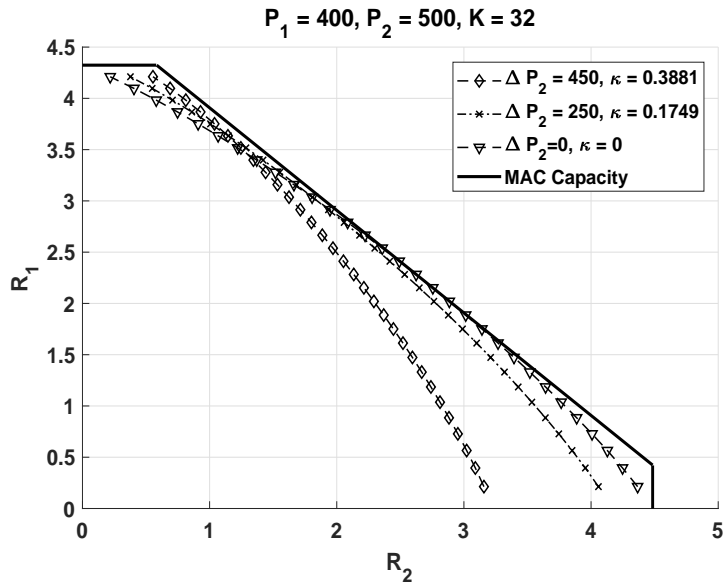


Figure 4.13: Performance of the hybrid analog-digital scheme using a digital code of rate  $\kappa$  for user 2, and an uncoded analog system ( $M = 1$ .)

The resulting rates are shown in Figure 4.13 for several cases of interest. Note that the results provided in Figure 4.13 show that the hybrid system is not optimal (it does not touch the capacity region for  $\kappa > 0$ ). This stems from the fact that the LDPC code operates at about 1.5 dB away from capacity at BER =  $10^{-7}$  (which translates to a loss of 0.08-0.2 bits depending on the specific code used). The loss observed in Figure 4.13 results purely from the sub-optimality of the digital code, since transmission of Gaussian sources is optimal for the AWGN channel [34] and we showed in the previous subsection that for  $M = 1$ , the analog system is optimal. To

corroborate this conclusion, Figure 4.14 shows the results assuming that the digital code is optimal (i.e., it achieves the bound in (4.37)).

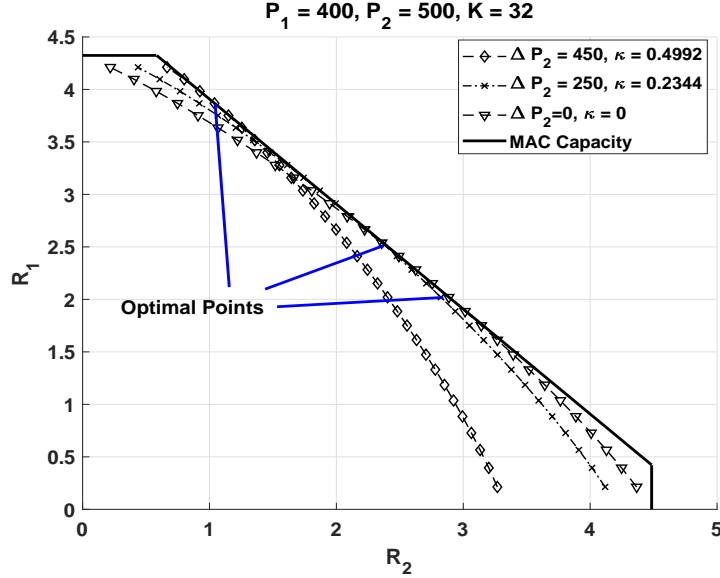


Figure 4.14: Performance of the hybrid analog-digital scheme using an optimal digital code and an uncoded analog system ( $M = 1$ ). Note that the performance is tangent to the MAC capacity meaning it is optimal for that specific rate pair.

Figure 4.15 presents the simulation results for a system with 3 users having  $P_1 = 10$ ,  $P_2 = 12$ , and  $P_3 = 15$ , and utilizing the orthogonal access scheme to transmit uncoded ( $M = 1$ ) zero mean Gaussian sources with unity variance over  $K = 128$  signaling times. For clarity, we only show one face of the capacity Polyhedron representing the maximum sum rate bound ( $R_1 + R_2 + R_3 < \frac{1}{2} \log(1 + P_1 + P_2 + P_3)$ ). We notice that the scheme is optimal (tangent to the MAC Capacity) at one point where  $\frac{P_i}{m_i} = \frac{P_j}{m_j}$ . It can easily be shown that the hybrid scheme can achieve any point in the capacity region by proper choice of digital codes for any two of the three users in the system, as described in Section 4.4.

## 4.6 Conclusion

We have proposed the use of a CDMA-like access scheme for the transmission of independent users through a MAC using analog joint source-channel coding. The proposed access scheme allows for the use of different rates for each user, and achieves

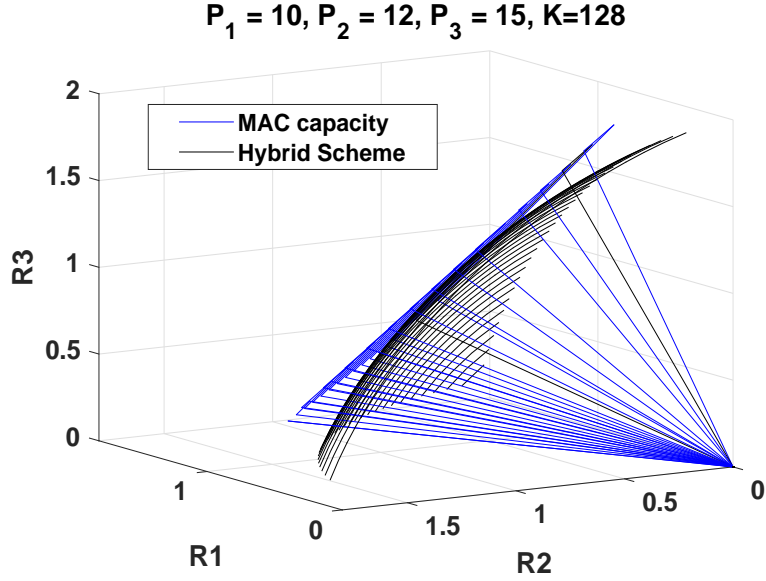


Figure 4.15: Performance of the analog-digital scheme for three users ( $N = 3$ ) when transmitting uncoded analog sources ( $M = 1$ ). Note that the performance is tangent to the MAC capacity meaning it is optimal for that specific rate pair.

the theoretical limit when the power is allocated optimally to each user. The sources are encoded by standard space-filling curves optimized for point-to-point AWGN channels. Simulation results show the optimality of the practical analog coding schemes when each user transmits the source symbols directly through the channel. The resulting performance when 2:1 spiral mappings are used to encode each source lies within 1 dB of the theoretical limit. We have also demonstrated a new hybrid analog-digital scheme that combines the use of orthogonal schemes with successive interference cancellation. We have proven analytically, assuming optimal coding, that the scheme achieves the MAC capacity at any desired rate pair by adjusting the power allocated to the SIC system. Finally, we have shown that practical systems based on this idea present a performance very close to the theoretical limits.

## Chapter 5

### ANALOG JSCC FOR THE BROADCAST CHANNEL

#### 5.1 Introduction

In this chapter, we continue with another important channel, the Broadcast Channel. In the Broadcast channel, there is one transmitter that wishes to communicate a set of messages to  $N$  receivers, where each receiver is interested only in a particular subset of the messages,  $M$ . A general framework for the Broadcast channel is shown in Figure 5.1. The channel is very common in cellular communication systems where there is a Base Station that wishes to transmit some common and private messages to the user equipment (cell phones for example) such as, signal strength, network information, base station location and phone call data.

The remainder of this chapter is organized as follows: Section 5.2 introduces the broadcast channel and discusses theoretical limits. We discuss the performance of separation-based schemes for the Broadcast channel in Section 5.3. Section 5.4 introduces the Alternating Sign-Scalar Quantizer Linear Coder (AS-SQLC) scheme, which is a modified version of the SQLC scheme, suited for the transmission of independent Gaussian sources. Section 5.5 explains and analyzes the advantage of the modified scheme over the classic SQLC scheme. In Section 5.6, we set the theoretical framework to analyze the distortion of the AS-SQLC scheme. In Section 5.7, we generalize the AS-SQLC scheme to transmit correlated Bivariate Gaussian Sources and derive the globally optimal decoding functions. We present the simulation results in Section 5.8, and discuss future work and conclude the Chapter in Section 5.9

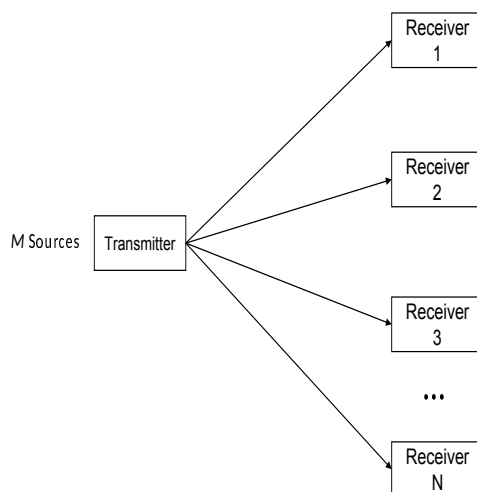


Figure 5.1: General framework for the Broadcast channel. There is one transmitter which has a set of messages or sources. The transmitter wishes to communicate each message to a subset of the receivers with a given fidelity. The desired fidelity level may be different for each receiver.

## 5.2 The Broadcast Channel

The broadcast channel was first considered by Cover in [65]. The problem formulation is the following: Suppose you have a central transmitter and several receivers. The central transmitter wishes to communicate a common message to all the receivers, as well as a private message to each receiver<sup>1</sup>. Cover showed in [65] that time sharing is strictly suboptimal for the broadcast channel in the general case<sup>2</sup>. He showed that the optimal way to achieve the channel capacity for Gaussian sources is via *superposition coding*. Next, we give a concrete example (taken from [40]) about the sub-optimality

---

<sup>1</sup> One might even consider a more general case where the central transmitter has  $W$  messages and each receiver is interested in a particular subset of the messages.

<sup>2</sup> Time Sharing or Frequency Sharing or CDMA or any other orthogonal scheme can achieve the capacity of the Broadcast Channel in special cases. For example for the two user Gaussian broadcast with the two receivers having the same noise variance, time sharing is optimal, as will be shown in Appendix B.

of time sharing in general for broadcast channels, showing the need to employ a superposition coding based system.

Dutch and Spanish speaker: Suppose you speak both Dutch and Spanish and you wish to communicate to two persons, one who only speaks Dutch and the other person only Spanish. Furthermore, suppose that each language has  $2^{20}$  words, and assume that there are no common words in Spanish and Dutch. Also assume that the speaker can speak at a rate of one word per second in any language, hence the speaker can speak at rate of 20 bits/second. If the speaker chose to communicate to the Dutch speaker half of the time and to the Spanish speaker half of the time (by speaking a word to the Spanish speaker and then a word to the Dutch speaker alternatively), then he would be communicating to each listener at a rate of half a word per second or equivalently 10 bits/second to each listener. Can he do better? In fact, yes. We note that we can communicate information via the *order* in which the speaker interleaves the words to each listener. This is possible because each listener can determine if the spoken word is either Spanish or Dutch (we have assumed that the two language alphabets are disjoint<sup>3</sup>). We can choose any order of the words as shown in Figure 5.2 below. Thus, in effect we can communicate that extra information of order. If we look at four consecutive time slots, there are four possible different orderings. Hence, we can communicate two extra bits in these four time slots(seconds). Thus we added an extra 0.5 bits of information and the overall communication rate would be 20.5 bits/second<sup>4</sup>.

Next, we formalize the above argument. However, note that this characterization is the one typically used when working with discrete digital systems, as will be shown in the next section. Since we are considering analog joint source channel coding systems here, we will give an alternate characterization of the broadcast channel that is specific to the case in which we are interested in sending analog Gaussian sources.

---

<sup>3</sup> I believe that the authors in [40] chose Spanish and Dutch in their example because Spanish and Dutch sound very different from each other, at least they do to the author.

<sup>4</sup> In fact by considering a larger word block length instead of four in the above example, it can be shown that in the limit of taking the block length to  $\infty$ , we can communicate at most 1 bit using the described scheme. Thus bringing the total number of transmitted bits to 21 bits/second [40].

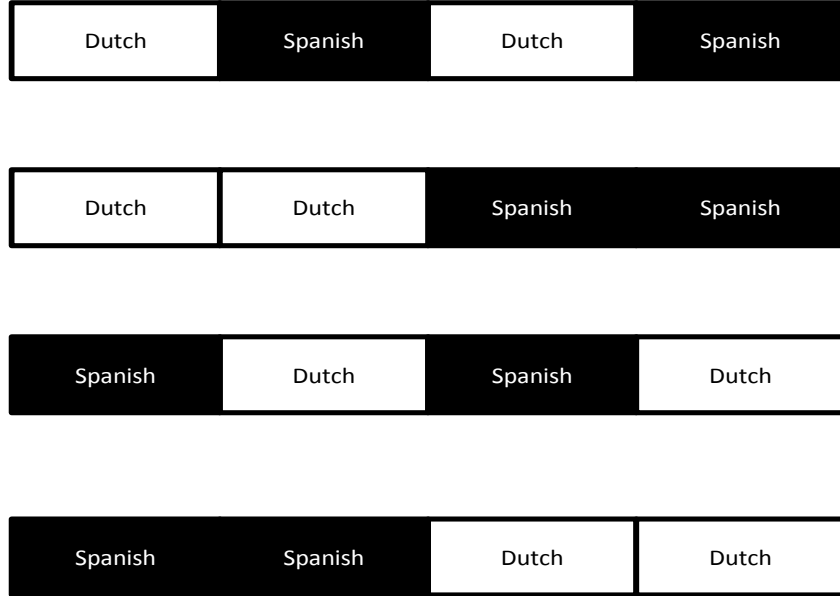


Figure 5.2: Different orderings of four messages in a four time slot communication system. Each order represents a message from a codebook.

We shall still consider the digital (discrete-values) version of the Broadcast channel because some of the arguments are similar and it is clearer to see the techniques in the digital domain.

### 5.2.1 Formal Characterization of the Discrete Broadcast Channel

Before we proceed, we discuss the terminology to be used in the rest of the chapter: A random variable will be denoted by capital letters  $\mathbf{X}, \mathbf{Y}$ . Samples will be denoted as lower-case letters  $x, y$ . A vector  $(x(1), x(2), \dots, x(n))$  will be denoted by  $x^n$ .

The following theoretical formulation is largely based on Cover's [40]. A two-user broadcast channel consists of an input alphabet  $\mathcal{X}$ , two output alphabets  $\mathcal{Y}_1$  and  $\mathcal{Y}_2$ , and a probability transition function  $p(y_1, y_2|x)$  for  $x \in \mathcal{X}, y_1 \in \mathcal{Y}_1$  and  $y_2 \in \mathcal{Y}_2$ .

We shall consider memoryless broadcast channels in which

$$p(y_1^n, y_2^n | x^n) = \prod_{i=1}^n p(y_1(i), y_2(i) | x(i)), \quad (5.1)$$

where  $i \in \mathbb{N}$  is the time index. The broadcast channel has one encoding function,  $f$ , and two decoding functions,  $g_1$  and  $g_2$ . The encoding function  $f$  is defined as

$$f = \{1, 2, 3, \dots, 2^{nR_1}\} \times \{1, 2, 3, \dots, 2^{nR_2}\} \rightarrow \mathcal{X}^n, \quad (5.2)$$

where  $R_i$  is user  $i$  information rate and it has units of bits per channel use. We define the decoding functions as

$$g_1 : \mathcal{Y}_1^n \rightarrow \{1, 2, \dots, 2^{nR_1}\} \quad (5.3)$$

$$g_2 : \mathcal{Y}_2^n \rightarrow \{1, 2, \dots, 2^{nR_2}\} \quad (5.4)$$

This means that the encoding function,  $f$ , takes as input a pair of two messages, one intended for user 1 and the other intended for user 2. At the decoders side, decoder  $i$  receives  $y_i^n \in \mathcal{Y}_i$  and estimates user  $i$  transmitted message among the possible choices of  $\{1, 2, \dots, 2^{nR_i}\}$ . We define the average probability of error as

$$P_e^{(n)} = P(\{g_1(y_1^n) \neq W_1\} | \{g_2(y_2^n) \neq W_2\}), \quad (5.5)$$

where  $(W_1, W_2)$  are assumed to be uniformly distributed over  $2^{nR_1} \times 2^{nR_2}$ . We say that a rate  $(R_1, R_2)$  is achievable for the broadcast channel if there exists a sequence of  $((2^{nR_1}, 2^{nR_2}), n)$  codes (functions  $(f, g_1, g_2)$ ) with  $\lim_{n \rightarrow \infty} P_e^{(n)} = 0$ .

A broadcast channel is said to be physically degraded if  $p(y_1, y_2, x) = p(y_1|x)p(y_2|y_1)$ . The channel is also said to be stochastically degraded if its conditional marginal distributions are the same as that of a physically degraded broadcast channel, i.e., if there

exists a distribution  $p'(y_2|y_1)$  such that

$$p(y_2|x) = \sum_{y_1} p(y_1|x)p'(y_2|y_1). \quad (5.6)$$

Since the capacity only depends on the marginal distributions, the capacity of the physically degraded broadcast channel is the same as that of the stochastically degraded channel, hence hereinafter we shall assume physical degradedness<sup>5</sup>.

### 5.2.2 Broadcasting Gaussian sources over the Gaussian Broadcast Channel

In this section, we will formally define the Gaussian Broadcast channel for transmitting a bivariate Gaussian source. Let  $(\mathbf{S}_1, \mathbf{S}_2)$  be a stationary, memoryless bivariate Gaussian distribution with zero mean and Covariance matrix  $\mathbf{C}$  given by

$$\mathbf{C} = \begin{bmatrix} 1 & \rho^2 \\ \rho^2 & 1 \end{bmatrix}, \quad (5.7)$$

with  $0 \leq \rho \leq 1$ , where we are assuming that each source has unity variance. Figure 5.3 shows the pdf of the Bivariate Gaussian source when  $\rho^2 = 0$  and  $\rho^2 = 0.9$ .

The encoder function  $f$  takes  $(\mathbf{S}_1^n, \mathbf{S}_2^n)$  and produces  $\mathbf{X}^n$ , the channel input. The output of the broadcast channel  $\mathbf{Y}_i$  is given by

$$\mathbf{Y}_i(k) = \mathbf{X}(k) + \mathbf{Z}_i(k), \quad i = 1, 2, \text{ and } k \in N_+, \quad (5.8)$$

where  $\mathbf{Y}_i(k)$  is the channel output observed by the  $i$ -th receiver at time  $k$  and  $\mathbf{Z}_i(k)$  is the zero mean independent Gaussian noise with variance  $N_i$  experienced by user  $i$  at time  $k$ . Without loss of generality, we assume  $N_2 \geq N_1$ .

---

<sup>5</sup> Physical degradedness means that the second received source can be obtained by getting the second source and actually (physically) modifying it via another channel between the first and second receiver. Statistical degradedness means the second source distribution looks like it was obtained by physical degradedness but in fact it may not. The Gaussian channel is always physically degraded.

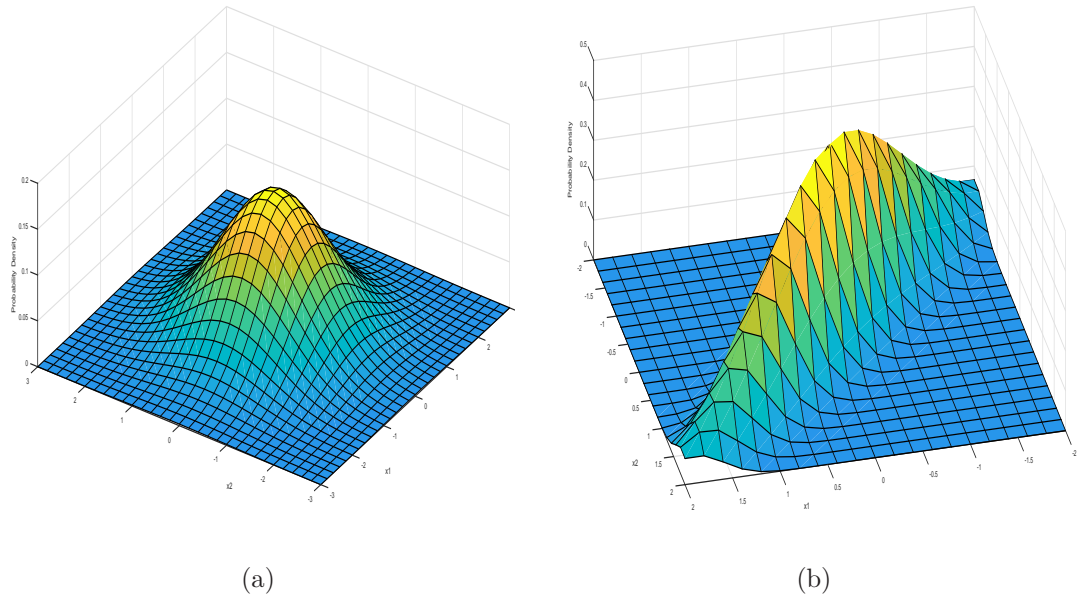


Figure 5.3: Bivariate Gaussian probability density function for  $\rho^2 = 0$  (left) and  $\rho^2 = 0.9$  (right).

The decoding functions  $g_i$  of the broadcast channel take  $\mathbf{Y}_i^n$  and produce an estimate  $\hat{\mathbf{S}}_i^n$  of the original transmitted source symbol  $\mathbf{S}_i^n$ . Note that the function  $g_i$  is only required to produce an estimate of the source for user  $i$ , although it can be helpful in the decoding if one of the users has an estimate about the other user's data. The Gaussian Broadcast channel for Gaussian sources is shown in Figure 5.4.

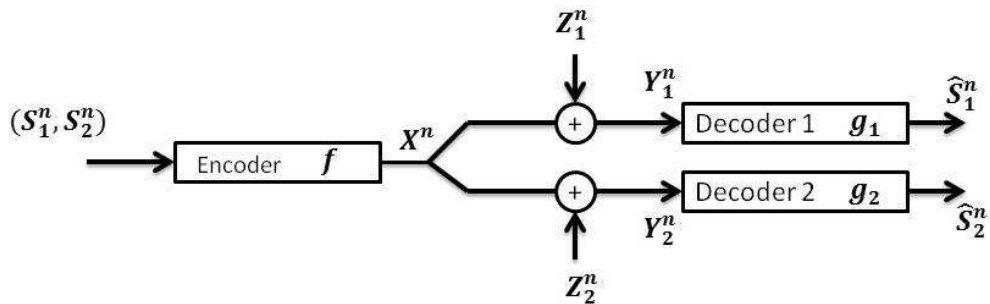


Figure 5.4: Broadcasting a Bivariate Gaussian source over the Gaussian Broadcast Channel.

To calculate the distortion between the original source symbol  $\mathbf{S}_i$  and the decoded source symbol  $\hat{\mathbf{S}}_i$ , we use the Mean Squared Error criteria given by

$$D_i(s_i^n, \hat{s}_i^n) = \frac{1}{n} \sum_{j=1}^n (s_i(j) - \hat{s}_i(j))^2, \quad i = 1, 2. \quad (5.9)$$

We also operate under an average transmit power constraint  $P$  defined as

$$\frac{1}{n} \sum_{j=1}^n x^2(j) \leq P. \quad (5.10)$$

Next we give the definition of achievability of a given distortion pair  $(D_1, D_2)$

**Definition** A distortion pair  $(D_1, D_2) \in \mathbb{R}_+ \times \mathbb{R}_+$  is achievable under power constraint  $P$  if for any  $\epsilon > 0$  there exists an  $A \in \mathbb{N}_+$  such that  $\forall n \geq A$ , there exists a broadcast channel code (functions  $f, g_1, g_2$ ) achieving a distortion pair of  $(d_1, d_2)$  such that  $D_i \geq d_i + \epsilon$  for  $i = 1, 2$ .

The collection of all the achievable distortion pairs under power constraint  $P$  for a given bivariate source is denoted by  $\mathcal{D}(P, \rho, N_1, N_2)$ . Such collection can be fully characterized by determining the following function

$$D_2(P, \rho, N_1, N_2, D_1) = \min_{(D_1, d_2) \in \mathcal{D}(P, \rho, N_1, N_2)} d_2. \quad (5.11)$$

The function in (5.11) basically says that to get the region  $\mathcal{D}(\cdot)$ , we should fix  $D_1$  and search for the minimum achieved  $d_2$  given that  $D_1$ . [66] gives such optimal distortion region for the two-user Gaussian Broadcast channel. The bound consists of three regions, and the authors in [66] proved that only a hybrid analog digital scheme could achieve the optimal performance. The authors claim that this is the first case in the literature of Network Information Theory that a hybrid scheme was shown to be required to achieve optimality. They have shown that using optimal digital codes, based on the separation principle (analyzed in [67]), is strictly suboptimal in certain regions. Similarly, uncoded (analog) transmission was analyzed thoroughly in [68] and again

shown to be strictly suboptimal in certain regions. This is indeed a very interesting result and reinforces the points discussed in the introduction about the challenges facing pure digital communication systems. Uncoded transmission, in which a linear combination of  $\mathcal{S}_1$  and  $\mathcal{S}_2$  is transmitted directly, is optimal under certain conditions. Figure 5.5 depicts these regions visually.

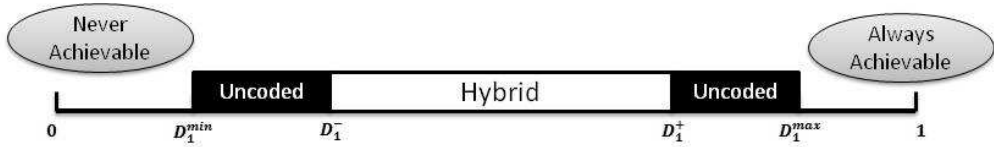


Figure 5.5: Optimal coding schemes and associated regions as described in [13]. Note that the maximum distortion incurred can not be larger than 1 because we are working with sources of variance 1.

A final observation about the Broadcast channel is that feedback indeed *increases* the capacity region [69] for certain classes of Broadcast Channels. This is true for most settings in Multi-Terminal communications, and it should not come as a surprise. On the other hand, we observe that feedback *does not* increase the capacity for point to point communications<sup>6</sup> [40]. This exemplifies the fact that point to point communication is a very special case of the general communication problem, and hence many simple schemes that are generally not optimal for the networked case could be optimal for the point to point case.

### 5.3 Separation Based solutions

This section explores the theoretical limits of separation based schemes<sup>7</sup>. It was shown in [66] that only a hybrid *joint* scheme achieves OPTA. We will discuss the gap in performance that separate source-channel coders incur compared to the optimal hybrid coding system.

<sup>6</sup> Although feedback does not increase capacity for point to point communications, it can reduce the error exponent as well as the complexity of the encoding/decoding significantly.

<sup>7</sup> The results in this section apply to any separation based scheme, whether it is digital, analog or a hybrid scheme.

We first begin with a simple scheme, Scheme A<sup>8</sup>, which encodes  $\mathbf{S}_1$  and  $\mathbf{S}_2$  as if they were independent, resulting in a distortion region given by

$$D_1 \geq \left(1 + \frac{\alpha P}{(1 - \alpha)P + N_1}\right)^{-1} \quad (5.12)$$

$$D_2 \geq \left(1 + \frac{(1 - \alpha)P}{N_2}\right)^{-1}, \quad (5.13)$$

for  $\alpha \in [0, 1]$ . The second scheme we consider, scheme B, decomposes  $\mathbf{S}_2$  into  $\mathbf{S}_2 = \rho\mathbf{S}_1 + \mathbf{E}$ , where  $\mathbf{S}_1 \perp \mathbf{E}$ . The scheme, first introduced in [70], would then treat  $\mathbf{S}_1$  and  $\mathbf{E}$  as two new independent sources, resulting in a distortion region given by

$$D_1 \geq \left(1 + \frac{\alpha P}{(1 - \alpha)P + N_1}\right)^{-1} \quad (5.14)$$

$$D_2 \geq (1 - \rho^2) \left(1 + \frac{(1 - \alpha)P}{N_2}\right)^{-1} + \rho^2 \left(1 + \frac{\alpha P}{(1 - \alpha)P + N_1}\right)^{-1}, \quad (5.15)$$

for  $\alpha \in [0, 1]$ . Scheme B *decorrelates*  $\mathbf{S}_2$  with  $\mathbf{S}_1$  and encodes the difference,  $\mathbf{E}$ . The third scheme, Scheme C, improves on scheme B by decorrelating  $\mathbf{S}_2$  with the quantized first source,  $\hat{\mathbf{S}}_1$ , and not with  $\mathbf{S}_1$  itself. This is an improvement since it is a more accurate representation at the decoder site, since the decoder can only decode and obtain  $\hat{\mathbf{S}}_1$ . Remember that the decoder for  $\mathbf{S}_2$  needs to decode the common message before decoding  $\mathbf{S}_2$ . The distortion achieved by scheme C is given by

$$D_1 \geq \left(1 + \frac{\alpha P}{(1 - \alpha)P + N_1}\right)^{-1} \quad (5.16)$$

$$D_2 \geq [1 - \rho^2(1 - D_1)] \left(1 + \frac{(1 - \alpha)P}{N_2}\right)^{-1}, \quad (5.17)$$

for  $\alpha \in [0, 1]$ .

None of the above schemes are optimal for the general case, although they progressively provide better performance. The authors in [67] claim that successive coding is the optimal scheme for separate Broadcast channel coding. The previous

---

<sup>8</sup> Following the notation in [67].

schemes (A,B,C) encoded  $\mathbf{S}_1$  as the common message and in the refinement layer they encoded some version of  $\mathbf{S}_2$ . Successive coding performs encoding for *both* ( $\mathbf{S}_1, \mathbf{S}_2$ ) at the common layer, as well as the refinement layer *jointly* [71]. The distortion region achieved by successive coding does not have a closed form expression and is given parametrically by

$$\begin{aligned} R_1(\alpha) &= \frac{1}{2} \log \frac{1 - \rho^2}{D_1(1 - \alpha^2\delta) - (\rho - \alpha\delta)^2} \\ R_2(\alpha) &= \left[ \frac{1}{2} \log \frac{1 - \alpha^2\delta}{D_2} \right]^+, \end{aligned} \quad (5.18)$$

where

$$\begin{aligned} \alpha &\in \left[ \rho, \min\left(\frac{1}{\rho}, \frac{\rho}{\delta}, \alpha^*\right) \right] \\ \delta &= 1 - D_1 \\ \alpha^* &= \sqrt{\frac{1 - D_2}{\delta}} \end{aligned} \quad (5.19)$$

This scheme was proved to be the best separation based scheme for the two-user Gaussian Broadcast channel in [71]. We shall benchmark our proposed communication system against the optimal successive coding scheme given by (5.18, 5.19). Figure 5.6 shows the performance of the three schemes A, B and C as well as the optimal separation based schemes of (5.18).

#### 5.4 Analog Mappings for The Broadcast Channel

As explained earlier, we are searching for an encoding function,  $g(\cdot)$ , that takes the data intended for the first user,  $s_1$ , and the second user,  $s_2$ , to produce the channel output,  $x$ . Each receiver observes a corrupted version of  $x$  and each employs a decoding function  $g_i$  to obtain its data,  $s_i$ .

Several schemes have been proposed for the Broadcast channel in the literature: The authors in [72, 61] used calculus of variation techniques to design the optimal encoder and decoder pairs, which performs well but is complex to design and train. The

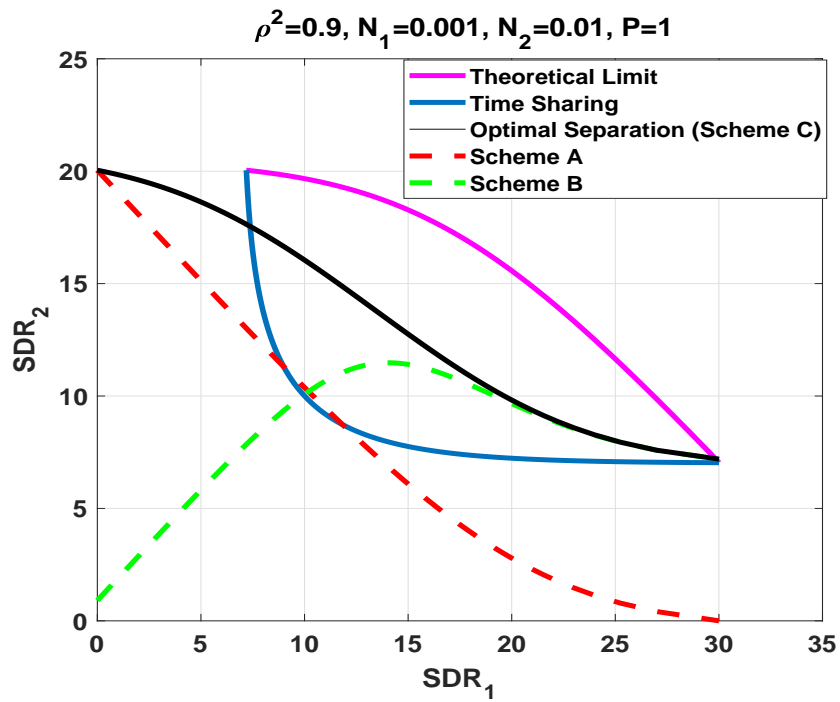
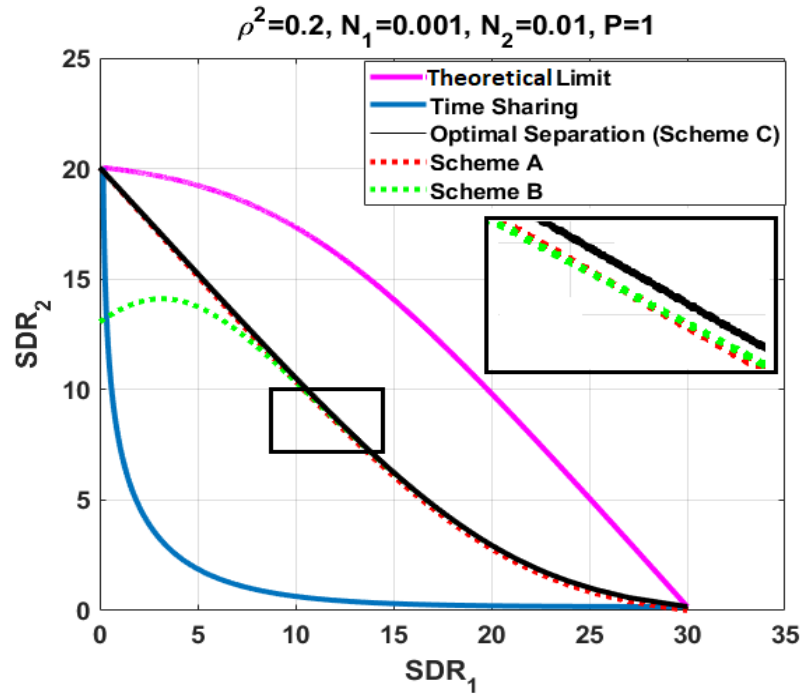


Figure 5.6: Different Separation Based schemes for different values of  $\rho$ . Notice that the optimal separation based scheme is equivalent to Scheme C.

authors in [73] performed optimizations on particular analog mappings, and designed a “distortion balancing” framework in which target users’ distortions can be easily achieved. The “distortion balancing” scheme performs well and is less complex than the schemes [72, 61]. In this Chapter, we consider an analog mapping scheme, with little encoding and decoding complexity, which offers excellent performance that will be shown to outperform the best separation-based scheme. The proposed scheme is a variant of the Nested Quantization and the Scalar Quantizer Linear Coder (SQLC) [58, 57] techniques, and is termed Alternating-Sign SQLC.

The mappings we consider here are based on a variant of Nested Quantization, NQ [58], called *Scalar Quantizer Linear Coder*, SQLC, which was proposed in [9] for the Multiple Access Channel (MAC). In SQLC, the first symbol,  $s_1$ , is passed through a uniform quantizer of step  $2\Delta$  to produce  $v_1$ . The second symbol,  $s_2$ , is scaled by  $\alpha$  and clipped to force it to lie in the interval  $[-\Delta, \Delta]$  to produce  $v_2$ . The sum of  $v_1 + v_2$  is sent through the channel after scaling it by a factor,  $\beta$ , which controls the power of the transmission system. That is

$$v_1 = 2\Delta \left\lceil \frac{s_1}{2\Delta} \right\rceil \quad (5.20)$$

$$v_2 = \mathcal{L}_{\pm\Delta}(\alpha s_2) \quad (5.21)$$

$$\eta = v_1 + v_2 \quad (5.22)$$

$$x = \beta \eta, \quad (5.23)$$

where  $\lceil \cdot \rceil$  rounds its argument to the nearest integer,  $\alpha$  controls the spread of the second symbol and  $\mathcal{L}_{\pm\Delta}[\cdot]$  forces its output to lie within the interval  $[-\Delta, \Delta]$ . That is

$$\mathcal{L}_{\pm\Delta}(\lambda) = \begin{cases} \lambda & \text{if } -\Delta \leq \lambda \leq \Delta \\ \Delta & \text{if } \lambda > \Delta \\ -\Delta & \text{if } \lambda < -\Delta \end{cases} \quad (5.24)$$

Note that  $\lceil \frac{s_1}{2\Delta} \rceil$  in (5.20) produces an *integer* (positive, negative or zero). This integer is then scaled by  $2\Delta$  to produce  $v_1$ . A system diagram of the AS-SQLC encoder is shown in Figure 5.7.

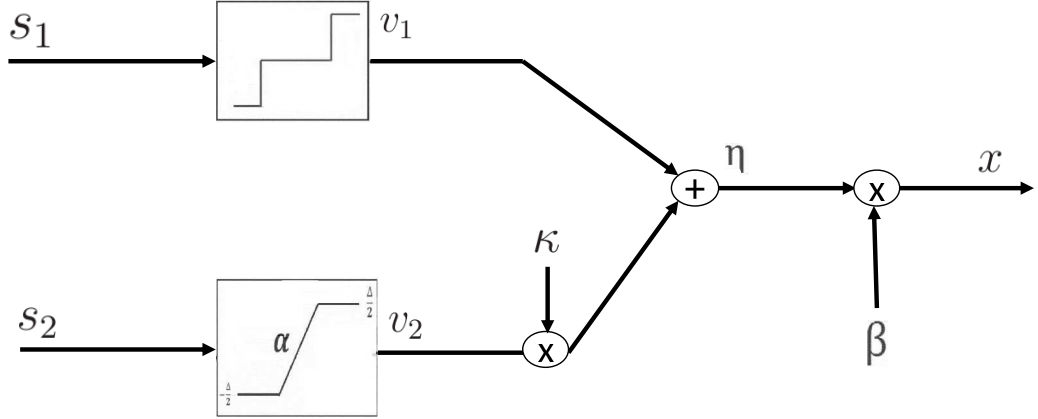


Figure 5.7: Encoder for an AS-SQLC system.

Each user of the Broadcast channel channel employs a channel decoder to decode the AS-SQLC scheme. The standard decoder, discussed in [13], receives  $y = x + z$ <sup>9</sup>, where  $z \sim \mathcal{N}(0, N_i)$ , and performs MMSE decoding on  $z$  to obtain the MMSE estimate of  $\eta$  as

$$\hat{\eta} = \frac{\beta}{N_i + \beta^2} y. \quad (5.25)$$

Then, the decoder quantizes  $\hat{\eta}$  according to (5.20) to obtain an estimate of the quantized first symbol,  $\hat{v}_1$ , as  $\hat{v}_1 = 2\Delta \lceil \frac{\hat{\eta}}{2\Delta} \rceil$ . The second symbol estimate is obtained by subtracting  $\hat{v}_1$  from  $\hat{\eta}$ , that is  $\hat{v}_2 = \hat{\eta} - \hat{v}_1$ . The transmitted symbol pair is estimated from  $(\hat{v}_1, \hat{v}_2)$  as

---

<sup>9</sup> Since there are two decoders, we should use a subscript for each of the users received data,  $y_i$ , and noise  $z_i$ . We will drop the superscript for simplicity, and note that the decoder is identical at the two users' sites, and is only parametrized by the noise variance  $N_i$ .

$$\hat{s}_1 = \hat{v}_1 \quad (5.26)$$

$$\hat{s}_2 = \frac{1}{\alpha} \hat{v}_2. \quad (5.27)$$

The system diagram of the decoder is shown in Figure 5.8<sup>10</sup>.

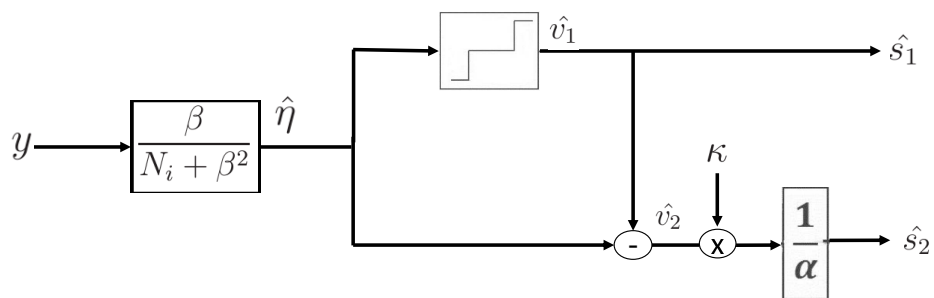


Figure 5.8: The decoder of AS-SQLC systems. There are two instances of the decoder, one at each user site. The decoder is parametrized by the received noise variance,  $N_i$ .

SQLC can be thought as equivalent to projecting the source pair  $(s_1, s_2)$  onto a space filling curve of dimension 1 to produce  $(v_1, v_2)$ , as shown in Figure 5.9. As Figure 5.9 shows, we project the source  $(s_1, s_2)$  to the nearest branch of the SQLC curve. If the noise moves that projected symbol to a different branch, the resulting distortion is typically severe. This effect is typically referred to as the threshold effect [13, 14], in which a small noise in the input causes a big distortion in the decoded symbol, and is caused by the discontinuity of the SQLC curve [13]. A modification of SQLC termed Alternating Sign SQLC was described in [13] to alleviate this problem. AS-SQLC works as SQLC with the difference in how  $v_2$  is generated: rather than using

---

<sup>10</sup> It is important to remark that (5.27) is suboptimal. In the next section, we discuss how to perform optimal decoding on the second source.

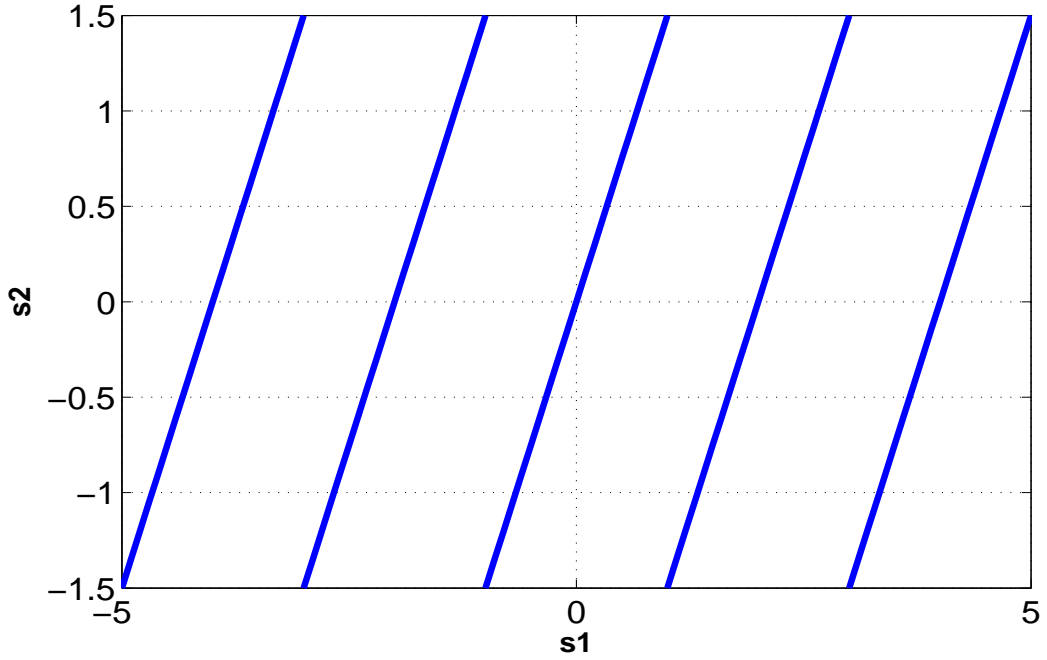


Figure 5.9: Space filling curve corresponding to the proposed SQLC system. Source symbols  $(s_1, s_2)$  are projected onto the curve to produce  $(v_1, v_2)$ .

(5.21), in AS-SQLC the second user symbol is generated according to

$$v_2 = \kappa \mathcal{L}_{\pm\Delta}(\alpha s_2) \quad (5.28)$$

where

$$\kappa = \begin{cases} +1 & \text{when } \lceil \frac{v_1}{2\Delta} \rceil \text{ is even} \\ -1 & \text{when } \lceil \frac{v_1}{2\Delta} \rceil \text{ is odd .} \end{cases} \quad (5.29)$$

At the decoder, we use the same procedure as in SQLC, with the difference on how  $\hat{y}_2$  is obtained. Specifically,  $\hat{y}_2$  is obtained by multiplying the estimate by the factor  $\kappa$  as follows

$$\hat{v}_2 = \kappa (\hat{\eta} - \hat{v}_1) \quad (5.30)$$

where

$$\kappa = \begin{cases} +1 & \text{when } \lceil \frac{\hat{v}_1}{2\Delta} \rceil \text{ is even} \\ -1 & \text{when } \lceil \frac{\hat{v}_1}{2\Delta} \rceil \text{ is odd.} \end{cases} \quad (5.31)$$

This is equivalent to projecting the source pair  $(s_1, s_2)$  onto the space filling curve shown in Figure 5.10. Note that this space filling curve is *continuous* and  $s_2$  does not experience any threshold effect. The complete system diagram including the transmitter and receiver is shown in Figure 5.11.

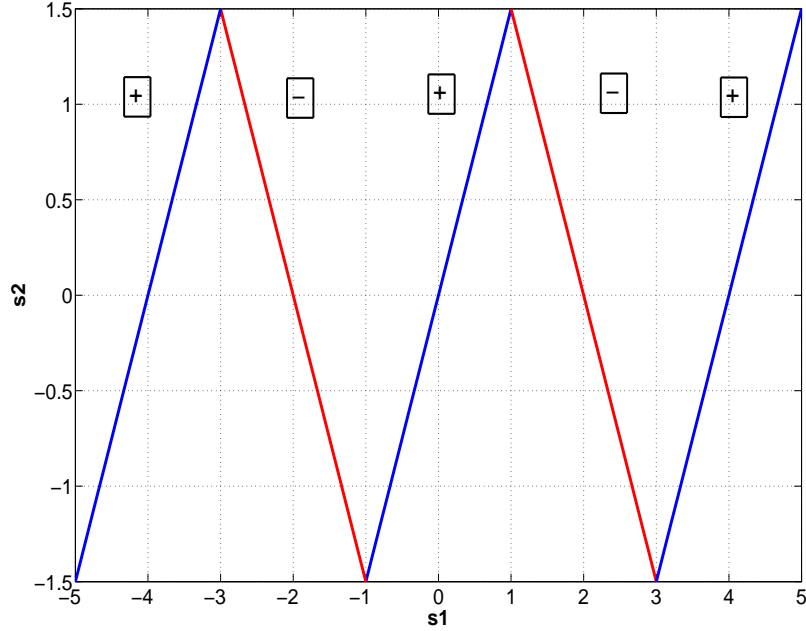


Figure 5.10: Space filling curve for AS-SQLC. The two sources  $(s_1, s_2)$  are projected onto the curve and the resulting pair is transmitted as indicated in the text. Notice the *continuity* of the curve, eliminating the threshold effect.

It is interesting to remark the difference between the space filling curve in Figure 5.10 and standard space filling curves designed for point to point communication, such as Shannon-Kotelnikov mappings (see [38] and [37]). Standard space filling curves are designed for a *symmetric* distortion case. For example, the 2:1 Archimedes spiral, discussed in Section 2.2.2, transmits two source symbols, which can be regarded as

each of the user' data in the Broadcast channel. The Archimedes spiral is designed to minimize the *average* distortion of both symbols. That is, the distortion incurred by user 1,  $D_1$ , is usually the same as the distortion incurred by user 2,  $D_2$ . However, the proposed space filling curve for the broadcast channel shown in Figure 5.10 has the advantage of being able to control the distortions incurred by each user. This is achieved by changing the quantization step,  $\Delta$ . If  $\Delta$  is small, source 1,  $s_1$ , will be finely quantized and the resulting distortion,  $D_1$ , will be small. At the same time, since  $\Delta$  is small, source 2,  $s_2$  will be “squeezed” and fit within the small interval  $[-\frac{\Delta}{2}, \frac{\Delta}{2}]$  so that  $D_2$  will be large. On the other hand, if  $\Delta$  is large, source 1 is quantized coarsely and incurs in a large distortion. At the same time,  $s_2$  is spread over a longer interval and  $D_2$  will be smaller.

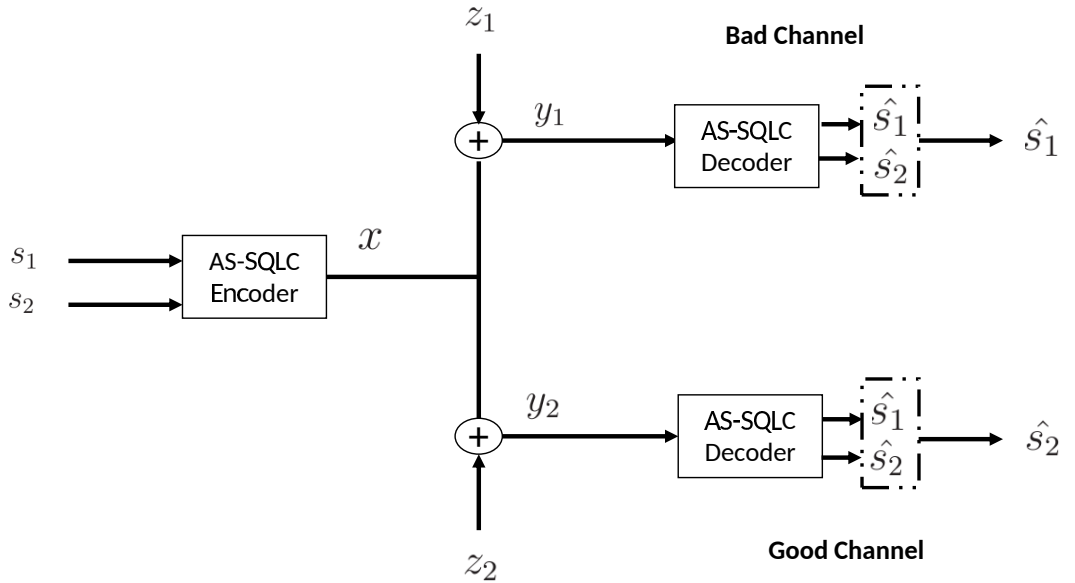


Figure 5.11: Complete system diagram of the AS-SQLC system.

## 5.5 Rationale of AS-SQLC

In this section, we discuss the rationale for the use of AS-SQLC over standard SQLC. Intuitively, there should be a performance gain as the threshold effect would

be eliminated, and we will quantify this gain here. As explained in Section 5.4, SQLC systems send a discrete component  $s_1$  and an analog component  $s_2$ . As shown in Figure 5.12(a), in SQLC the analog component experiences a threshold effect due to the way the separation between the discrete and analog components is handled. On the other hand, when using AS-SQLC, the analog source does not experience a threshold effect (Figure 5.12(b)).

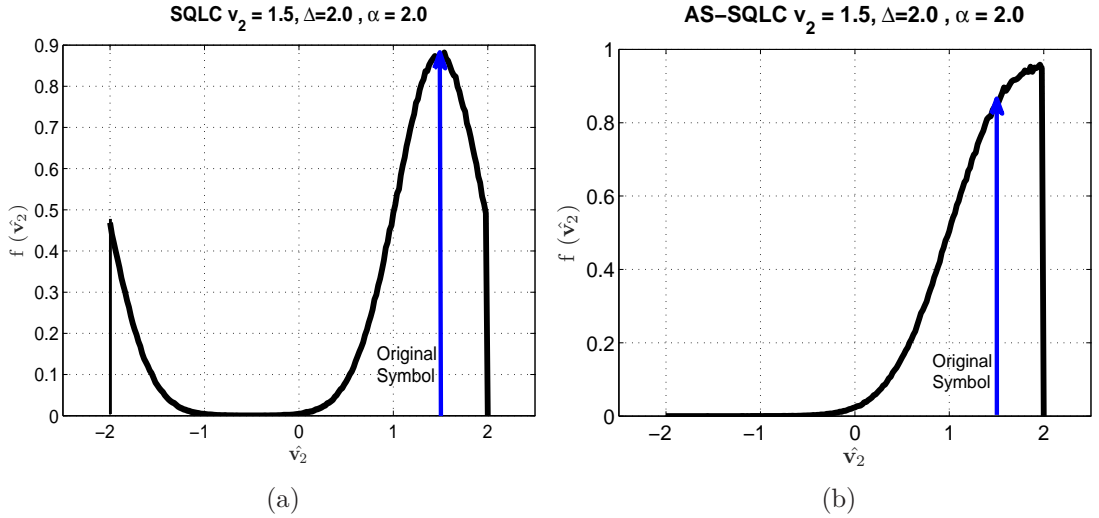


Figure 5.12: Distribution of  $\hat{v}_2$ , when  $v_2 = 1.5$ . (a) SQLC; (b) AS-SQLC. Notice the disappearance of the threshold effect in 5.12(b).

Next, we calculate the achievable information rate for both schemes (SQLC and AS-SQLC) by calculating the mutual information between the transmitted source,  $\mathbf{S}_2$ , and the received symbol at the input to the second source decoder,  $\hat{\mathbf{V}}_2$ . This is given by

$$I(\mathbf{S}_2, \hat{\mathbf{V}}_2) = h(\hat{\mathbf{V}}_2) - h(\hat{\mathbf{V}}_2 | \mathbf{S}_2) \int_{\hat{v}_2} f(\hat{v}_2) \log\left(\frac{1}{f(\hat{v}_2)}\right) - \int_{s_2} \int_{\hat{v}_2} f(s_2, \hat{v}_2) \log\left(\frac{f(s_2)}{f(s_2, \hat{v}_2)}\right), \quad (5.32)$$

for  $\hat{v}_2 \in \hat{\mathbf{V}}_2 = [-\Delta, \Delta]$  and  $s_2 \in \mathbf{S}_2 = [-\Delta, \Delta]$ . An example of the distribution of  $\mathbf{V}_2$  for different values of  $\Delta$  and  $\alpha$  is shown in Figure 5.13.

The mutual information in (5.32) depends on three factors,  $\Delta$ ,  $\alpha$  and  $N_2$ . Evaluating (5.32) analytically is difficult because of the highly non-linear nature of the

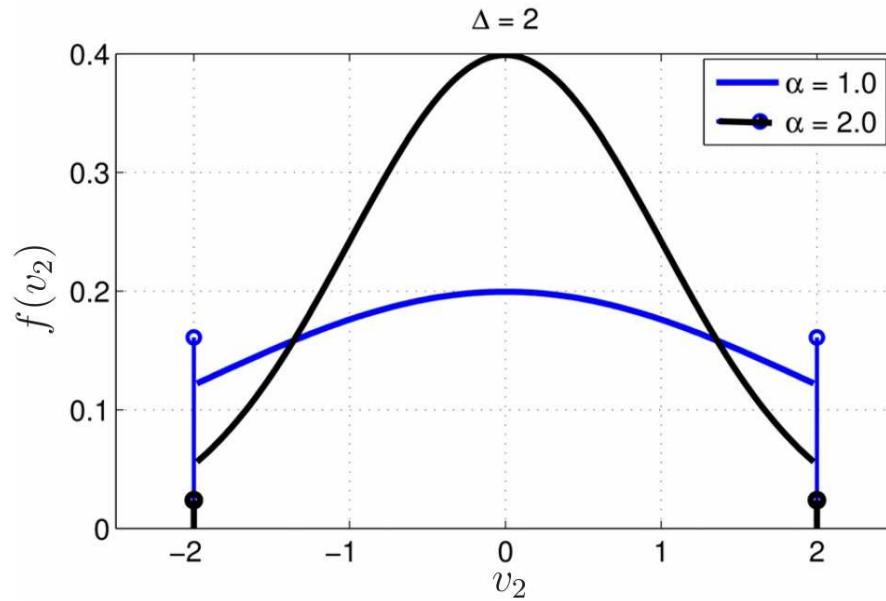


Figure 5.13: Distribution of  $\mathbf{V}_2$  for two different values of  $\alpha$ . Increasing  $\alpha$  makes the distribution more uniform but increases the percentage of data that gets clipped.

channel due to the potential clipping and reversing of the received symbol. Thus, we evaluated (5.32) via Monte Carlo techniques. The results are shown in Figure 5.14.

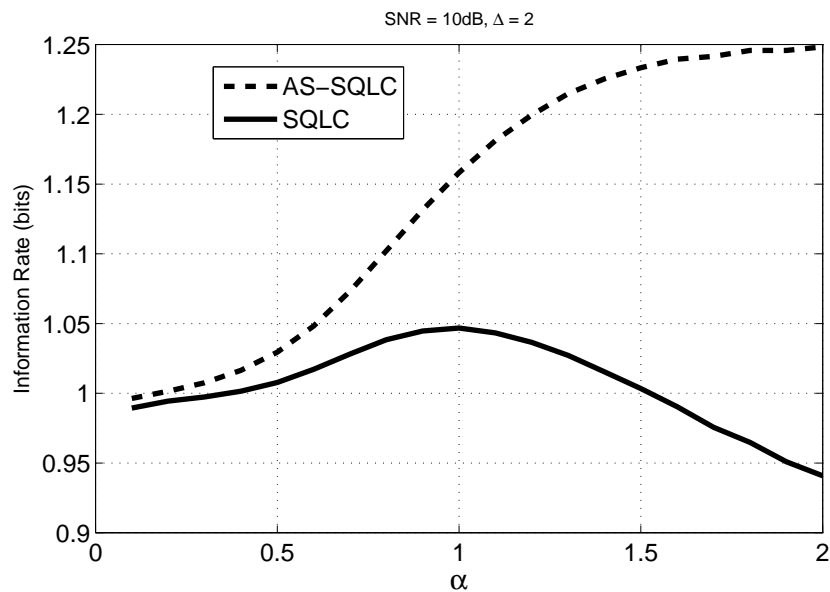


Figure 5.14: Information rates obtained by the SQLC and the AS-SQLC systems.

As shown in Figure 5.13, increasing  $\alpha$  increases the spread of  $\mathbf{S}_2$  so that the

interval  $[-\Delta, \Delta]$  is filled in more uniformly, while at the same time it increases the percentage of  $\mathbf{S}_2$  that gets clipped. For SQLC systems, increasing  $\alpha$  has the initial effect of increasing the information rate of the system since the sources are spread more uniformly in  $[-\Delta, \Delta]$ . However, further increases in  $\alpha$  put more symbols near the edge at  $\pm\Delta$ , and causes these symbols to experience the threshold effect, which significantly decreases the information rate. On the other hand, the AS-SQLC system does not suffer from the threshold effect and we continue to see information rate improvements with  $\alpha$ , as the symbols spread more uniformly over  $[-\Delta, \Delta]$ . Of course, the improvement plateaus for high values of  $\alpha$  (increases of  $\alpha$  above 2.0, not shown in Figure 5.14, results in a decrease in the information rate, as more data symbols are clipped to  $\pm\Delta$ ). Note the SQLC and AS-SQLC schemes are identical in the treatment of the first source  $\mathbf{S}_1$ , and the above analysis was only needed for  $\mathbf{S}_2$ .

## 5.6 Distortion Analysis and Optimal Decoder

The distortion measure used here is the mean squared error distortion (MSE). The MSE distortion experienced by the second source  $\mathbf{S}_2$  is given by

$$D_2 = \frac{1}{\sqrt{2\pi}} \int_{s_2} e^{-\frac{s_2^2}{2}} \int_{z_2} \frac{1}{\sqrt{2\pi N_2}} e^{-\frac{z_2^2}{2N_2}} (s_2 - \Psi(\hat{v}_2))^2 dz_2 ds_2, \quad (5.33)$$

where  $\hat{y}_2$  is shown in Figure 5.8, and  $\Psi(\cdot)$  is the decoding function. We now discuss how to obtain the integration regions for (5.33), which are key to obtaining the optimal decoding function,  $\Psi$ . In [13]  $\hat{s}_2$  was chosen for simplicity to be

$$\hat{s}_2 = \Psi(\hat{v}_2) = \frac{1}{\alpha} \hat{y}_2. \quad (5.34)$$

However, (5.34) is not the optimal decoding rule that minimizes (5.33). Our aim is to calculate the optimal decoding rule,  $\Psi$ . We begin by obtaining a direct relationship between  $\hat{v}_2$  and  $s_2$ . To that end, we observe that the relationship depends on the

branch where the noise allocates the received symbol. Hence

$$\hat{v}_2 = \begin{cases} \mathcal{L}_{\pm\Delta}(\alpha s_2) + n & \text{if } -\Delta < \mathcal{L}_{\pm\Delta}(\alpha s_2) + n < \Delta \\ 2\Delta - \mathcal{L}_{\pm\Delta}(\alpha s_2) - n & \text{if } \Delta < \mathcal{L}_{\pm\Delta}(\alpha s_2) + n < 3\Delta \\ -2\Delta - \mathcal{L}_{\pm\Delta}(\alpha s_2) - n & \text{if } -3\Delta < \mathcal{L}_{\pm\Delta}(\alpha s_2) + n < -\Delta, \end{cases} \quad (5.35)$$

and so on for every branch.

Following (5.35), we can break (5.33) into several branches and eliminate the non-linearity resulting from the quantization of the received symbol  $x$ . Specifically, we can break the non-linearity resulting from the clipping function by considering the three regions of  $\mathcal{L}_{\pm\frac{\Delta}{2}}(\cdot)$  separately (similar to (5.24)), so that  $D_2$  is given by

$$D_2 = D_2^\Delta + D_2^{center} + D_2^{-\Delta}, \quad (5.36)$$

where  $D_2^{center}$  is the distortion incurred by  $s_2 \in [-\frac{\Delta}{\alpha}, \frac{\Delta}{\alpha}]$ ,  $D_2^\Delta$  is the distortion experienced by  $s_2 > \frac{\Delta}{\alpha}$ , and  $D_2^{-\Delta}$  is the distortion experienced by  $s_2 < -\frac{\Delta}{\alpha}$ .

$$\begin{aligned} D_2^{center} = & \frac{1}{\sqrt{2\pi}} \int_{-\frac{\Delta}{\alpha}}^{\frac{\Delta}{\alpha}} e^{-\frac{s_2^2}{2}} \int_{-\Delta-\alpha s_2}^{\Delta-\alpha s_2} \frac{1}{\sqrt{2\pi N_2}} e^{-\frac{z_2^2}{2N_2}} (s_2 - \Psi(\hat{v}_2))^2 dz_2 ds_2 + \\ & \frac{1}{\sqrt{2\pi}} \int_{-\frac{\Delta}{\alpha}}^{\frac{\Delta}{\alpha}} e^{-\frac{s_2^2}{2}} \int_{\Delta-\alpha s_2}^{3\Delta-\alpha s_2} \frac{1}{\sqrt{2\pi N_2}} e^{-\frac{z_2^2}{2N_2}} (s_2 - \Psi(\hat{v}_2))^2 dz_2 ds_2 \\ & \frac{1}{\sqrt{2\pi}} \int_{-\frac{\Delta}{\alpha}}^{\frac{\Delta}{\alpha}} e^{-\frac{s_2^2}{2}} \int_{-3\Delta-\alpha s_2}^{-\Delta-\alpha s_2} \frac{1}{\sqrt{2\pi N_2}} e^{-\frac{z_2^2}{2N_2}} (x_2 - \Psi(\hat{v}_2))^2 dz_2 ds_2 + \dots \end{aligned} \quad (5.37)$$

The terms in (5.37) correspond to the case over the main branch and the two cases over the neighboring branches. The dots mean that we should add other neighboring branches to get a better estimate of (5.37). To obtain  $D_2^\Delta$  and  $D_2^{-\Delta}$ , we simply perform the outer integration on  $s_2$  over  $[\frac{\Delta}{\alpha}, \infty]$  and  $[-\infty, -\frac{\Delta}{\alpha}]$ , respectively, rather than over  $[-\frac{\Delta}{\alpha}, \frac{\Delta}{\alpha}]$ , and also replace  $\alpha s_2$  in the inner integral. Note that although all the terms in (5.37) contain  $\hat{v}_2$ , its value is different and its specific realization is given according to (5.35).

Once we have expressed  $D_2$  as a sum of linear terms, we have to find the decision function  $\Psi$  that minimizes that distortion. Obtaining the optimal decoding function is a classical variational problem that can be solved by variational techniques. A similar problem was studied in [74, 60, 61], where the authors jointly designed the encoder/decoder pair and proved that their solution was a local minima but not a global one. Here, the encoding function is specified in (5.10). This greatly simplifies the process of finding the optimal decoding function. Indeed, the decoding function is nothing but a map that takes an observed symbol  $\hat{v}_2 \in [-\Delta, \Delta]$  and produces a decision  $\Psi(\hat{v}_2)$ . Notice that if we choose the value of  $\Psi(b) = q$ , then this choice has no effect on how we should proceed in choosing the optimal  $\Psi(a)$  when  $b \neq a$ <sup>11</sup>. This means that we fix the received symbol  $\hat{v}_2 = b$  and find the optimal  $\Psi(b)$ , which is a single number rather than an entire function, and repeat the procedure for all values of  $b$ .

Once we have fixed the received symbol to be  $\hat{v}_2 = b$ , we need to integrate over all admissible values of  $s_2$  and  $n$  in (5.36). To that end, note that once a value of  $s_2$  is chosen, then  $z_2$  is determined by which branch  $b$  is in (since we do not know which branch  $b$  lies in, we have a sum in (5.37)). For instance, if  $|\alpha s_2| < \Delta$  and  $b$  lies in the first branch, then from (5.35)  $z_2 = b - \alpha s_2$ .

Hence given that we received  $b$ , the goal is to find the value of  $q$  that minimizes the distortion at this point. Equation (5.36) can be written as

$$D_2 = \min_q \sum_{\mathbf{S}_2} \sum_{\text{noise branches}} \frac{1}{\sqrt{2\pi}} \int_{\mathbf{S}_2} e^{-\frac{s_2^2}{2}} \int_{\mathcal{R}_{z_2}} \frac{1}{\sqrt{2\pi N_2}} e^{-\frac{z_2^2}{2N_2}} (s_2 - q)^2 dz_2 ds_2, \quad (5.38)$$

where  $\mathcal{R}_{z_2}$  is an integration region to determine the probability of the noise,  $z_2$

$$\mathcal{R}_{z_2} = [z_2 - \epsilon, z_2 + \epsilon] \text{ for } \epsilon > 0. \quad (5.39)$$

---

<sup>11</sup> This was not the case in [74], since there it was necessary to obtain the optimal encoding function as well, which made the problem global.

Setting the derivative of (5.38) (w.r.t  $q$ ) to 0, we obtain the optimal value of  $q$  as

$$\hat{q} = \frac{\sum \sum \frac{1}{\sqrt{2\pi}} \int e^{-\frac{s_2^2}{2}} \int \frac{1}{\sqrt{2\pi N_2}} e^{-\frac{z_2^2}{2N_2}} dz_2 ds_2}{\sum \sum \frac{1}{\sqrt{2\pi}} \int e^{-\frac{s_2^2}{2}} \int \frac{1}{\sqrt{2\pi N_2}} e^{-\frac{z_2^2}{2N_2}} x_2 dz_2 ds_2}. \quad (5.40)$$

The optimal function  $\Psi$  is shown in Figure 5.15(a) when SNR=8 dB,  $\Delta = 1$  and  $\alpha = 1.2$ , while Figure 5.15(b) shows the optimal  $\Psi$  for SNR=20 dB,  $\Delta = 1$  and  $\alpha = 1.2$ . The optimal decoding function differs in several ways from the simple detector given in (5.27). First, the difference depends on the operating SNR. When all other parameters are fixed, increasing the SNR has the tendency to “dampen” the decoding function and flatten it out near  $\pm\Delta$  as evident in Figure 5.15(b). Also increasing  $\alpha$  has the effect of “stretching” the function as seen in Figure 5.15(a).

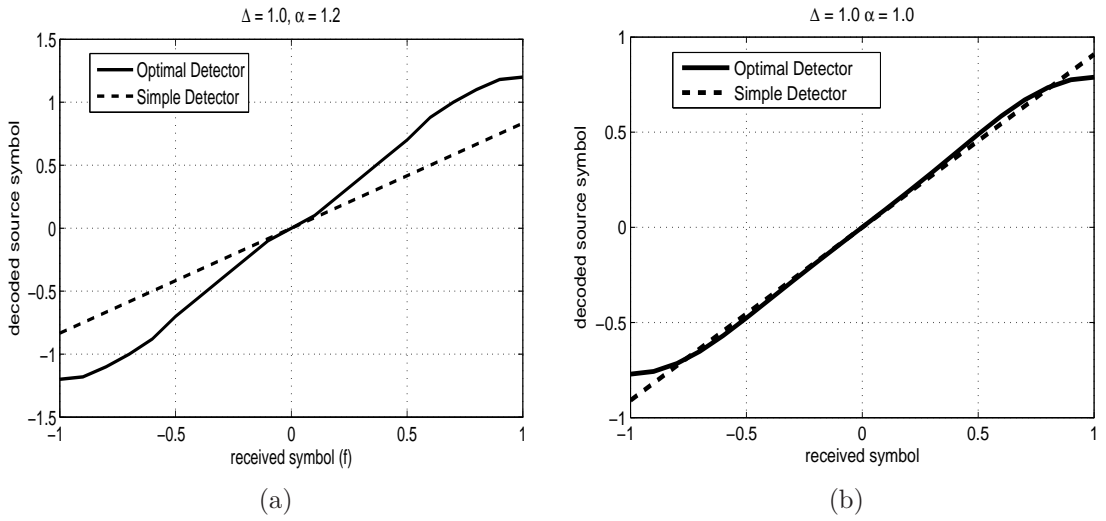


Figure 5.15: Optimal detector function  $\Psi$  vs the suboptimal function in [13]. (a) SNR=8 dB,  $\Delta = 1.0, \alpha = 1.2$ ; (b) SNR=20 dB,  $\Delta = 1.0, \alpha = 1.0$ .

## 5.7 AS-SQLC Generalization to Correlated Sources

This section shows how AS-SQLC can be generalized for correlated sources. We will modify the scheme in Section 5.4 by adding a pre-encoding block at the transmitter (and a corresponding decoder at the receiver). The pre-encoding block is a  $2 \times 2$  matrix,  $\mathbf{H} = [a \ b ; c \ d]$ , that is applied to  $[\mathbf{S}_1 \ \mathbf{S}_2]'$  before the AS-SQLC encoder to produce

$[\mathbf{W}_1 \ \mathbf{W}_2]' = \mathbf{H} \cdot [\mathbf{S}_1 \ \mathbf{S}_2]'$ . The system diagram described in section 5.4 can be thought of as a special case of this system when  $\mathbf{H}$  is set to the identity matrix,  $\mathbf{I}$ . The generalized system diagram is shown in Figure 5.16.

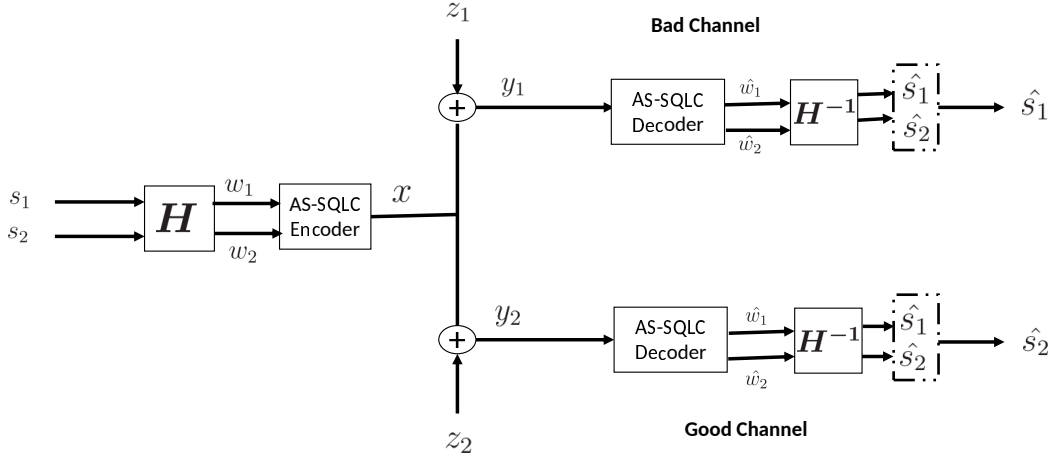


Figure 5.16: Complete system diagram of the generalized AS-SQLC system for transmitting correlated sources.

The intuition behind having a pre-encoder is captured by observing that the Bivariate Gaussian source can be written as a combination of 3 different mutually independent i.i.d single Gaussian normal sources  $\mathbf{E}, \mathbf{I}_1, \mathbf{I}_2$ . Specifically,

$$\mathbf{S}_1 = \rho \mathbf{E} + \sqrt{1 - \rho^2} \mathbf{I}_1 \quad (5.41)$$

$$\mathbf{S}_2 = \rho \mathbf{E} + \sqrt{1 - \rho^2} \mathbf{I}_2. \quad (5.42)$$

If we use  $\mathbf{H} = [1 \ 0; -1 \ 1]$ , then  $\mathbf{W}_1 = \mathbf{S}_1$  and  $\mathbf{W}_2 = \sqrt{1 - \rho^2} \mathbf{I}_2 - \sqrt{1 - \rho^2} \mathbf{I}_1$ . The power of  $\mathbf{W}_2$  is  $2(1 - \rho^2)$ , while  $\mathbf{S}_2$  has a power of 1. When the correlation,  $\rho$ , is very high,  $\mathbf{W}_2$  has much less power than  $\mathbf{S}_2$ <sup>12</sup>. Thus,  $\mathbf{W}_2$  can potentially communicate the extra necessary information, that along with  $\mathbf{S}_1$ , required by the receiver to faithfully reconstruct  $\mathbf{S}_2$  at a lower power cost. This argument is not very quantitative, but it is

<sup>12</sup> If  $\mathbf{H} = \mathbf{I}$  is used, then we would not see the power reduction in  $\mathbf{W}_2$ , since it will have the same power as  $\mathbf{S}_2$ .

meant to show that we can save energy on encoding  $\mathbf{S}_2$  in the refinement layer. This line of thinking here is similar to that of scheme C in section 5.3, namely, trying to encode the *marginal* ( $\mathbf{S}_2|\mathbf{S}_1$ ). Our proposed analog scheme is not completely successful in that regard because, given  $\mathbf{S}_1$ , we only need to encode  $\sqrt{1-\rho^2} \mathbf{I}_2$ , yet we also capture  $\sqrt{1-\rho^2} \mathbf{I}_1$ . This is not a problem produced by the choice of the pre-encoding matrix  $\mathbf{H}$ , but rather inherent to the system architecture, where we are operating *algebraically* on the sources (scheme C and other Information Theoretic constructs assume *statistical* processing of the data that involves the law of large numbers). We cannot fully exploit the statistical properties of the source since by construction our system is a zero delay one. Another reason that justifies the use of the precoding matrix  $\mathbf{H}$  is that, as mentioned before, AS-SQLC is very suitable for asymmetric sources (or rather achieving asymmetric distortion criteria). The pre-coding matrix gives the system designer extra parameters to configure the source distribution for the AS-SQLC scheme input. Without the precoding matrix  $\mathbf{H}$ , the two inputs to the AS-SQLC (at the quantization and refinement layer) would be indeed symmetric.

### 5.7.1 Distortion Analysis and Decoder Design

In this subsection, we generalize the distortion analysis performed in Section 5.6 to the case of correlated sources. Moreover, Section 5.6 only derived the optimal decoder for the analog source branch,  $\mathbf{S}_2$ , and not for  $\mathbf{S}_1$ . Here, we derive the optimal decoder for *both* components. Again we use the MSE as the distortion metric we want to minimize

$$D_1 = \int_{z_1} \int_{s_1} \int_{s_2} p(z_1, s_1, s_2) (g_1(f(s_1, s_2) + z_1) - s_1)^2 ds_2 ds_1 dz_1 \quad (5.43)$$

$$D_2 = \int_{z_2} \int_{s_1} \int_{s_2} p(z_2, s_1, s_2) (g_2(f(s_1, s_2) + z_2) - s_2)^2 ds_2 ds_1 dz_2, \quad (5.44)$$

where the output of  $f(\cdot, \cdot)$  is subject to an average power constraint  $P$ . This general problem formulation will lead us to jointly find an encoding function and two decoding functions ( $f, g_1, g_2$ ). This is a non trivial variational problem and was addressed in [72].

The solution in [72] used practical iterative methods to find an optimal  $(f, g_1, g_2)$ . For a fixed encoding function,  $f$ , a (locally) optimum  $(g_1, g_2)$  would be found, then for a fixed  $(g_1, g_2)$  a (locally) optimum  $f$  would be found. The algorithm iterates for a fixed number of iterations or until a certain criteria is met.

Here, we follow a simple approach, fixing the encoding function  $f$  based on the AS-SQLC scheme described in Section 5.7. Given the encoding function, we obtain the decoding functions  $(g_1, g_2)$ . Note that the AS-SQLC scheme has three different parameters  $(\Delta, \alpha, \mathbf{H})$ , and we will search over all possible values<sup>13</sup>  $(\Delta, \alpha, \mathbf{H})$  to find the corresponding  $D_1, D_2$ . Hence we will have a table of  $(\Delta, \alpha, \mathbf{H}, D_1, D_2)$ , and we can perform a table lookup to decide which encoder parameters to use for a given  $(D_1, D_2)$ .

The analysis done in Section 5.6 assumed that the first step in decoding was to simply decode  $\hat{s}_1$  using a simple MMSE inverse to the quantization process. The decoder would map the received symbol to the nearest quantization “center”. The optimal decoder for  $s_2$  was then derived. That analysis also assumed no correlation between  $s_1$  and  $s_2$ . In this section, we generalize that analysis and we come up with the generalized optimal decoder for both  $s_1, s_2$  and for general  $\rho$ .

We can denote  $f(s_1, s_2) + z_i$  by  $h_i$  in (5.43). Moreover, we can replace the integrand over  $z_i$  by one over  $h_i$  (notice that the noise is linear and it is a mere translation of the original integrand). Moreover, as discussed earlier, for a fixed  $f$ , we can minimize  $D_1$  and  $D_2$  *independently*. Hence, from (5.43), the optimal attainable distortion can be written as

$$D_i^{opt} = \min_{g_i} \int_{h_i} \int_{s_1} \int_{s_2} p(h_i, s_1, s_2) (g_i(h_i) - s_i)^2 ds_2 ds_1 dh_i, \quad (5.45)$$

for  $i = 1, 2$ . Equation (5.45) is searching for a function that takes a received symbol  $h_i$  and gives out a single number. This is very similar to what we did in Section 5.6 but instead of integrating over one variable ( $s_2$  previously), we are integrating over both

---

<sup>13</sup> Note that it is not technically possible to search over all values of  $(\Delta, \alpha, H)$  since they are *continuous* variables. We will be *sampling* the domain of each variable at adequately finer steps.

$(s_1, s_2)$  jointly. Similar to Section 5.6, we can obtain a map of received and optimal decoded values. Hence for a particular received symbol,  $h_i = \zeta_i$ , the corresponding optimal decoded value  $g_i(\zeta_i) = q$ , obtained by setting the derivative of (5.45) to zero, is given by

$$g_i(t) = q = \frac{\int_{s_1} \int_{s_2} p(s_1, s_2) p(\zeta_i | s_1, s_2) s_2 ds_2 ds_1}{\int_{s_1} \int_{s_2} p(s_1, s_2) p(\zeta_i | s_1, s_2) ds_2 ds_1}. \quad (5.46)$$

Notice that we have broken  $p(\zeta_i, s_1, s_2)$  into  $p(s_1, s_2)p(\zeta_i | s_1, s_2)$ . The first term,  $p(s_1, s_2)$  is the probability distribution of a normally distributed jointly Gaussian source with a correlation of  $\rho$ . The latter term,  $p(\zeta_i | s_1, s_2)$ , can be obtained by noting that  $\zeta_i$  is given by<sup>14</sup>

$$\zeta_i = \Delta \lceil \frac{as_1 + bs_2}{\Delta} \rceil + \kappa \mathcal{L}_{\pm\Delta}(\alpha(cs_1 + ds_2)) + z_i = \mu + z_i \quad (5.47)$$

Hence  $p(\zeta_i | s_1, s_2)$  follows a Gaussian distribution with mean,  $\mu$ , as shown in (5.47), and variance  $N_i$ . Notice that we did not break (5.46) into parts similar to (5.36), but instead the equation for  $\zeta_i$  in (5.47) implicitly takes care of that. Yet, the problem formulation in Section 5.6 was carried out to shed light into the system behavior. Figure 5.17 shows the complete system diagram when the optimal decoders are used at both receivers. Notice that the encoder remains unchanged.

### 5.7.2 Optimal Decoders

Figure 5.18 shows the optimal decoding functions when the source correlation is zero. Figure 5.18(a) shows the case when the system encoding parameters are set to  $\Delta = 1.5$  and  $\alpha = 1.2$ , while Figure 5.18(b) uses  $\Delta = 2.0$  and  $\alpha = 1.5$ . All remaining parameters are fixed for the systems in subfigures (a) and (b) to  $P = 1$ ,  $N_1 = 0.02$ ,  $N_2 = 10N_1$ . As we can see from Figure 5.18, the optimal decoding function,  $g_1$ , for the first source  $s_1$  is very similar in both systems (a) and (b), while the shape of the optimal decoding function,  $g_2$ , for the second source  $s_2$  strongly depends on  $\Delta$  and  $\alpha$ . The optimal decoding function takes into account the different *folds* of the Gaussian noise

---

<sup>14</sup>  $\mu$  is a constant given  $(s_1, s_2)$ .

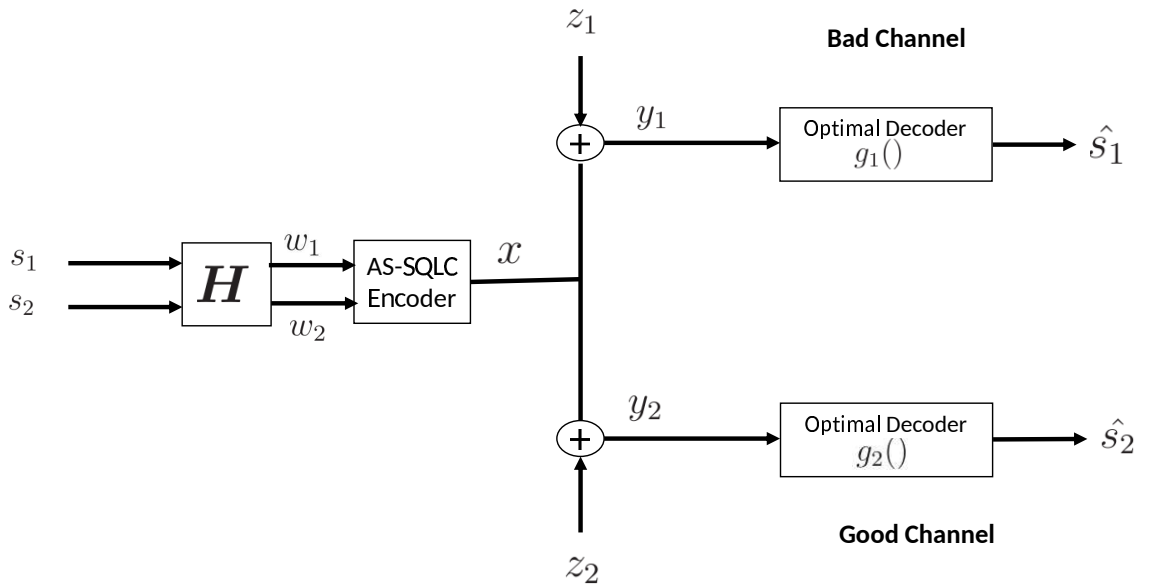


Figure 5.17: Complete system diagram of the AS-SQLC system with optimal decoders.

distribution that happen around  $\pm k\Delta$ , as well as the fact that source  $x_2$  gets clipped at  $\pm\Delta$ .

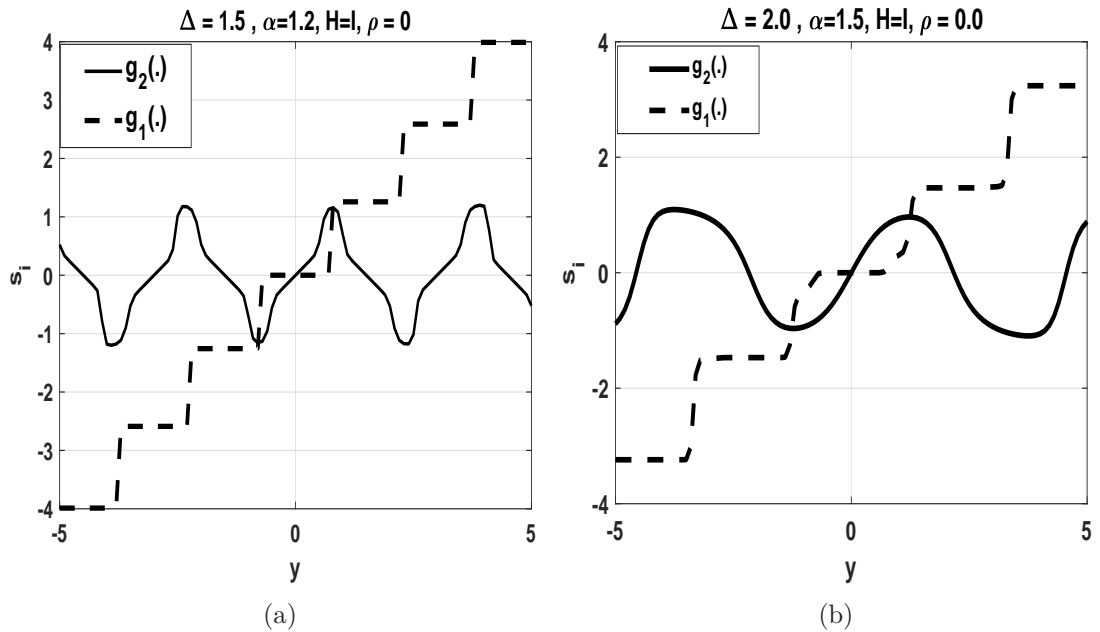


Figure 5.18: Optimal decoders for  $P = 1, N_1 = 0.04, N_2 = 10N_1, \rho^2 = 0, \mathbf{H} = \mathbf{I}$ . (a) uses  $\Delta = 1.5$  and  $\alpha = 1.2$  as encoding parameters, while (b) uses  $\Delta = 2.0$  and  $\alpha = 1.5$ .

Figure 5.19 shows the optimal decoding functions when the source correlation is 0.9. Figure 5.19(a) shows the case when  $\mathbf{H}$  is set to  $\mathbf{I}$  and 5.19(b) demonstrates the case when  $\mathbf{H} = [1 \ 0; -1 \ 1]$ . All remaining parameters are fixed for the systems in (a) and (b) to  $P = 1, N_1 = 0.02, N_2 = 10N_1, \Delta = 1.5, \alpha = 1.2$ . Notice that  $\hat{x}_2$  is less clipped in Figure 5.19(b), which leads to less spurious errors. Moreover, the decoder utilizes the high source correlation properly, as apparent from the observation that  $\hat{x}_1$  in Figure 5.19(b) is very close to  $\hat{x}_2$ . In fact, the system in Figure 5.19(b) performs about 3 dB better than the system in Figure 5.19(a).

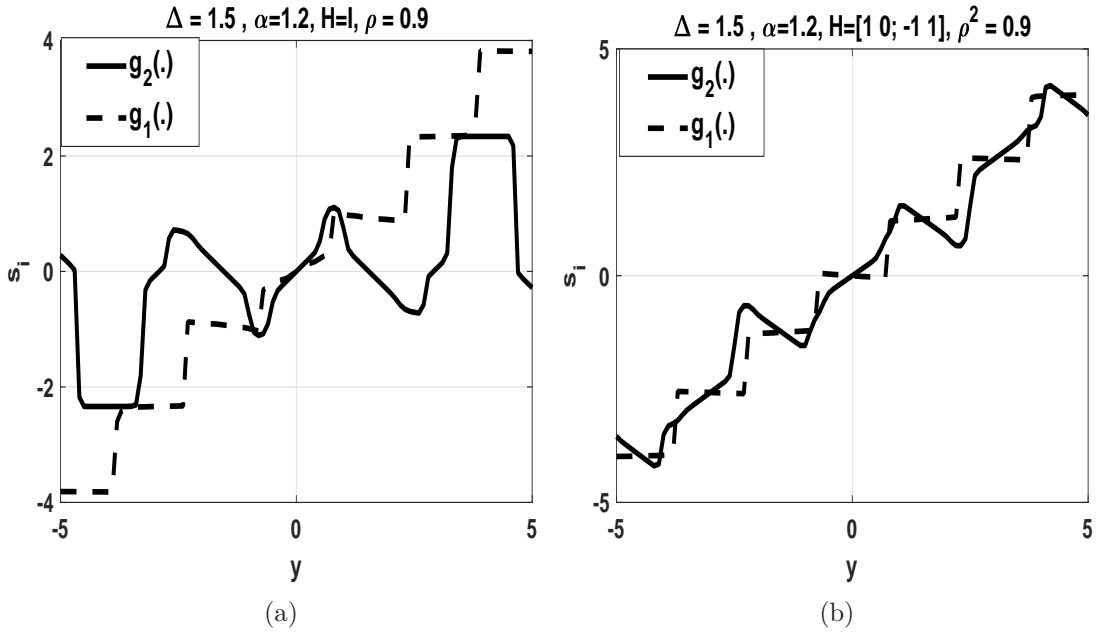


Figure 5.19: Optimal decoders for  $P = 1, N_1 = 0.04, N_2 = 10N_1, \rho^2 = 0.9$ . 5.19(a) uses the identity matrix as the precoding matrix  $\mathbf{H}$ , while 5.19(b) uses  $[1 \ 0; -1 \ 1]$  as  $\mathbf{H}$ .

Next, we highlight the effect that different system parameters have on the shape of the optimal decoders. In Figure 5.20, we have two optimal decoder function pairs for two cases: the first case considers  $N_1 = N_2 = 0.1$ , and is shown in Figure 5.20(a). The second case considers  $N_1 = N_2 = 0.01$  and is shown in Figure 5.20(b). All remaining system parameters are exactly the same. Notice that as the noise variance increases, the optimal decoding function appears as “stretched” and not very “sharp” as opposed to the low noise case. This is expected because when the noise increases, the optimal

MMSE detector strongly weighs in the effect of neighboring signal points, hence it appears as a “smoothing filter”, as seen in Figure 5.20(b).

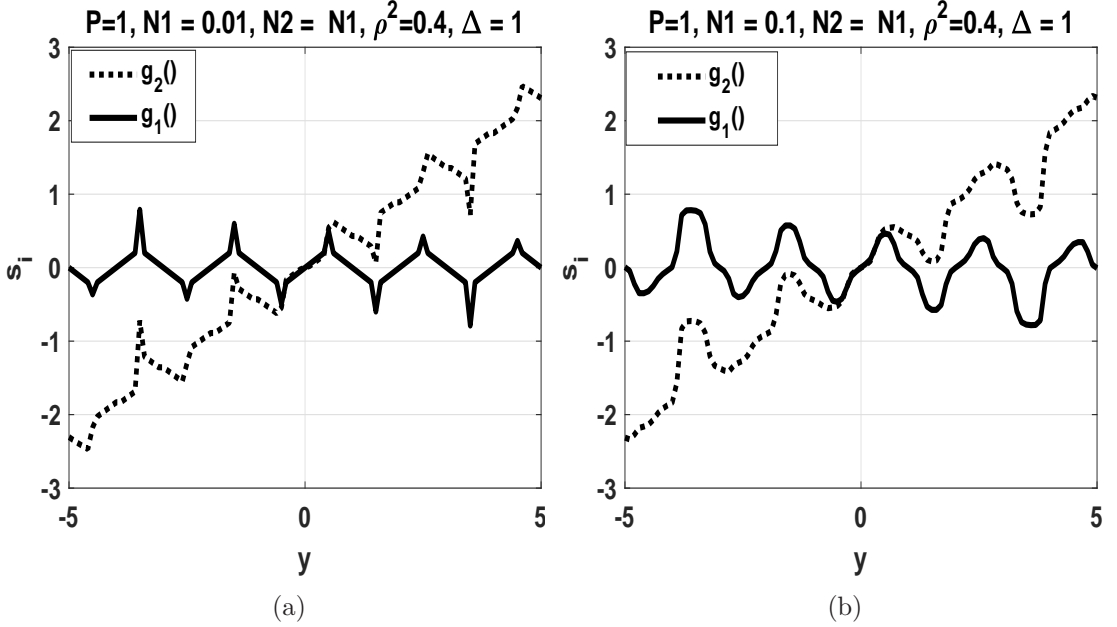


Figure 5.20: Optimal decoders for  $P = 1, \rho^2 = 0.4, \Delta = 1, \mathbf{H} = [1 \ 0 ; -0.9 \ 1]$ . (a) considers  $N_1 = N_2 = 0.01$ , while for (b) considers  $N_1 = N_2 = 0.1$ .

Finally, we demonstrate the effect that the source correlation  $\rho^2$  has on the shape of the optimal decoders. Figure 5.21 presents the results for a system with parameters  $P = 1, N_1 = N_2 = 0.1, \Delta = 1, \mathbf{H} = [1 \ 0 ; -0.4 \ 1]$ . The only difference between Figure 5.21(a) and 5.21(b) is the value of the source correlation,  $\rho^2$ , which is set to  $\rho^2 = 0.4$  in (a), and  $\rho^2 = 0.9$  in (b). We can see in Figure 5.21(b) that the shape of the optimal decoding function for the second source  $\hat{x}_2$  follows quite closely the decoded value of  $\hat{s}_1$  when  $\rho^2$  increases. This is explained by the observation that there is more relevant information in  $\hat{s}_1$  about  $s_2$ .

## 5.8 Simulation Results

In this section, we present the simulation results of the complete Broadcast system. To recap, we will be sending a Bivariate Gaussian source  $(\mathbf{X}_1, \mathbf{X}_2)$  with zero mean and a covariance matrix  $\mathbf{C} = [1 \ \rho^2 ; \rho^2 \ 1]$  using the AS-SQLC scheme. We will

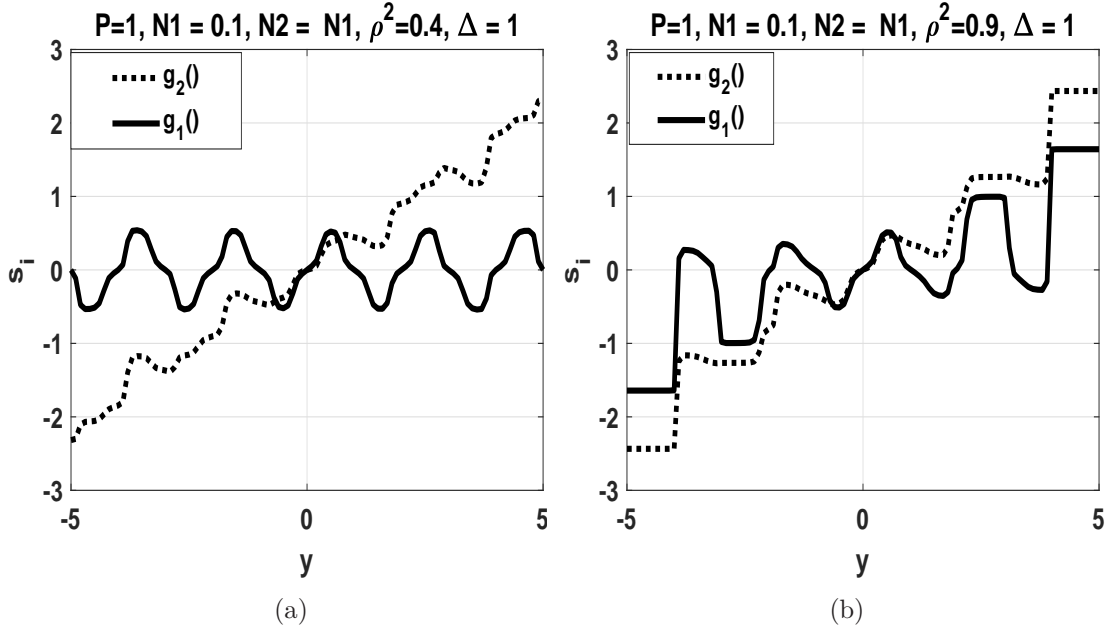


Figure 5.21: Optimal decoders for  $P = 1, N_1 = N_2 = 0.1, \Delta = 1$ . (a) has a source correlation,  $\rho^2 = 0.4$ , while (b) has a source correlation  $\rho^2 = 0.9$ . Notice that the second source  $\hat{s}_2$  in 5.21(b) closely follows the decoded values of  $\hat{x}_1$  has  $\rho^2 = 0.9$ .

use the system described in Figure 5.16, which has parameters  $\mathbf{H}, \Delta, \alpha$ , to transmit the users' data and perform simulations on different values of  $(\mathbf{H}, \Delta, \alpha)$ .

Figures 5.22, 5.23 and 5.24 show different combinations of system parameters and source correlation values. The “Theoretical limit” curve shown in the figures is obtained as explained in Section 5.2.2, while the “Optimal Separation Scheme” curve is obtained as explained in Section 5.3. As explained in Section 5.2.2, an instance of the Broadcast channel is characterized by  $(P, N_1, N_2, \rho^2)$ . For each instance, we perform a global search to find the parameters  $(\mathbf{H}, \Delta, \alpha)$  achieving the best performance (using the naïve decoding method described in Figure 5.16). The “Naïve decoding” curves in Figures 5.22 to 5.24 show the results of the naïve decoding method. Note that each point on the “naïve decoding” curve potentially has different system parameters  $(\mathbf{H}, \Delta, \alpha)$ . Then, for each point on the “naïve decoding” curve, we perform optimal decoding (as described in Figure 5.17) using the same system parameters  $(\mathbf{H}, \Delta, \alpha)$ . The results of the optimal decoding method are marked as “Optimal decoding” in the figures.

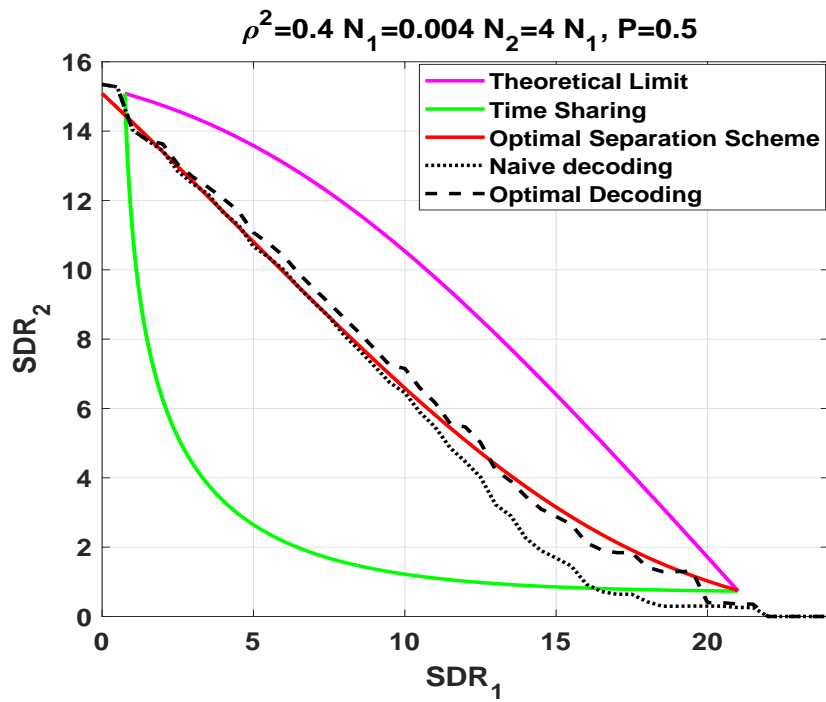
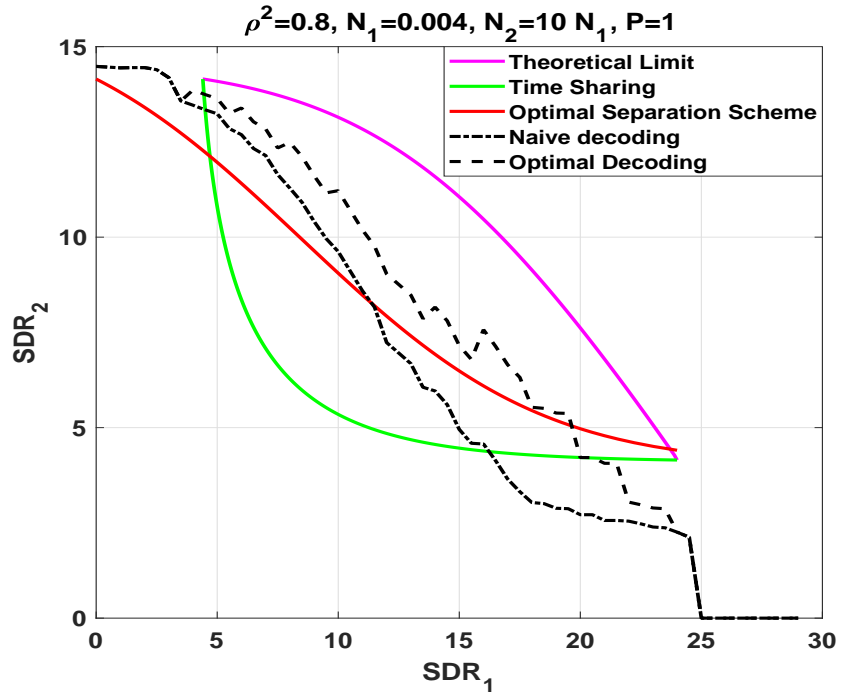


Figure 5.22: System performance under different conditions: (a)  $\rho^2 = 0.8, N_1 = 0.004, N_2 = 10N_1, P = 1$ , (b)  $\rho^2 = 0.4, N_1 = 0.004, N_2 = 4N_1, P = 1$ .

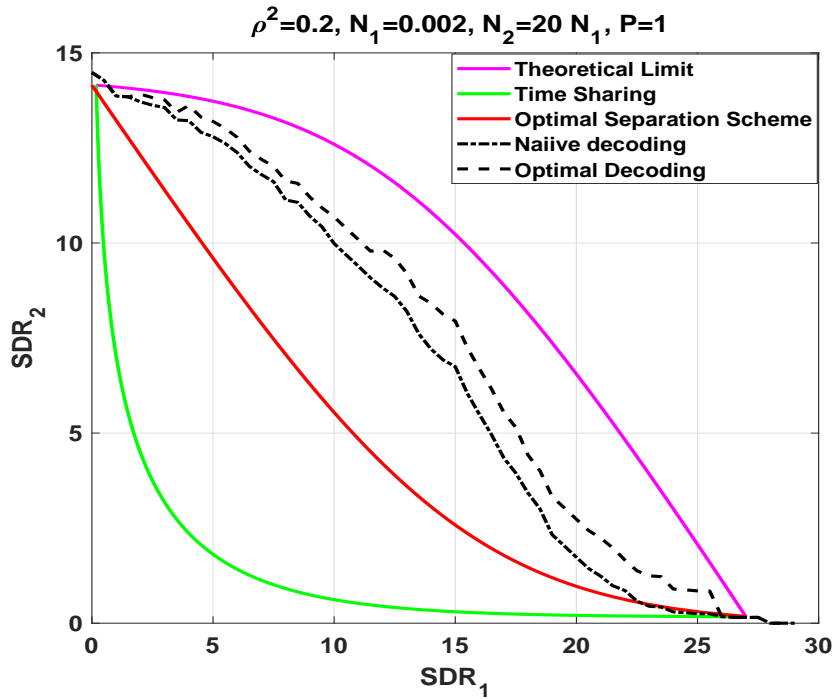
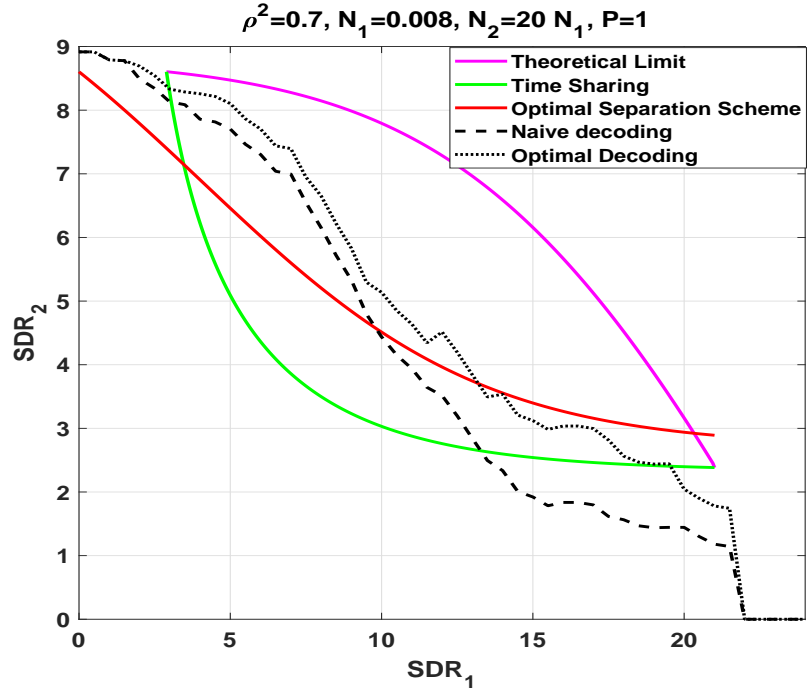
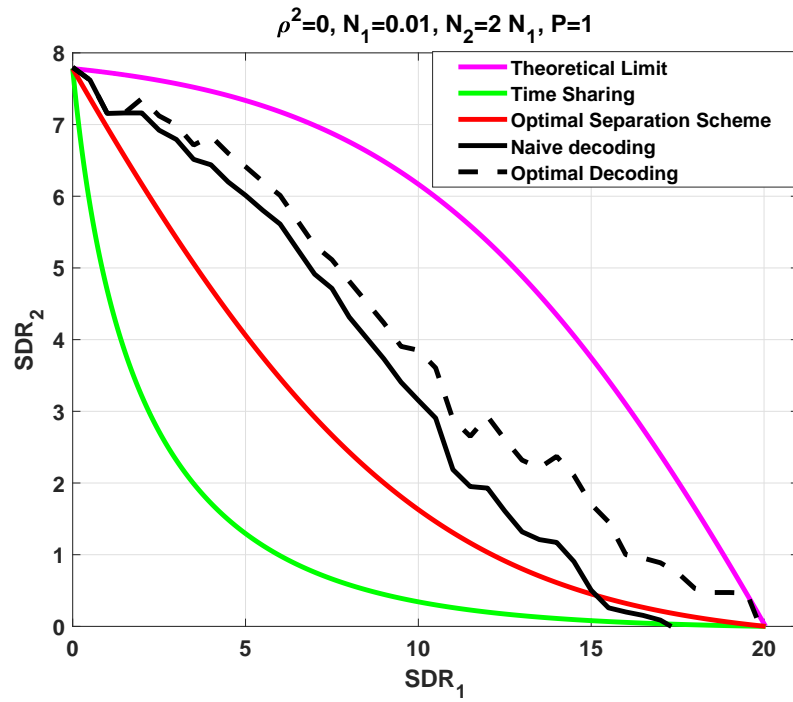
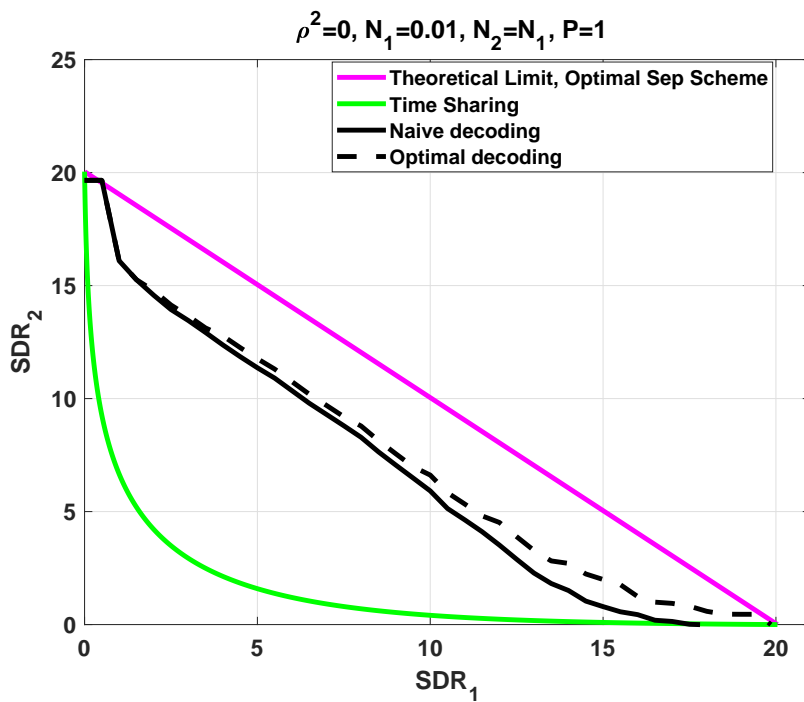


Figure 5.23: System performance under different conditions: (a)  $\rho^2 = 0.7, N_1 = 0.008, N_2 = 20N_1, P = 1$ , (b)  $\rho^2 = 0.2, N_1 = 0.002, N_2 = 20N_1, P = 1$ .



(a)



(b)

Figure 5.24: System performance under different conditions: (a)  $\rho^2 = 0, N_1 = 0.01, N_2 = N_1, P = 1$ , (b)  $\rho^2 = 0, N_1 = 0.01, N_2 = 2N_1, P = 1$ .

It is interesting to note that the AS-SQLC scheme is suitable for a wide range of source correlation values  $\rho^2$ , and noise variances  $N_1, N_2$ . Figure 5.24 shows that the proposed AS-SQLC works well for the case when there is great divergence in the noise variances. Specifically, when the difference between  $N_1$  and  $N_2$  is high, the scheme can beat the best known separation based system. This holds true across different source correlation values. On the other hand, as shown in Figure 5.24(b), when  $N_1 = N_2$  the separation based scheme is *optimal* and outperforms the AS-SQLC scheme. We should note, however, that the equal noise case is not very interesting in the Broadcast channel, since it can easily be shown that a variant of time sharing on an optimal point to point scheme can achieve the upper bound<sup>15</sup>. In general, the separation based scheme is not optimal even when  $\rho = 0$ , as shown in Figure 5.24(a). In this case the proposed AS-SQLC scheme outperforms the separation based scheme by 1-5 dB. We also note that the gain from the optimal decoding method is more pronounced for higher source correlation values. For example, in Figure 5.22 the largest gain is in Figure 5.22(a), where  $\rho^2 = 0.8$ , is 5 dB, while for Figure 5.22(b) the gain is only 3 dB when  $\rho^2 = 0.4$ .

We would like to remark that the results of the proposed systems in Figures 5.22 to 5.24 could be improved. The reason is that we have used a brute force approach by trying all combinations for  $\Delta, \alpha, \mathbf{H}$  for the naïve decoding, which allowed us to find the best  $SDR_2$  for each  $SDR_1$  (we performed binning to within 0.5 dB). Then, we used the system parameters of those optimal naïve points to calculate the optimal decoding function for those parameters, and hence obtain the optimal decoding results as shown in Figures 5.22 to 5.24. It is possible that the system could perform better, since the best parameters for the optimal decoder may be different than the best parameters for the naïve decoder.

---

<sup>15</sup> See Appendix B.

## 5.9 Conclusion

We have discussed the optimization of the decoding functions for analog joint source-channel coding systems based on non-linear mappings for the transmission of independent and correlated Gaussian messages over the two user Gaussian Broadcast Channel. We have introduced an optimization procedure that allows us to obtain optimized decoding functions in an easier manner, and assessed the performance improvements through simulation results. In general, we have corroborated that optimization is more critical when the SNR is low and when data clipping is more pronounced (small  $\Delta$ , large  $\alpha$ ). For the case of correlated sources, we have shown through Monte-Carlo simulation that the proposed scheme, and the optimal decoding technique, outperform any separation based scheme.

## Chapter 6

### CONCLUSION AND FUTURE WORK

This dissertation has studied the application of analog joint source channel coding in different environments. We first studied the non-linear acoustic underwater channel and showed how to adapt space filling curves to channel non-linearity. We derived the capacity for a simplified non-linear channel using the Blahut-Arimoto algorithm, and postulated a capacity bound for the end-to-end non-linear acoustic channel. We showed, via Monte Carlo simulations, that the proposed communication system provides excellent performance.

We then moved to the Multiple Access Channel. We proposed an analog CDMA-like communication scheme suitable for the transmission of analog codes over the MAC for an arbitrary number of users. The scheme was proven to achieve the theoretical limits for the special case when the users' communication rates (degrees of freedom) are allocated proportionally to the communication power each user utilizes. We then proposed a hybrid analog-digital scheme, which is an extension of the CDMA-like access scheme. The hybrid scheme uses analog and digital codes to communicate over the MAC, and was proven optimal for any point in the MAC region. In future work, we will study how to extend the scheme to transmit correlated Gaussian sources for different scenarios, such as MIMO and fading channels.

We then moved to the Broadcast channel, where we developed an analog scheme, AS-SQLC, for the transmission of Bivariate Gaussian sources. We derived an optimal decoding method for AS-SQLC systems, which offers significant performance gains, particularly at low SNR. We demonstrated that the AS-SQLC scheme, with the help of the optimal decoding functions, can outperform the best separation based scheme.

In future work, we will look for faster ways to arrive at the optimal AS-SQLC system parameters, and extend the scheme to broadcast channels with fading.

In summary, we have shown that analog JSCC system can be successfully used, in different scenarios, with impressive results. The relative ease and simplicity of designing the encoders and decoders was demonstrated. Although analog JSCC systems are a viable alternative to canonical digital systems, they lack a comprehensive framework similar to that of digital codes. For instance, there is still no known analog JSCC technique that works well for arbitrary source/channel bandwidth ratios, even for the point-to-point channel. In the future, we will investigate the application of JSCC to other channels that have gained recent interest, such as relay channels and wiretap channels.

## BIBLIOGRAPHY

- [1] C. E. Shannon, "A Mathematical Theory of Communication," *The Bell System Technical Journal*, 27:379-423, 1948.
- [2] T. A. Ramstad, "Shannon Mappings for Robust Communication," *Teletronikk*, 98(1):114-128, 2002.
- [3] S. Y. Chung, "On the Construction of Some Capacity-Approaching Coding Schemes," *Ph.D. thesis, Massachusetts Institute of Technology*, September 2000.
- [4] E. Hodgson, G. Brante, R. D. Souza and J. L. Rebelatto, "On the physical layer security of analog joint source channel coding schemes," 2015 IEEE 16th International Workshop on Signal Processing Advances in Wireless Communications (SPAWC), Stockholm, 2015, pp. 585-589.
- [5] A. Erdozain, P. M. Crespo and B. Beferull-Lozano, "Multiple Description Analog Joint Source-Channel Coding to Exploit the Diversity in Parallel Channels," in *IEEE Transactions on Signal Processing*, vol. 60, no. 11, pp. 5880-5892, November 2012.
- [6] O. Fresnedo, F. J. Vazquez-Araujo, J. Garcia-Frias, M. Gonzalez-Lopez and L. Castedo, "Comparison between Analog Joint Source-Channel Coded and Digital BICM Systems," 2011 IEEE International Conference on Communications (ICC), Kyoto, 2011, pp. 1-5.
- [7] S. Guruacharya and E. Hossain, "Self-Sustainability of Energy Harvesting Systems: Concept, Analysis, and Design," in *IEEE Transactions on Green Communications and Networking*, vol. 2, no. 1, pp. 175-192, March 2018.
- [8] G. Bedi, G. K. Venayagamoorthy, R. Singh, R. R. Brooks and K. C. Wang, "Review of Internet of Things (IoT) in Electric Power and Energy Systems," in *IEEE Internet of Things Journal*, vol. 5, no. 2, pp. 847-870, April 2018.
- [9] P. Floor, et al, "Zero-Delay Joint Source-Channel Coding for a Bivariate Gaussian on a Gaussian MAC," *IEEE Transactions on Communications* 60(10), pp. 3091-3102 (2012).
- [10] P. A. Floor, A. N. Kim, T. A. Ramstad, I. Balasingham, N. Wernersson and M. Skoglund, "On Joint Source-Channel Coding for a Multivariate Gaussian on a Gaussian MAC," in *IEEE Transactions on Communications*, vol. 63, no. 5, pp. 1824-1836, May 2015.

- [11] Lapidoth, A., Tinguely, S.: “Sending a Bivariate Gaussian Source over a Gaussian MAC,” *IEEE Transactions on Information Theory* 56(6), pp. 2714-2752 (2010).
- [12] O. Fresnedo, J. P. Gonzalez-Coma, M. Hassanin, L. Castedo and J. Garca-Fras, “Evaluation of Analog Joint Source-Channel Coding Systems for Multiple Access Channels,” in *IEEE Transactions on Communications*, vol. 63, no. 6, pp. 2312-2324, June 2015.
- [13] M. Hassanin, “Non Linear Joint Source Channel Coding For Broadcast Channels,” *Master’s thesis, The University of Delaware*, August 2015.
- [14] M. Hassanin, J. Garcia-Frias and L. Castedo, “Analog joint source channel coding for Gaussian Broadcast Channels,” 2014 IEEE International Conference on Acoustics, Speech and Signal Processing (ICASSP), Florence, 2014, pp. 4264-4268.
- [15] Fresnedo, O., Vzquez-Araujo, F., Castedo, L., Gonzalez Lpez, M., Garca Frias, J. “Analog Joint Source-Channel Coding in MIMO Rayleigh Fading Channels,” *Proceedings of 20th European Signal Processing Conference (EUSIPCO 2012)*, Bucharest, Romania (August 2012).
- [16] Fresnedo, O., Vzquez, F., Castedo, L., Garca-Frias, J. “Analog Joint Source-Channel Coding for OFDM Systems,” *Proceedings of 14th IEEE International Workshop on Signal Processing Advances in Wireless Communications (SPAWC 2013)*, Darmstadt, Germany (June 2013).
- [17] G. Brante, R. Souza, and J. Garcia-Frias, “Spatial Diversity Using Analog Joint Source Channel Coding in Wireless Channels,” *Communications, IEEE Transactions on*, vol. PP, no. 99, pp. 1 –11, 2012.
- [18] H. Liao. “Multiple access channels,” *Ph.D. thesis, Department of Electrical Engineering, University of Hawaii*, Honolulu, 1972.
- [19] R. Ahlswede. “Multi-way communication channels,” In *Proc. 2nd Int. Symp. Inf. Theory (Tsahkadsor, Armenian S.S.R.)*, pages 2352. Hungarian Academy of Sciences, Budapest, 1971.
- [20] P. Bergmans. “Random coding theorem for broadcast channels with degraded components,” *IEEE Trans. Inf. Theory*, IT-19:197207, 1973.
- [21] R. G. Gallager. “Capacity and coding for degraded broadcast channels,” *Probl. Peredachi Inf.*, 10(3):314, 1974.
- [22] J. H. Cox et al., “Advancing Software-Defined Networks: A Survey,” in *IEEE Access*, vol. 5, pp. 25487-25526, 2017.
- [23] “KDKA Begins to Broadcast, 1920”, *Public Broadcasting Services (PBS)*, <http://www.pbs.org/wgbh/aso/databank/entries/dt20ra.html>, doi: April 2017.

- [24] Robert G. Gallager, “Low-Density Parity Check Codes”, *Ph.D. thesis, Massachusetts Institute of Technology*, 1963.
- [25] David Forney, 6-451 Principles of Digital Communication II, Spring 2005. (Massachusetts Institute of Technology: MIT OpenCourseWare), <http://ocw.mit.edu> (Accessed March 10, 2017). License: Creative Commons BY-NC-SA.
- [26] John Proakis, “Fundamentals of Communication Systems,” Pearson Publishing, 2nd edition, December 2004.
- [27] Y. Yuli, “Audio Coding, Theory and Applications,” Springer 2010, p.40
- [28] A. Gersho and R. M. Gray, “Vector Quantization and Signal Compression,” Springer Science and Business Media, 1991.
- [29] C. Berrou, A. Glavieux and P. Thitimajshima, “Near Shannon limit error-correcting coding and decoding: Turbo-codes. 1,” *Communications*, 1993. ICC ’93 Geneva. Technical Program, Conference Record, IEEE International Conference on, Geneva, 1993, pp. 1064-1070 vol.2
- [30] Sae-Young Chung, G. D. Forney, T. J. Richardson and R. Urbanke, “On the design of low-density parity-check codes within 0.0045 dB of the Shannon limit,” in *IEEE Communications Letters*, vol. 5, no. 2, pp. 58-60, Feb 2001.
- [31] P. A. Floor, T. A. Ramstad and N. Wernersson, “Power Constrained Channel Optimized Vector Quantizers used for Bandwidth Expansion,” 2007 4th International Symposium on Wireless Communication Systems, Trondheim, 2007, pp. 667-671.
- [32] A. Fuldseth, “Robust subband video compression for noisy channels with multi-level signaling,” *Ph.D. dissertation, Norwegian University of Science and Technology*, 1997.
- [33] I. Iglesias “Extensions of Compressed Sensing by Exploiting Prior Knowledge,” *Ph.D thesis, University of Delaware*, Fall 2011.
- [34] T. Goblick, Jr., “Theoretical limitations on the transmission of data from analog sources,” *IEEE Transactions on Information Theory*, vol. 11, no. 4, pp. 558–567, October 1965.
- [35] V. A. Kotelnikov, “The Theory of Optimum Noise Immunity,” *New York: McGraw-Hill Book Company, Inc*, 1959.
- [36] C. E. Shannon, “Communication in The Presence of Noise,” *Proc. IRE*, 10-21, January 1949.
- [37] F. Hekland, P. Floor, and T. Ramstad, “Shannon-kotel-nikov mappings in joint source-channel coding,” *Communications, IEEE Transactions on*, vol. 57, no. 1, pp. 94 –105, January 2009.

- [38] Y. Hu, J. Garcia-Frias, and M. Lamarca, “Analog Joint Source-Channel Coding Using Non-linear Curves and MMSE decoding,” *Communications, IEEE Transactions on*, vol. 59, no. 11, pp. 3016 –3026, November 2011.
- [39] Yury Polyanskiy, “Channel coding: non-asymptotic fundamental limits”, *Ph.D. thesis, Princeton University*, 2010.
- [40] T. M. Cover and J. A. Thomas, “Elements of information theory”, New York, NY, USA: Wiley-Interscience, 1991.
- [41] RI Underwater US Government report  
”<http://www.dtic.mil/dtic/tr/fulltext/u2/a046687.pdf>”
- [42] D. Lucani, M. Stojanovic, and M. Medard, “On the relationship between transmission power and capacity of an underwater acoustic communication channel,” in *OCEANS 2008 - MTS/IEEE Kobe Techno-Ocean*, April 2008, pp. 1 –6.
- [43] M. Stojanovic, “Underwater Acoustic Communications: Design Considerations on the Physical Layer,” *Wireless on Demand Network Systems and Services, 2008. WONS 2008. Fifth Annual Conference on*, Garmisch-Partenkirchen, 2008, pp. 1-10.
- [44] S. Jiang, S Georgakopoulos: “Electromagnetic Wave Propagation into Fresh Water”, *Journal of Electromagnetic Analysis and Applications*, Volume 3, pp 261-266, July 2011.
- [45] M. Hassanin and J. Garcia-Frias, “Analog Joint Source Channel Coding over Non-linear Acoustic Channels,” 2013 47th Annual Conference on Information Sciences and Systems (CISS), Baltimore, MD, 2013, pp. 1-6.
- [46] A. Song, M. Badiy, H.-C. Song, W. S. Hodgkiss, M. B. Porter, and the KauaiEx Group, “Impact of ocean variability on coherent underwater acoustic communications during the Kauai experiment (KauaiEx),” *J. Acoust. Soc. Am.*, vol. 123, no. 2, pp. 856-865, February 2008
- [47] R. Blahut, “Computation of Channel Capacity and Rate-distortion Functions,” *Information Theory, IEEE Transactions on*, vol. 18, no. 4, pp. 460 – 473, July 1972.
- [48] I. Csiszar, “On the Computation of Rate-Distortion Functions (corresp.),” *Information Theory, IEEE Transactions on*, vol. 20, no. 1, pp. 122 – 124, January 1974.
- [49] O. Ndili and T. Ogunfunmi, “Achieving Maximum Possible Download Speed on ADSL Systems,” in *Signal Processing Systems, 2007 IEEE Workshop on*, October 2007, pp. 407 –411.

- [50] S. Shamai and I. Bar-David, “The Capacity of Average and Peak-power-limited Quadrature Gaussian Channels,” *Information Theory, IEEE Transactions on*, vol. 41, no. 4, pp. 1060–1071, July 1995.
- [51] J. Dauwels, “On Graphical Models for Communications and Machine Learning: Algorithms, Bounds, and Analog Implementation,” *Ph.D. thesis, Swiss Federal Institute of Technology, Zurich*, May 2006.
- [52] P. Almers, F. Tufvesson, O. Edfors and A. F. Molisch, “Measured capacity gain using water filling in frequency selective MIMO channels,” *The 13th IEEE International Symposium on Personal, Indoor and Mobile Radio Communications*, 2002, pp. 1347-1351 vol.3.
- [53] O. Fresnedo, F. J. Vazquez-Araujo, L. Castedo and J. Garcia-Frias, “Low-Complexity Near-Optimal Decoding for Analog Joint Source Channel Coding Using Space-Filling Curves,” in *IEEE Communications Letters*, vol. 17, no. 4, pp. 745-748, April 2013.
- [54] C. Belfiore and J. Park, J.H., “Decision feedback equalization,” *Proceedings of the IEEE*, vol. 67, no. 8, pp. 1143 – 1156, August 1979.
- [55] M. Hassanin, and J. Garcia-Frias, “A hybrid digital-analog scheme for the Multiple Access Channel,” *IEEE CISS’14*, March 2014.
- [56] O. Fresnedo, L. Castedo, M. Hassanin and J. Garcia-Frias, “Analog Joint Source Channel Coding for Block Fading Multiple Access Channels,” *2014 IEEE International Conference on Acoustics, Speech and Signal Processing (ICASSP)*, Florence, 2014, pp. 4254-4258.
- [57] P. A. Floor, A. N. Kim, T. A. Ramstad, I. Balasingham, N. Wernersson and M. Skoglund, “On Joint Source-Channel Coding for a Multivariate Gaussian on a Gaussian MAC,” in *IEEE Transactions on Communications*, vol. 63, no. 5, pp. 1824-1836, May 2015.
- [58] S. Servetto, “Lattice Quantization with Side Information, Codes, Asymptotics, and Applications in Sensor Networks,” *IEEE Transactions on Information Theory* 53(2), pp. 714-731 (2007).
- [59] C. Illangakoon and P. Yahampath, “Hybrid Digital-Analog Communication of a Bivariate Gaussian Source over a Fading MAC,” *2016 IEEE 84th Vehicular Technology Conference (VTC-Fall)*, Montreal, QC, 2016, pp. 1-5.
- [60] J. Kron, F. Alajaji and M. Skoglund, “Low-Delay Joint Source-Channel Mappings for the Gaussian MAC,” in *IEEE Communications Letters*, vol. 18, no. 2, pp. 249-252, February 2014.

- [61] M. S. Mehmetoglu, E. Akyol and K. Rose, “Deterministic Annealing-Based Optimization for Zero-Delay Source-Channel Coding in Networks,” in *IEEE Transactions on Communications*, vol. 63, no. 12, pp. 5089-5100, December 2015.
- [62] Z. Ding, X. Lei, G. K. Karagiannidis, R. Schober, J. Yuan and V. K. Bhargava, “A Survey on Non-Orthogonal Multiple Access for 5G Networks: Research Challenges and Future Trends,” in *IEEE Journal on Selected Areas in Communications*, vol. 35, no. 10, pp. 2181-2195, October 2017.
- [63] ETSI Standard EN 302 307 V1.1.1: Digital Video Broadcasting (DVB); Second generation framing structure, channel coding and modulation systems for Broadcasting, Interactive Services, News Gathering and other broadband satellite applications (DVB-S2), European Telecommunications Standards Institute, Valbonne, France, 2005-03.
- [64] M. Hassanin, Bo Lu and J. Garcia-Frias, “Application of Analog Joint Source-Channel Coding to Broadcast Channels,” 2015 IEEE 16th International Workshop on Signal Processing Advances in Wireless Communications (SPAWC), Stockholm, 2015, pp. 610-614.
- [65] T. Cover, “Broadcast channels,” *IEEE Transactions on Information Theory*, vol.18, no. 1, pp. 214, January 1972.
- [66] C. Tian, S. Diggavi and S. Shamai, “The Achievable Distortion Region of Sending a Bivariate Gaussian Source on the Gaussian Broadcast Channel,” *IEEE Transactions on Information Theory*, vol. 57, no. 10, pp. 6419–6427, October 2011.
- [67] Yang Gao; Tuncel, E., “Separate source-channel coding for broadcasting correlated Gaussians,” *IEEE ISIT’11*, August 2011.
- [68] S. Bross, A. Lapidoth, S. Tinguely, “Broadcasting Correlated Gaussians,” *IEEE Transactions on Information Theory*, vol. 56, no. 7, pp. 3057–3068, July 2010.
- [69] M. Gastpar, A. Lapidoth, Y. Steinberg and M. Wigger, “Coding Schemes and Asymptotic Capacity for the Gaussian Broadcast and Interference Channels With Feedback,” in *IEEE Transactions on Information Theory*, vol. 60, no. 1, pp. 54-71, January 2014.
- [70] R. Soundararajan and S. Vishwanath, “Hybrid coding for Gaussian broadcast channels with Gaussian sources,” 2009 IEEE International Symposium on Information Theory, Seoul, 2009, pp. 2790-2794. doi: 10.1109/ISIT.2009.5205795
- [71] J. Nayak and E. Tuncel, “Successive Coding of Correlated Sources,” in *IEEE Transactions on Information Theory*, vol. 55, no. 9, pp. 4286-4298, September 2009.

- [72] A. Abou Saleh, F. Alajaji and W. Y. Chan, "Source-Interference Recovery Over Broadcast Channels: Asymptotic Bounds and Analog Codes," in *IEEE Transactions on Communications*, vol. 64, no. 8, pp. 3406-3418, August 2016
- [73] P. Suarez-Casal, O. Fresnedo, L. Castedo and J. Garcia-Frias, "Analog Transmission of Correlated Sources Over BC With Distortion Balancing," in *IEEE Transactions on Communications*, vol. 65, no. 11, pp. 4871-4885, Nov. 2017.
- [74] E. Akyol, K. Rose, and T Ramstad, "Optimized analog mappings for distributed source channel coding," *Proc. IEEE Data Compression Conference*, Snowbird, Utah. March 2010.
- [75] S. Boyd and L. Vandenberghe, "Convex Optimization," New York, NY, USA: Cambridge University Press, 2004.

## Appendix A

### POWER ALLOCATION

In this appendix, we corroborate that the algorithm derived in Section 3.3.1 converges to the global maximum. We will first see that the function

$$f(P_1, P_2, \dots, P_N) = \sum_{i=1}^N C_d\left(\frac{|H_i|^2 \gamma_d P_i}{\sigma_{n^2}^i}\right) + \lambda \sum_{i=1}^N P_i \quad (\text{A.1})$$

is concave. We first notice that  $C_d(x)$  is concave in  $x$ . This is clear from Figure 3.8, in which we can see that the second derivative,  $C''$ , will always be negative. The function  $f(P_1, P_2, \dots, P_N)$  is a multivariate function and to show that a point is a local maxima we have to form the Hessian matrix  $\mathbf{K}$ , which is an  $N \times N$  matrix with entries

$$\mathbf{K}_{ij} = \frac{\partial^2 f}{\partial P_i \partial P_j}. \quad (\text{A.2})$$

It is clear from (A.1) that the off diagonal entries are all zero and that the diagonal entries are  $(\frac{|H_i|^2 \gamma_d}{\sigma_{n^2}^i})^2 C''(\frac{|H_i|^2 \gamma_d P_i}{\sigma_{n^2}^i})$ . These diagonal entries are all negative for any value of  $P_i \in [a^2, b^2]$  since  $C''(x)$  is itself negative. For a point  $(P_1, P_2, \dots, P_N)$  to be a maximum, the eigenvalues of the Hessian have to be negative [75]. Since our Hessian matrix is diagonal, it is clear that all eigenvalues (diagonal elements) are negative and thus the local maxima we find is also a global maxima. One final technicality to note is that our optimization region is convex, meaning that  $P_i$  belongs to the interval  $[a^2, b^2]$ . This is a necessary condition to guarantee convergence to the global minima/maxima.

## Appendix B

### SIMPLE SCHEMES FOR THE BROADCAST CHANNEL

In this appendix, we discuss simple schemes for the Broadcast channel. In the simplest scheme, the broadcast channel can be converted into a point to point communication system by ignoring one of the sources and transmitting only the remaining source. In this case, the Broadcast channel becomes a single point-to-point channel for the user intended to receive that information. For example, ignoring user 1 and transmitting only  $S_1$ , user 2 achieves a distortion of  $D_2^{min}$  and user 1 achieves a distortion of  $D_1^{max}$ . Similarly we can get  $D_1^{min}$  and  $D_2^{max}$ , where

$$D_1^{max} = \frac{(1 - \rho^2)P + N_1}{P + N_1}, \quad D_2^{min} = \frac{N_2}{P + N_2} \quad (\text{B.1})$$

$$D_1^{min} = \frac{N_1}{P + N_1} \quad D_2^{max} = \frac{(1 - \rho^2)P + N_2}{P + N_2} \quad (\text{B.2})$$

Then, we can use time sharing to obtain linear combinations of the extremal distortions: Since the uncoded scheme is optimal at the two extreme points, we can transmit source 1 a fraction  $\zeta$  of the time and achieve  $D_1^{min}$ , while at the same time source 2 would be achieving  $D_2^{max}$  [68]. Also, for the  $1 - \zeta$  fraction of time that source 1 is not being transmitted, source 2 is being transmitted over the channel, achieving a distortion of  $D_2^{min}$ , while the distortion of source 1 is  $D_1^{max}$ . Hence the set of time sharing solutions can be expressed parametrically with respect to  $\zeta$  as

$$D_1(\zeta) = \zeta D_1^{min} + (1 - \zeta) D_1^{max} \quad (\text{B.3})$$

$$D_2(\zeta) = (1 - \zeta) D_2^{max} + \zeta D_2^{min} \quad (\text{B.4})$$

We denote this scheme as *Naïve* time sharing, since at the times where one source is being transmitted the other source is experiencing *maximal* distortion. We note that we can actually devise a smarter time sharing solution that performs much better, at the cost of a more complicated system design.

In this smart time sharing solution, we perform time sharing on the extreme rates of the broadcast channel *capacity* region  $C_1$  and  $C_2$ <sup>1</sup>. Using similar arguments to (B.3), the time sharing rates that can be achieved are given by:

$$R_1(\zeta) = \zeta C_1 \tag{B.5}$$

$$R_2(\zeta) = (1 - \zeta) C_2. \tag{B.6}$$

Since in this dissertation we focus on transmitting one Gaussian source to each user using the channel once ( $\kappa = 1$ ), we must perform source compression (bandwidth reduction) on the original sources to keep the source/channel bandwidth at unity. For example, if  $\zeta = \frac{1}{3}$ , then, in three time slots, the first source will be transmitted in one of the time slots, while the second source would occupy the remaining two time slots. Hence, for source 1 we must use a 3 : 1 compression system that takes three Gaussian source symbols and produces one symbol. Similarly source 2 utilizes a 3 : 2 compression system, that produces two symbols. Then, the encoded two symbols are transmitted in the two allocated time slots. This is demonstrated in Figure B.1.

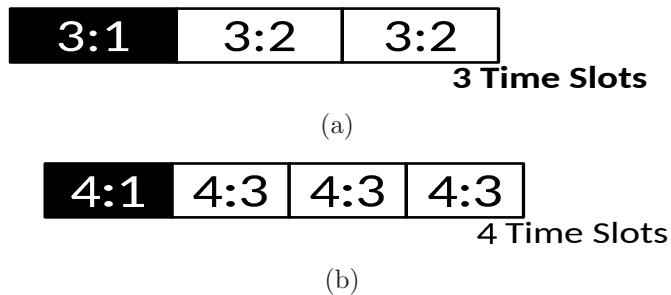


Figure B.1: Smart time sharing: (a) shows the case when  $\zeta = \frac{1}{3}$  and, (b) shows the case when  $\zeta = \frac{1}{4}$ .

---

<sup>1</sup> For an AWGN channel,  $C_i = \frac{1}{2} \log_2(1 + \frac{P}{N_i})$ .

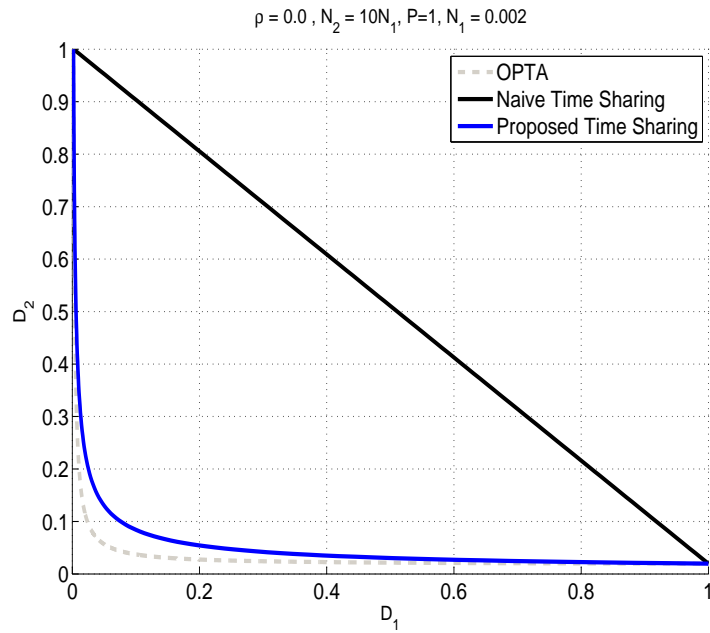
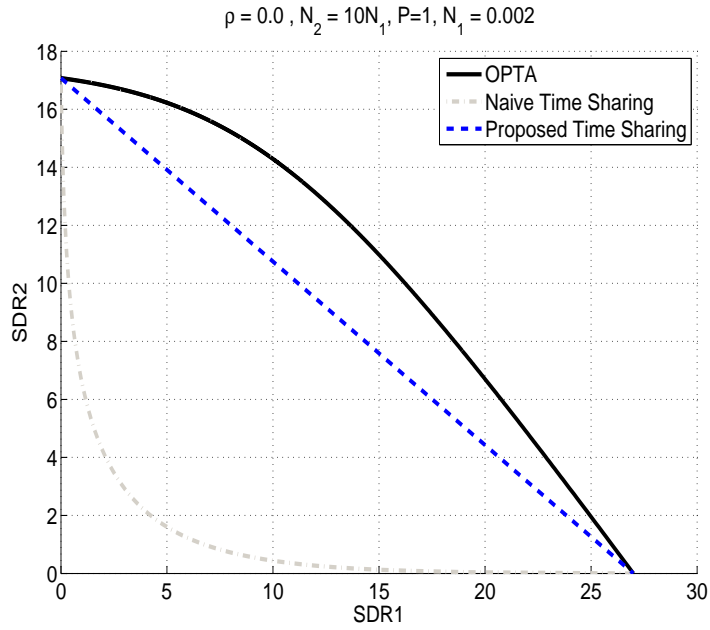


Figure B.2: OPTA curves for  $P = 1$ ,  $N_1 = 0.002$ ,  $N_2 = 10N_1$  and  $\rho = 0$ : (a) depicts the log scale; and, (b) depicts the linear scale.

The performance of the smart time sharing system is shown in Figure B.2, where we used a time-frame of 1024 time-slots. Note that the smart time sharing

system requires re-design of the complete system at every optimal distortion pair, a task that is not to be taken lightly. Again note the sub-optimality of the smart time sharing scheme: although it requires complete system re-design at each point, it is still suboptimal in general. Smart time sharing is only optimal for a *symmetric* Broadcast channel (when the two users' receiver noise variances are equal,  $N_1 = N_2$ ).